On the stabilization and enhancement of the reduced-order models for compressible flows

by

Elnaz Rezaianzadeh

B.S., Shahid Beheshti University, Iran, 2013

M.S., New Mexico State University, United States, 2016

AN ABSTRACT OF A DISSERTATION

submitted in partial fulfillment of the
requirements for the degree

DOCTOR OF PHILOSOPHY

Alan Levin Department of Mechanical and Nuclear Engineering
Carl R. Ice College of Engineering

KANSAS STATE UNIVERSITY
Manhattan, Kansas

2020

Abstract

Projection-based model reduction offers a physically informed, and mathematically rigorous framework to bypass the prohibitive amount of computational resources required by the direct numerical simulations in fluid dynamics, and enable the recurrent computations that dominate many-queries applications. Projection of the governing equations onto a low-dimensional space, however, does not guarantee to naturally inherit the stability properties of the high-fidelity model. Symmetrization of the Reduced-Order Model (ROM) through a least squares Petrov-Galerkin projection, or by Galerkin projection using the symmetry inner product, provides theoretical error bounds, and generates more stable ROMs. This study shows that besides being more stable, the symmetrized ROMs are more controllable and robust. The stability guarantees by symmetrization or energy-based inner products, assume that the subspace constructed for projection, accurately captures the coherent structures that are the main ingredients in the dynamics of the flow. However, when the high-fidelity simulations contain nonlinear phenomena (e.g. unsteady shock waves, and turbulence), truncation of the high-frequency modes through dimensionality reduction with a linear approach like Proper Orthogonal Decomposition (POD), that is biased towards the most energetic modes, may result in losing structures with critical contributions in the dynamical evolution of the system. As a result, especially when the governing equations lack any intrinsic dissipative mechanisms to contain the generated errors (e.g. the Euler equations), symmetrization alone is not sufficient to preserve stability. Therefore, a complete framework is proposed in this study for the enhancement of ROMs for compressible flows, through ROM symmetrization, and post-ROM stabilization.

Two optimization-based non-intrusive stabilization methods are developed here: a Hybrid method for the stabilization of ROMs as Linear Time-Invariant (LTI) systems, and an eigenvalue reassignment method for stabilization of nonlinear ROMs (ERN algorithm). The

Hybrid method is a two-step approach: in step one (efficiency-oriented), the left reduced order basis of the ROM is minimally modified in a convex optimization problem; in step two (accuracy-oriented), an eigenvalue reassignment method is used to stabilize the most energetic eigen-modes. The ERN algorithm, on the other hand, confines the nonlinear ROM to maintain a negative total power for stability; and the distance between the nonlinear ROM and Full-Order Model (FOM) attractors is directly minimized as the eigenvalues of the linear dynamics matrix (control parameters) are reassigned in the complex plane.

A computational bottleneck occurs in strongly nonlinear systems (e.g. advection-dominated flows), where the slow decay of the projection error requires more base functions to accurately span the high-fidelity solutions with a linear subspace. Hence to sufficiently describe a strongly nonlinear system, ROMs have higher dimensions intrinsically. Nevertheless, the truncation of such ROMs may still bring in instability, and their relatively higher dimension (i.e. large coefficient matrices) leads to a large number of control parameters which may potentially prevent the stabilization algorithm being feasible in computation. As a remedy, this study introduces a multi-stage layout for robust stabilization of nonlinear ROMs with the ERN algorithm, in strongly nonlinear systems, where a linear ROM typically fails to capture the true dynamics.

The proposed methods are applied on POD-Galerkin ROMs based on the snapshots of two supersonic flow applications. The high-fidelity simulations are performed with a Weighted Essentially Non-Oscillatory (WENO) shock capturing scheme, integrated with the immersed boundary method. The two applications involve strong shock-wake interactions in the downstream, where the unsteady shock oscillations as a result of the interaction of shock waves with vortices, exhibit strong nonlinearities that are not completely resolved in the leading POD modes. Thus, the missing high-frequency contributions of this phenomenon trigger strong instabilities in the linear and nonlinear ROMs, and enable a thorough investigation of the ideas that are developed in this research for the stabilization and enhancement of ROMs.

On the stabilization and enhancement of the reduced-order models for compressible flows

by

Elnaz Rezaianzadeh

B.S., Shahid Beheshti University, Iran, 2013

M.S., New Mexico State University, United States, 2016

A DISSERTATION

submitted in partial fulfillment of the
requirements for the degree

DOCTOR OF PHILOSOPHY

Alan Levin Department of Mechanical and Nuclear Engineering
Carl R. Ice College of Engineering

KANSAS STATE UNIVERSITY
Manhattan, Kansas

2020

Approved by:

Major Professor
Mingjun Wei

Copyright

Abstract

Projection-based model reduction offers a physically informed, and mathematically rigorous framework to bypass the prohibitive amount of computational resources required by the direct numerical simulations in fluid dynamics, and enable the recurrent computations that dominate many-queries applications. Projection of the governing equations onto a low-dimensional space, however, does not guarantee to naturally inherit the stability properties of the high-fidelity model. Symmetrization of the Reduced-Order Model (ROM) through a least squares Petrov-Galerkin projection, or by Galerkin projection using the symmetry inner product, provides theoretical error bounds, and generates more stable ROMs. This study shows that besides being more stable, the symmetrized ROMs are more controllable and robust. The stability guarantees by symmetrization or energy-based inner products, assume that the subspace constructed for projection, accurately captures the coherent structures that are the main ingredients in the dynamics of the flow. However, when the high-fidelity simulations contain nonlinear phenomena (e.g. unsteady shock waves, and turbulence), truncation of the high-frequency modes through dimensionality reduction with a linear approach like Proper Orthogonal Decomposition (POD), that is biased towards the most energetic modes, may result in losing structures with critical contributions in the dynamical evolution of the system. As a result, especially when the governing equations lack any intrinsic dissipative mechanisms to contain the generated errors (e.g. the Euler equations), symmetrization alone is not sufficient to preserve stability. Therefore, a complete framework is proposed in this study for the enhancement of ROMs for compressible flows, through ROM symmetrization, and post-ROM stabilization.

Two optimization-based non-intrusive stabilization methods are developed here: a Hybrid method for the stabilization of ROMs as Linear Time-Invariant (LTI) systems, and an eigenvalue reassignment method for stabilization of nonlinear ROMs (ERN algorithm). The

Hybrid method is a two-step approach: in step one (efficiency-oriented), the left reduced order basis of the ROM is minimally modified in a convex optimization problem; in step two (accuracy-oriented), an eigenvalue reassignment method is used to stabilize the most energetic eigen-modes. The ERN algorithm, on the other hand, confines the nonlinear ROM to maintain a negative total power for stability; and the distance between the nonlinear ROM and Full-Order Model (FOM) attractors is directly minimized as the eigenvalues of the linear dynamics matrix (control parameters) are reassigned in the complex plane.

A computational bottleneck occurs in strongly nonlinear systems (e.g. advection-dominated flows), where the slow decay of the projection error requires more base functions to accurately span the high-fidelity solutions with a linear subspace. Hence to sufficiently describe a strongly nonlinear system, ROMs have higher dimensions intrinsically. Nevertheless, the truncation of such ROMs may still bring in instability, and their relatively higher dimension (i.e. large coefficient matrices) leads to a large number of control parameters which may potentially prevent the stabilization algorithm being feasible in computation. As a remedy, this study introduces a multi-stage layout for robust stabilization of nonlinear ROMs with the ERN algorithm, in strongly nonlinear systems, where a linear ROM typically fails to capture the true dynamics.

The proposed methods are applied on POD-Galerkin ROMs based on the snapshots of two supersonic flow applications. The high-fidelity simulations are performed with a Weighted Essentially Non-Oscillatory (WENO) shock capturing scheme, integrated with the immersed boundary method. The two applications involve strong shock-wake interactions in the downstream, where the unsteady shock oscillations as a result of the interaction of shock waves with vortices, exhibit strong nonlinearities that are not completely resolved in the leading POD modes. Thus, the missing high-frequency contributions of this phenomenon trigger strong instabilities in the linear and nonlinear ROMs, and enable a thorough investigation of the ideas that are developed in this research for the stabilization and enhancement of ROMs.

Table of Contents

List of Figures

List of Tables

Acknowledgments

Earning a Ph.D. degree is not just another academic milestone. Through the doctoral studies, one becomes part of an academic family that carries a particular culture, that directly affects their professional attribute, and sometimes their personality. This culture is the legacy of the research group in which they have grown up as a graduate student, and typically remains with them through their professional life. I have been honored to earn my Ph.D. degree under the supervision of Prof. Mingjun Wei. The day I knocked on the door of his office to talk about a position in his group as a Master's student, I was not aware that I will be working with one of the most humble, patient, and principled people in the academia. He has set a remarkable example for me to prioritize the right values when making important decisions in my career. It is only fair to be, first and foremost, thankful to my advisor, Prof. Mingjun Wei, for his wise guidance, and kind support through all these years. This is not the end of his part in my life as an advisor. Down the road, I will always look back, and learn more from my years in his group.

I would like to acknowledge my Ph.D. supervisory committee: Prof. Mohammad Hosni, Prof. Chih-hang Wu, Prof. Hitesh Bindra, Prof. Doina Caragea, and Prof. Bala Natarajan, for their constructive comments, inspiration, and support. I am especially thankful to Prof. Caragea for her guidance towards the future extension of this research. I appreciate the Interim Head of the Department of Mechanical and Nuclear Engineering, Prof. Steven Eckels, for granting me the opportunity to teach an undergraduate course, and for his thoughtful support. I cannot be thankful enough to the staff of the MNE Department at KSU: Catherine Sandoval, Shelly Reves-Klinkner, and Mitzi Farmer, for being incredibly kind and helpful.

I am grateful for the support from the Army Research Lab (ARL), through the Army High Performance Computing Research Center (AHPCRC), and Micro Autonomous Systems and Technology (MAST) Collaborative Technology Alliance (CTA), that has enabled this research.

Special thanks go to my labmates, and friends, who helped me enjoy every step of this journey. I would like to appreciate Ameneh Tavakol, Amir Shaghaghi, Tayebeh Kakeshpour, and Negar Orangi-Fard: the true friends who have laughed with my smile, and sympathized with my sorrow. The everlasting moments they have built in my memory are priceless.

Words are not adequate to express how grateful I am to have a wonderful supporting family. Although physically far away, my parents have mentally remained by my side in every single moment along this path. They could not be more supportive, and more understanding. It takes superpowers to make someone feel you beside them when you are an Earth-diameter apart, and they have done this for me. At the end, I cannot miss the opportunity to thank my younger brother Arshia, who has inspired me with his persistent enthusiasm in science.

Dedication

To my parents, Sima and Abbas, for their endless love, and constant support.

Chapter 1

Introduction

Recurrent simulations of the dynamics for flow control, design and optimization processes are fueling a large motion towards the development and enhancement of the Reduced-Order Models (ROM) to facilitate online prediction of the flow field, where fast or real-time application of the High-Fidelity Models (HFM) based on the discretization of the governing partial differential equations are beyond the current capabilities of high performance computing[2–5]. The competition between the projection-based model reduction techniques and the more or less black-box models that have been traditionally developed by system identification and operator inference algorithms, has entered a new phase by the steep growth in the success factor of machine learning and deep neural architectures. The physically and mathematically rigorous nature of projection-based ROMs is balanced by the non-intrusive framework of black-box methods. However, many if not most of the fluid dynamics applications cannot withstand the slightest deviation of the ROM dynamics from the original high-dimensional attractor, which magnifies the value of the projection-based ROMs that contain strong physical and mathematical connections with the Full-Order Model (FOM), rather than the purely data-driven models with little or no knowledge about the conservation laws that govern the fluid dynamics[6;7]. Added to this factor is the computationally intensive process of training the artificial neural networks that requires prohibitively large number of high-fidelity snapshots compared to what is consumed for the dimensionality reduction in

projection-based model reduction techniques.

Projection-based ROMs are founded over dimensionality reduction, in conjunction with orthogonal projection or residual minimization[8–10]. Proper Orthogonal Decomposition (POD) constructs a linear subspace that spans the space of the high-fidelity snapshots with the fewest number of modes among the linear dimensionality reduction methods[11–13]. Being biased towards the most energetic flow structures, POD fails to capture the high-frequency signatures that are crucial in the dynamics of nonlinear fluid systems, such as supersonic flows with unsteady shock waves, turbulent flows, and advection-dominated flows in general. Thus, subsequent projection of the governing equations onto the POD subspace through the Galerkin projection, or by residual minimization in Petrov-Galerkin methods results in unstable or inaccurate ROMs that need closure modeling or post-ROM stabilization to recover the missing high-frequency modal information[14–21]. Projection of the governing equations over nonlinear manifolds has recently gained attention in applications where the POD subspace comes short in resolving the true dynamics of the flow[22;23]. However, the computational overhead that is usually the aftermath of learning a compact nonlinear manifold, and preserving computational efficiency in model reduction of non-polynomial nonlinear ROMs has slowed down these nonlinear manifolds in replacing the POD subspace with its powerful mathematical properties. Thus, post-ROM algorithms are designed in this study to compensate for the limitations of a linear subspace without interfering with the standard model reduction routine.

Lack of an energy-based inner product definition, evolution of ROMs that do not necessarily satisfy the energy equation, and as a result, the unbounded growth of numerical errors becomes a challenge in the POD-Galerkin ROMs of compressible flows. Stability is preserved through the error bounds provided by energy-conserving inner product definitions[8], as such one that is obtained by symmetrization of the governing equations in the Galerkin projection[24–27]. The need for rigorous error bounds is addressed through similar approaches in other model reduction techniques, for example via the least-squares residual minimization in the Petrov-Galerkin projection[10;28;29], or the balancing transformations in ROMs created based on the Balanced Proper Orthogonal Decomposition (BPOD), which is equivalent to

the POD-Galerkin projection when the observability Gramian is used as the inner product[9]. ROMs constructed through these channels, although more stable, they cannot survive the rather large errors that are generated as a result of the incomplete modal representation in nonlinear systems[14;27]. This study exhibits the broader impact of symmetrization on model reduction. It is shown in this work that symmetrization of ROMs in compressible flows enhances the controllable space of ROMs, and directly contributes to the robustness of stabilization.

Post-ROM treatment offers a non-intrusive approach for ROM stabilization once the original ROM is already built[14;30–34], thus provides an obvious advantage in its independence of different model order reduction techniques. The most trivial approach towards stabilization is to use numerical viscosity to attenuate the otherwise unbounded numerical errors. Lucia and Beran[31] used numerical dissipation, along with the Linear Quadratic Regulation (LQR) method to separately stabilize the low-, and high-frequency modes in the POD-Galerkin ROM based on the Euler equations. The ad-hoc nature of stabilization with numerical dissipation, and the risk of a high computation cost imposed by solving the Riccati equation in the LQR method in larger ROMs compromises the robustness of this approach. Closure modeling via eddy-viscosity models has been used in the POD-based ROMs as a stabilization and calibration method[19;35]. Despite the physics-based derivation of these models for incompressible flow ROMs that contain energy-conserving quadratic terms[36], it is challenging to preserve their robustness in compressible flows. Thus, such closure terms usually involve empirical choices of the structure and parameters that prevent generalization.

Optimization-based ROM stabilization methods are a more robust class of solutions for control and calibration of the low-dimensional systems. For the linear ROMs with time-invariant operators, Amsallem and Farhat[14] developed a stabilization method that implicitly modifies the left reduced-order basis of the ROM subject to the Lyapunov stability condition, where the right reduced-order basis is preserved to maintain accuracy. The stabilization algorithm is implemented as a convex optimization problem that ensures computational efficiency. However, since the optimization problem does not have direct access to the ROM outputs, there is a risk of over-modification of the bases through the stabilization of highly

unstable ROMs, that may lead to deviation of the dynamics from the FOM response[15;37]. This method was further evolved by Balajewicz et al.[33;38] for projection-based nonlinear ROMs of compressible and incompressible flows, where the system operators are modified by rotation of the subspace in a constrained optimization problem, thus these approaches also inherit the potential difficulties of the method of Amsallem and Farhat[14] in highly unstable systems, where stabilization with minimal modification or rotation of the bases is not possible, and a more aggressive alteration of the bases results in large deviations from the original dynamics[15].

In order to keep the ROM on the same attractor as the FOM, a natural objective is to minimize the deviation of the output of the two systems. This is achieved by transferring the eigenvalues of the linear ROM to the left half of the complex plain in a stabilization method developed by Kalashnikova et al.[30]. Direct monitoring of the ROM accuracy in this method is an advantage obtained at the cost of the additional computational effort for solving a nonlinear optimization problem that is not necessarily convex. Thus, the method can become intractable as the number of unstable modes increases. This has led to the advent of a new Hybrid stabilization method in this study, that integrates the computational efficiency of the method of Amsallem and Farhat[14] in its first step, with the accuracy of the method of Kalashnikova et al.[30] in a second step to directly monitor the accuracy of ROM through the stabilization of the most energetically-dominant modes[15]. Separate calibration of the low- and high-frequency components in the Hybrid method, reduces the computational burden on the method of Kalashnikova et al.[30], and prevents over-modification of the system through control, thus contributes to the robustness of the stabilization algorithm, especially in highly unstable ROMs with a large number of unstable modes.

When the nonlinear dynamical system evolves in close proximity to a fixed point, linearized ROMs are efficient alternatives, with a potential to accurately predict the dynamics of the HFM. There is also a lot of variability in the stabilization approaches that are developed for LTI systems. This is in contrast to the nonlinear ROMs that are both mathematically and computationally more challenging to process and post-process. Thus, when it comes to the stabilization of the nonlinear ROMs, one is left with only a few methods that are mainly

developed for a certain type of problems, and fail to respond to a more general category of applications. The presence of strongly nonlinear phenomena (e.g. turbulence, unsteady shock waves, chemical reactions, etc.), that compromise accuracy and even the viability of a linearized model, is a norm rather than exception in the fluid dynamics applications. Thus, there is a high demand for nonlinear ROM stabilization methods that can satisfy the requirements of a broader class of problems in this sector.

A new method is proposed in this study for the stabilization of nonlinear ROMs, that is initially inspired by the method of Kalshnokova et al.[30]. This approach uses eigenvalue reassignment in a nonlinear ROM, therefore named the ERN algorithm, to match the dynamical response of the nonlinear ROM with that of the FOM. To that end, the eigenvalues of the linear term in the nonlinear ROM are used as control parameters to drive the nonlinear system, while the deviation of the nonlinear ROM output from the FOM is directly monitored in the objective function, and a negative total power constraint guides the optimization to ensure the stability of ROM is recovered through the control. The negative total power constraint, although inspired by the conservation of the turbulent kinetic energy in fluid dynamics, is compatible with the notion of time-stability in generic nonlinear systems. Thus the proposed method can be easily extended for the stabilization of ROMs that originate in other fields of science and engineering.

Solving a constrained nonlinear optimization problem that is not necessarily convex, requires a global optimization solver, hence the cost of stabilization with the ERN algorithm grows nonlinearly with the number of unstable modes. Projection over the POD modes, and other linear subspaces is popular for its computational efficiency and mathematically rigorous implementation. This practical advantage however is tainted in strongly nonlinear systems that need a lot of base functions to capture the nonlinearity, while adding the typically less-accurate higher modes to the system further damages the stability of ROM. In the meantime, the control space of ROM becomes more complicated as the dimension of the optimization problem in the stabilization algorithm increases with the number of unstable modes, which makes it more challenging and even practically impossible at some point to capture the precise location of the global minimum point. Hence stabilization of the typically

larger ROMs of the strongly nonlinear systems, with the bare bone ERN algorithm, impairs the computational efficiency and accuracy of ROM, and may become intractable in the worst case. It is notable that the other optimization-based ROM stabilization methods that are discussed here are also prone to failure in such systems, either because of a nonlinear multi-modal objective function that makes it challenging to preserve accuracy and computational efficiency in higher dimensions, or due to the lack of a direct control of ROM accuracy that may result in aggressive modification of the system.

In order to address this challenge and expand the applications of the ERN algorithm, a multi-stage stabilization layout is proposed in this work, that breaks the problem of the stabilization of the target ROM into that of a few smaller ROMs, and uses the eigenvalues of the stabilized smaller ROMs at each stage to guide the higher-dimensional optimization problem of the larger ROMs, and accelerate convergence. This new layout has improved the computational efficiency and robustness of the ERN algorithm in the higher-dimensional ROMs of the strongly nonlinear systems.

Two supersonic flow applications serve as the probe to observe the performance of the proposed stabilization methods. The first case is the classic problem of the supersonic flow over a circular cylinder, which is further complicated by shock-vortex interactions that introduce unsteady shock oscillations and lead to highly unstable POD-Galerkin ROMs. The second case is the supersonic flow over a triangular prism, with strong shock-wake interactions and a similar destabilizing effect on the constructed ROMs. This application requires 60 POD modes to converge to the FOM energy. Using the bare bone ERN algorithm to stabilize the large number of unstable modes imposes a high computation cost. The proposed multi-stage configuration has enabled efficient implementation of the ERN algorithm, and allowed the global optimization solver to accurately capture the global minimum point, which is not otherwise possible with the complicated control landscape of the 60-dimensional ROM.

Despite ROMs constructed based on the common L^2 inner product, and the more promising symmetry inner product, are both unstable due to the presence of the strongly nonlinear shock-wake interactions in these applications, the influence of symmetrization on the controllable space of the ROMs and their overall robustness requires further attention. Control-

lability analysis of the linear ROMs via the controllability Gramian, and sensitivity analysis of the nonlinear ROMs in this work have revealed that the symmetry ROMs are not only more stable, but they are also more controllable and more robust, thus feasible to stabilize without sacrificing the accuracy.

The dissertation is outlined as follows: High-fidelity simulations of the Euler equations for the two supersonic flow applications that are used to test the performance of the proposed methods are briefly reviewed in chapter 2. The standard model reduction process through POD-Galerkin projection, and the form of the governing equations used for construction of the linear and nonlinear ROMs are discussed in chapter 3. Chapter 4 is dedicated to the Hybrid method that is developed for the stabilization of ROMs as LTI systems. The results of application of this method for the stabilization of the linear POD-Galerkin ROM of the supersonic flow over the circular cylinder are also discussed in this chapter. Nonlinear ROM stabilization, the ERN stabilization algorithm, and the results of the stabilization of the nonlinear POD-Galerkin ROM of the same application are addressed in chapter 5. In chapter 6, the discussion about the ERN algorithm is further expanded by introducing the multi-stage layout and comparing the performance of the vanilla ERN algorithm against the multi-stage approach in application to the nonlinear ROM of the supersonic flow over the triangular prism. At the end, in chapter 7 the influence of the inner product definition is unfolded. In particular, the impact of symmetrization on the stability, controllability, and robustness of the linear and nonlinear ROMs is discussed. The highlights of the proposed methods and their applications are summarized, followed by the final comments, and the future perspective of the research in chapter 8.

Chapter 2

High-Fidelity Simulations of the Euler Equations

The two-dimensional nonlinear Euler equations are solved by a fifth-order Weighted Essentially Non-Oscillatory (WENO) method, which advances in time with a third-order Total Variation Diminishing (TVD) Runge-Kutta scheme. The shock capturing method works in conjunction with a positive-preserving finite difference conservative scheme to avoid negative pressure[39;40] in presence of discontinuities. An immersed boundary method by Chaudhury et al.[1] is implemented with three layers of ghost points to define the solid boundary of a circular cylinder, and a triangular prism, in the supersonic flow applications of this study. Dirichlet (boundary condition) and outflow conditions are applied at the left and right boundaries of the domain respectively, along with reflective boundary condition at the top and bottom walls. The high-fidelity numerical algorithm used in this study has been extensively benchmarked in previous work[39;40] including validations against an exact solution for supersonic flow over a wedge and established numerical solutions[41;42] for shock reflections and interactions of a flow passing a forward facing step.

2.1 Governing Equations of the Full-Order Model

The WENO scheme solves the conservation form of the nonlinear Euler equations:

$$\frac{\partial \boldsymbol{U}}{\partial t} + \frac{\partial \boldsymbol{F}(\boldsymbol{U})}{\partial x} + \frac{\partial \boldsymbol{G}(\boldsymbol{U})}{\partial y} = 0, \tag{2.1}$$

where,

$$\boldsymbol{U} = \begin{pmatrix} \rho \\ \rho u \\ \rho v \\ E \end{pmatrix}, \boldsymbol{F}(\boldsymbol{U}) = \begin{pmatrix} \rho u \\ \rho u^2 + P \\ \rho uv \\ u(E+p) \end{pmatrix}, \boldsymbol{G}(\boldsymbol{U}) = \begin{pmatrix} \rho v \\ \rho uv \\ \rho v^2 + p \\ v(E+p) \end{pmatrix},$$

and ρ, u, v, p, and E are respectively the density, horizontal, and vertical components of velocity, pressure, and total energy (including internal energy and kinetic energy). The system of equations is closed with the ideal gas equation of state:

$$p = (\gamma - 1)[E - \frac{\rho(u^2 + v^2)}{2}], \tag{2.2}$$

where $\gamma = 1.4$ is the ratio of specific heats, which corresponds to air at standard conditions. These equations are solved assuming an impermeable adiabatic condition on the solid boundaries.

2.2 Supersonic Flow over a Circular Cylinder

Numerical data of snapshots are generated for a Mach 2.8 flow passing a fixed cylinder in a two-dimensional channel with solid walls at the top and bottom. After $146,700$ time steps, with step size $dt = 5 \times 10^{-4}$ (non-dimensionalized by the incoming flow speed and the diameter of the cylinder), of transition from the beginning of simulations for the flow to reach steady state, a total of 101 snapshots are then collected every 20 time steps over a grid of 601×401 points with $dx = dy = 0.02$ (non-dimensionalized by the diameter of the

cylinder). As shown in Figure 2.1, a standing bow shock is formed in front of the cylinder, and the reflected shock waves from the channel walls exhibit strong interactions with the

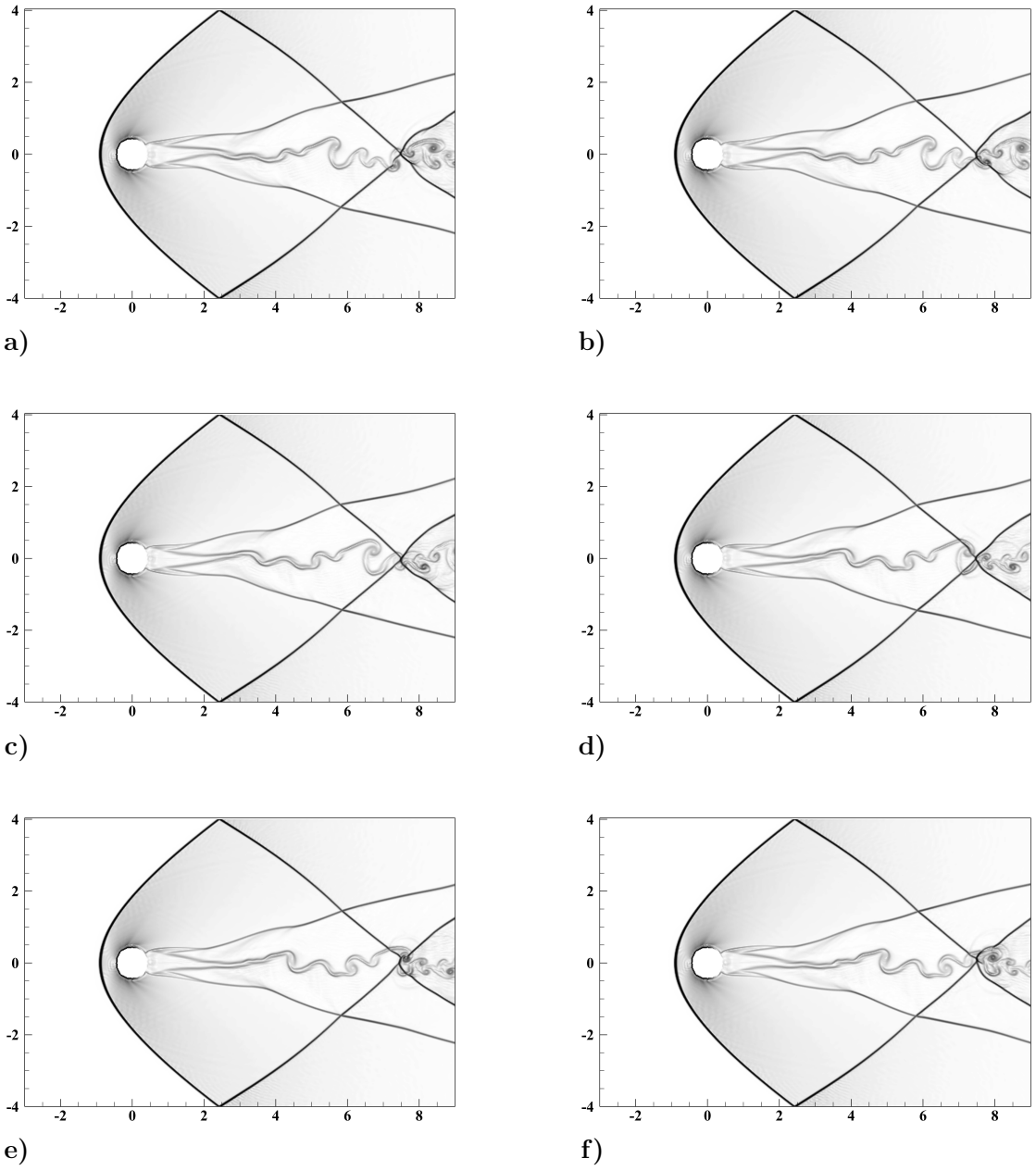

Figure 2.1: Numerical Schlieren of evenly spaced snapshots collected from the numerical simulation of a supersonic flow passing a circular cylinder.

wake structure after the cylinder. The discontinuity of shock waves and the strong shock-wake interactions all contribute to the challenge for an accurate numerical simulation and

more important to the numerical instability of a ROM built from the simulation data.

2.3 Supersonic Flow over a Triangular Prism

The two-dimensional Euler equations are solved in a 2000×500 grid with $dx = dy = 5.45 \times 10^{-3}$ (non-dimensionalized with respect to the height of the triangle) in this case, to simulate the Mach 3.5 flow over a triangular prism depicted in the snapshot in Figure 2.2. The incident

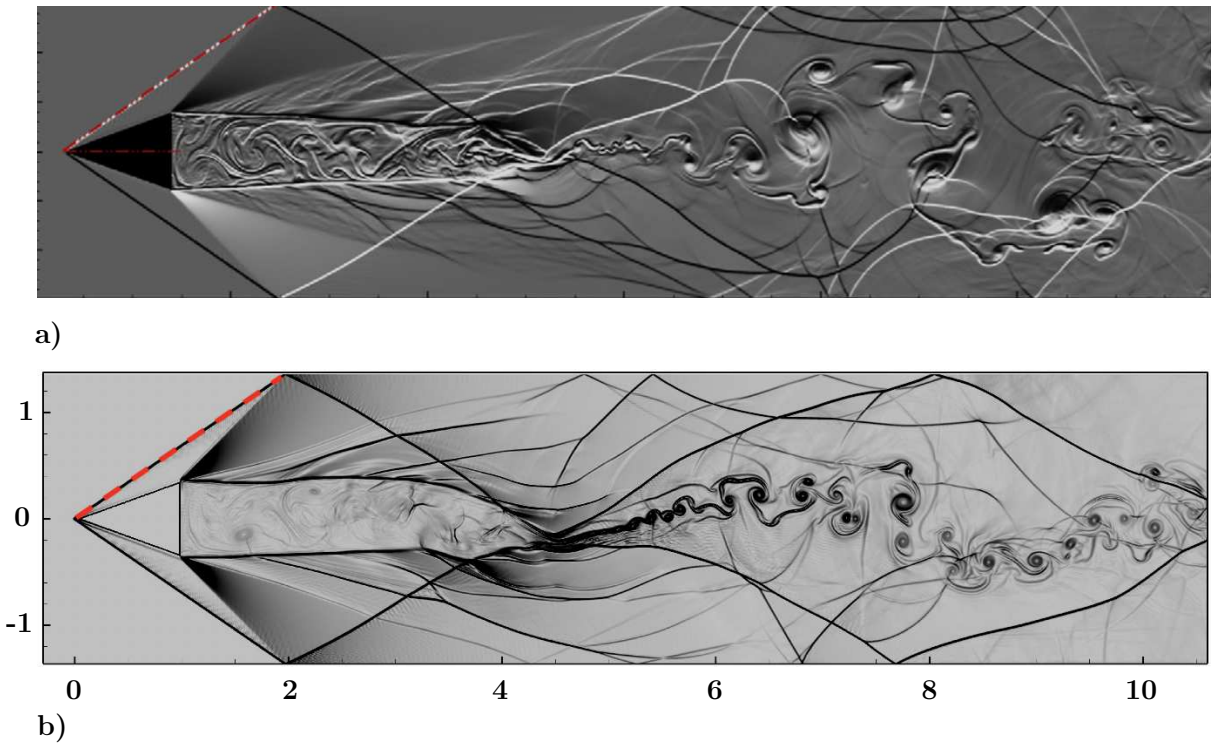

Figure 2.2: a) Numerical Schlieren of a typical snapshot shown in Chaudhuri et al.[1]. The red dash-dotted line shows the theoretical shock angle. b) Numerical Schlieren of a different snapshot computed with our WENO code. The red dashed line shows the incident shock angle in the numerical simulation of Chaudhuri et al.[1].

shock angle captured by the WENO scheme agrees well with the numerical simulation of Chaudhuri et al.[1], that is validated against the theoretical result. The theoretical shock angle β shown in this figure is computed by:

$$tan\theta = 2cot\beta \left[\frac{Ma^2 sin^2\beta - 1}{Ma^2(\gamma + cos2\beta) + 2} \right], \tag{2.3}$$

where Ma is the Mach number, and $\theta = 20^\circ$ is the deflection angle[1].

In order to compute the POD modes in this case, 550 snapshots are collected every 20 time steps, when the flow reaches steady state conditions after $200,000$ time steps with $dt = 2.05 \times 10^{-4}$ (non-dimensionalized with respect to the incoming flow velocity and height

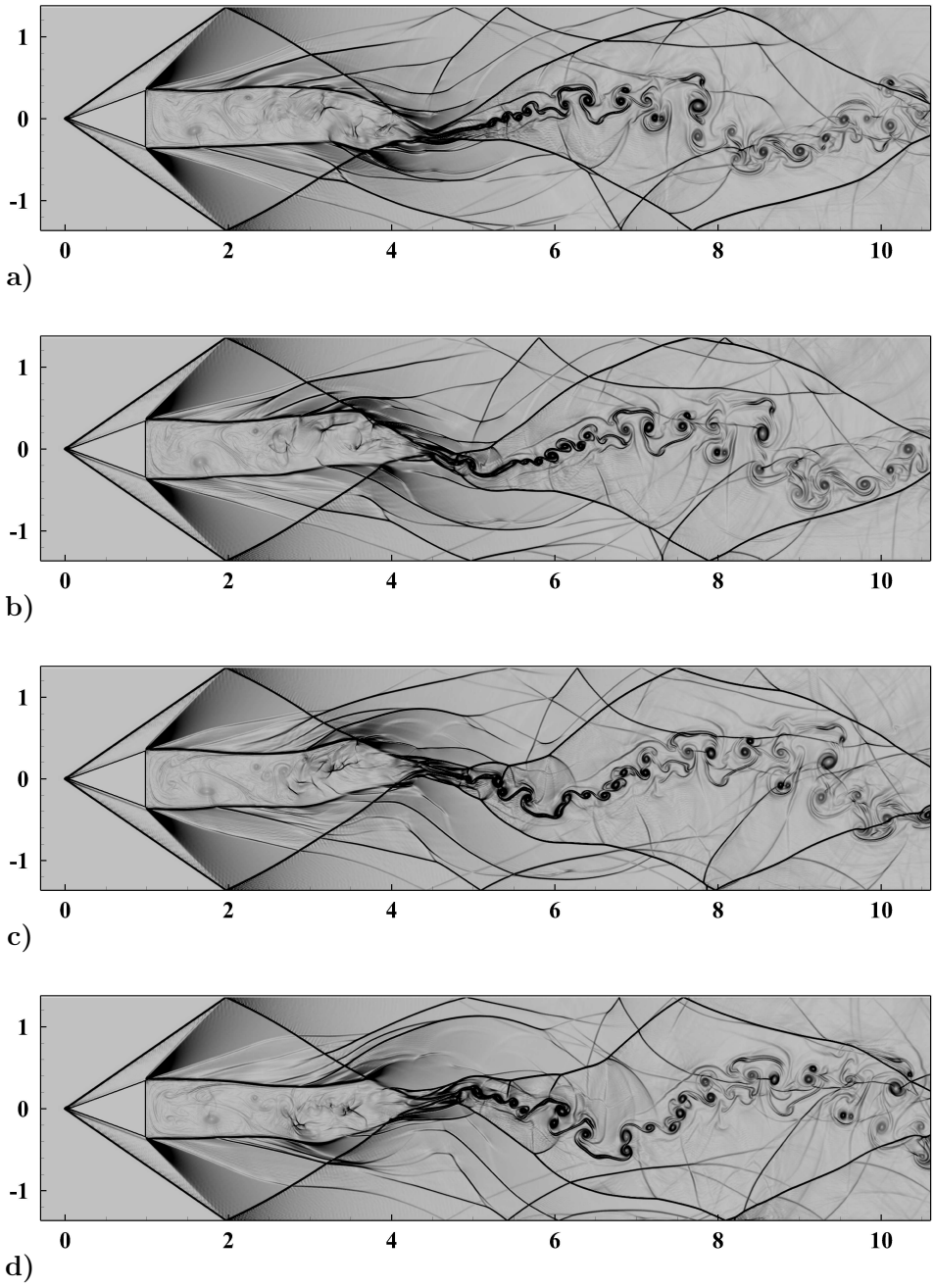

Figure 2.3: Numerical Schlieren of evenly spaced snapshots collected from the numerical simulation of a supersonic flow passing a triangular prism.

of the triangle). Dirichlet and outflow conditions are implemented at the left and right boundaries, and reflective conditions are used at the upper and lower walls. Figure 2.3 shows numerical Schlieren of typical evenly spaced snapshots. The shock-wake interactions in this flow field also trigger large instabilities in the POD-Galerkin ROMs.

Chapter 3

Reduced-Order Modeling by POD-Galerkin Projection

Model order reduction techniques, such as POD-Galerkin projection approach, provide a systematic and mathematically rigorous manner to develop ROMs. By forming a set of optimal bases suitable for the problem, and projecting the dynamics inherent from the governing equations onto a lower-dimensional space defined by these base functions, the constructed ROM is expected to capture the basic dynamics of interest, such as large coherent flow structures[12], at the cost of losing some resolution in less-appealing components. Thus, dimensionality reduction that serves as the foundation for the projection-based reduced-order modeling has branched into various methods, such as Proper Orthogonal Decomposition (POD)[12], reduced-basis method[43], balanced truncation[44], approximate balanced truncation or balanced POD[9], and Dynamic Mode Decomposition (DMD)[45] to name a few. Proper Orthogonal Decomposition (POD) as a popular choice for base functions is attractive due to the optimality in energy capture when high-order modes are truncated to reduce the degrees of freedom for computation[4;5;11–13;15;24;26;46–48]. In other words, the subspace defined by POD modes captures the most energy compared to any other linear subspace with the same dimension. Galerkin projection provides a straightforward manner to represent the governing equations (e.g. Euler equations in the current study) in a low-dimensional space

defined by chosen bases. This section includes basic formulation of model order reduction on Euler equations.

3.1 Governing Equations of the Nonlinear ROM

The specific volume form of the nonlinear Euler equations are used to construct the reduced-order models:

$$\frac{\partial \boldsymbol{q}}{\partial t} = -\boldsymbol{F}_1 \frac{\partial \boldsymbol{q}}{\partial x} - \boldsymbol{F}_2 \frac{\partial \boldsymbol{q}}{\partial y}, \tag{3.1}$$

where,

$$\boldsymbol{q} = \begin{pmatrix} u \\ v \\ p \\ \varsigma \end{pmatrix}, \boldsymbol{F}_1 = \begin{pmatrix} u & 0 & \varsigma & 0 \\ 0 & u & 0 & 0 \\ \gamma p & 0 & u & 0 \\ -\varsigma & 0 & 0 & u \end{pmatrix}, \boldsymbol{F}_2 = \begin{pmatrix} v & 0 & 0 & 0 \\ 0 & v & \varsigma & 0 \\ 0 & \gamma p & v & 0 \\ 0 & -\varsigma & 0 & v \end{pmatrix}.$$

$\gamma = 1.4$ is the ratio of specific heats, and u, v, p, and ς are the horizontal and vertical components of velocity, pressure, and specific volume, respectively. Using specific volume instead of the density in the nonlinear Euler equations generates a ROM with quadratic nonlinearities after projection, for which the operators can be precomputed in an offline manner, thus facilitates bypassing hyper-reduction techniques. The specific volume form of the Euler equations is a simple example of a lifted nonlinear model. A systematic framework has been developed in the literature for efficient model reduction of general nonlinear systems via the lifting transformations[49;50]. This is particularly important as directly handling the nonlinear ROMs in non-polynomial form can easily multiply the cost of stabilization up to an infeasible point.

3.2 Governing Equations of the Linear ROM

The nonuniform flow field $\boldsymbol{q}(\boldsymbol{x}, t)$ is averaged over time to obtain a steady base flow $\bar{\boldsymbol{q}}(\boldsymbol{x})$ for linearization. Knowing that $\boldsymbol{q}(\boldsymbol{x}, t) = \bar{\boldsymbol{q}}(\boldsymbol{x}) + \boldsymbol{q}'(\boldsymbol{x}, t)$, Euler equations are then linearized

about the mean flow before projection on to the base functions[24;37]:

$$\frac{\partial \boldsymbol{q}'}{\partial t} = -\boldsymbol{B}_1 \frac{\partial \boldsymbol{q}'}{\partial x} - \boldsymbol{B}_2 \frac{\partial \boldsymbol{q}'}{\partial y} - \boldsymbol{B}_3 \boldsymbol{q}', \tag{3.2}$$

where,

$$\boldsymbol{B}_1 = \begin{pmatrix} \bar{u} & 0 & \bar{\varsigma} & 0 \\ 0 & \bar{u} & 0 & 0 \\ \gamma\bar{p} & 0 & \bar{u} & 0 \\ -\bar{\varsigma} & 0 & 0 & \bar{u} \end{pmatrix}, \boldsymbol{B}_2 = \begin{pmatrix} \bar{v} & 0 & 0 & 0 \\ 0 & \bar{v} & \bar{\varsigma} & 0 \\ 0 & \gamma\bar{p} & \bar{v} & 0 \\ 0 & -\bar{\varsigma} & 0 & \bar{v} \end{pmatrix},$$

$$\boldsymbol{B}_3 = \begin{pmatrix} \frac{\partial \bar{u}}{\partial x} & \frac{\partial \bar{u}}{\partial y} & 0 & \frac{\partial \bar{p}}{\partial x} \\ \frac{\partial \bar{v}}{\partial x} & \frac{\partial \bar{v}}{\partial y} & 0 & \frac{\partial \bar{p}}{\partial y} \\ \frac{\partial \bar{p}}{\partial x} & \frac{\partial \bar{p}}{\partial y} & \gamma\nabla\cdot\bar{u} & 0 \\ \frac{\partial \bar{\varsigma}}{\partial x} & \frac{\partial \bar{\varsigma}}{\partial y} & 0 & -\nabla\cdot\bar{u} \end{pmatrix},$$

3.3 Proper Orthogonal Decomposition (POD)

Proper Orthogonal Decomposition (POD), also known as Karhunen Loéve Transform, or Principal Component Analysis (PCA), is an empirical, linear dimensionality reduction method to obtain the trial bases that optimally span the space of the high-fidelity snapshots:

$$\boldsymbol{q}'(\boldsymbol{x}, t) = \sum_{i=1}^{M} \boldsymbol{a}_i(t)\boldsymbol{\phi}_i(\boldsymbol{x}), \tag{3.3}$$

where $\boldsymbol{q}'$ is the state perturbation. In the modal expansion (3.3), M is the number of POD modes retained after truncation, $\boldsymbol{\phi}_i$ is the i^{th} base function (i.e. mode), and $\boldsymbol{a}_i$ is the i^{th} modal coefficient. These coefficients are obtained by projection of the FOM state onto the POD subspace, and typically serve as a reference for validation of the ROM solution.

Optimality is defined here in the sense of an energy-based inner product definition. Thus, the POD modes are obtained by solving the optimization problem that maximizes the average energy in projection of the high-fidelity snapshots $\boldsymbol{q}'(\boldsymbol{x},t)$ onto the POD subspace $\boldsymbol{\phi}(\boldsymbol{x})$:

$$max_{\phi\in\mathscr{H}(\Omega)}\frac{(\langle\boldsymbol{q}',\boldsymbol{\phi}\rangle^2)}{\|\boldsymbol{\phi}\|^2}, \tag{3.4}$$

subject to $\|\boldsymbol{\phi}\| = 1$. Where, $\|.\|$ is the inner product norm, $(.)$ is the time or ensemble average, $\boldsymbol{x} \in \Omega$, and $\mathscr{H}$ is the Hilbert space that contains the solution snapshots, and is associated with the inner product $\langle.,.\rangle$. This optimization problem is identically represented by an eigenvalue problem on the operator $\mathscr{R} = (\boldsymbol{q}' \otimes \boldsymbol{q}'^*)$:

$$\mathscr{R}\boldsymbol{\phi} = \sigma\boldsymbol{\phi}, \tag{3.5}$$

that scales with the dimension N of the high-fidelity snapshots, where $\boldsymbol{q}'^* \in \mathscr{H}^*$ is the dual of $\boldsymbol{q}'$. Thus, in order to make this eigenvalue problem tractable, when the number of snapshots K is smaller than the number of grid points N, the method of snapshots by Sirovich[13] is employed by solving the eigenvalue problem:

$$\boldsymbol{W}\boldsymbol{\zeta} = \sigma\boldsymbol{\zeta}, \tag{3.6}$$

where $\boldsymbol{W}_{ij} = \langle\boldsymbol{q}'_j,\boldsymbol{q}'_i\rangle$ is the $K \times K$ correlation matrix of the snapshots. The eigenvalues σ represent the average projection energy, and are arranged in descending order. Thus, truncation of the eigenvectors corresponding to the eigenvalues with $\sum_{i=M+1}^{K}\sigma_i \ll \sum_{i=1}^{K}\sigma_i$ yields a low-dimensional space that represents most of the flow energy. The POD modes are then computed:

$$\boldsymbol{\phi} = \sum_{i=1}^{K}\boldsymbol{\zeta}_i\boldsymbol{q}'_i. \tag{3.7}$$

The average ensemble energy captured by the first M POD modes is higher than any other linear subspace. Despite the optimality of the POD subspace in the sense of the average energy, naive truncation of the high-frequency modal information may result in the loss of

important dynamical signatures in advection-dominated flows, especially when the HFM is based on the Euler equations that are the extreme form of such cases[22;51]. As a result, construction of ROMs over the POD subspace with insufficient resolution of the nonlinearities compromises the stability of the low-dimensional system.

3.4 Galerkin Projection

Let $\boldsymbol{R}$ be the residual of the discretized system of the governing PDEs (in this case, the nonlinear Euler equations):

$$\boldsymbol{R} = \frac{\partial \boldsymbol{q}'}{\partial t} + \boldsymbol{F}_1 \frac{\partial \boldsymbol{q}'}{\partial x} + \boldsymbol{F}_2 \frac{\partial \boldsymbol{q}'}{\partial y}. \tag{3.8}$$

Substituting the POD expansion (3.3) in Equation (3.8) results in a rectangular residual matrix that represents the over-determined system of equations. Enforcing the residual $\boldsymbol{R}$ to be orthogonal to the test subspace $\boldsymbol{\psi}$:

$$\langle \boldsymbol{R}, \boldsymbol{\psi}(x, y) \rangle = 0, \tag{3.9}$$

yields an $M \times M$ system of equations. Where, $\boldsymbol{\psi}^T \boldsymbol{\phi} = \boldsymbol{I}$, and $\boldsymbol{I}$ is the identity matrix. The system of equations (3.9) is in general solved in an optimization problem to find the test subspace that minimizes the residual through the Petrov-Galerkin method. In the special occasion where the test and trial subspaces are identical (i.e. $\boldsymbol{\psi} = \boldsymbol{\phi}$), this procedure is called Galerkin projection. Thus, Galerkin projection of the nonlinear Euler equations over the POD subspace constructs the M-dimensional ROM ODEs:

$$\dot{\boldsymbol{a}}_i = C_i + \sum_{j=1}^{M} L_{ij} \boldsymbol{a}_j + \sum_{j,k=1}^{M} Q_{ijk} \boldsymbol{a}_j \boldsymbol{a}_k, \qquad i = 1, \ldots, M. \tag{3.10}$$

The specific volume form of the Euler equations gives rise to the nonlinear ROM ODEs in constant-linear-quadratic form, where matrix $\boldsymbol{L}$, and tensor $\boldsymbol{Q}$ are efficiently precomputed offline with zero computational overhead in the online stage of the model reduction.

Similarly, for the linearized Euler equations:

$$\boldsymbol{R} = \frac{\partial \boldsymbol{q}'}{\partial t} + \boldsymbol{B}_1 \frac{\partial \boldsymbol{q}'}{\partial x} + \boldsymbol{B}_2 \frac{\partial \boldsymbol{q}'}{\partial y} + \boldsymbol{B}_3 \boldsymbol{q}', \tag{3.11}$$

and following the same procedure yields the linear ROM ODEs:

$$\dot{\boldsymbol{a}}_i = C_i + \sum_{j=1}^{M} L_{ij} \boldsymbol{a}_j, \qquad i = 1, \ldots, M. \tag{3.12}$$

Equations (3.10), and (3.12) are solved by a time-advancement method, for instance the fourth-order Runge-Kutta scheme used in this study.

3.5 Choice of Inner Product

Inner product maps the Hilbert space containing flow field solutions to a metric space. The inner product definition that is used to identify the low-dimensional space and project the governing equations onto the subspace directly affects the numerical properties of projection-based ROMs. Energy-based norms provide error bounds that facilitate preserving the stability of high-fidelity simulations through model reduction. This advantage is naturally obtained in the model reduction of incompressible flows via the common L^2 inner product[12;52;53]. A direct generalization of L2 inner product for compressible flows is:

$$\langle \boldsymbol{q}_1', \boldsymbol{q}_2' \rangle = \int_\Omega (u_1' u_2' + v_1' v_2' + \beta p_1' p_2' + \beta \varsigma_1' \varsigma_2') d\Omega, \tag{3.13}$$

where $\beta = 1$ is a weighting coefficient. Since the conventional definition of L^2 does not satisfy energy conservation as compressibility effects prevail, compressible flows impose an additional challenge for defining a physically meaningful inner product that delivers similar stability guarantees through model reduction. Rowley[8;46] suggested physics-based inner product definitions for compressible flows with application to the isentropic Navier-Stokes equations. The most predominant effort in deriving a suitable inner product for compressible

flows is perhaps conducted by Barone et al.[24]. Inspired by the semibounded operators in the symmetrized equations, they derived a symmetry inner product for the linearized Euler equations, and showed that the Galerkin projection with this inner product guarantees stability bounds for ROMs constructed over the same governing equations.

Linear and nonlinear ROMs of this study are separately constructed by both L^2, and symmetry inner products. It is shown in chapter 7 that compressible flow ROMs based on the symmetry inner product are more stable, robust, and controllable compared to those based on the L^2 norm[27].

Although the nonlinear Euler equations are also symmetrizable, the corresponding symmetry inner product contains higher-order perturbation terms that multiply the computation cost of model reduction[60], thus similar to the linear ROMs, the nonlinear POD-Galerkin ROMs of this work are also constructed by the symmetry inner product of the linearized Euler equations:

$$\langle \boldsymbol{q}_1', \boldsymbol{q}_2' \rangle_{\boldsymbol{H}} = \int_\Omega [\bar{\rho}(u_1' u_2' + v_1' v_2') + \frac{1+\alpha^2}{\gamma \bar{p}} p_1' p_2' + \alpha^2 \gamma \bar{\rho}^2 \bar{p} \varsigma_1' \varsigma_2' + \alpha^2 \bar{\rho}(\varsigma_2' p_1' + \varsigma_1' p_2')] d\Omega, \tag{3.14}$$

where H is the symmetric positive definite matrix that symmetrizes the linearized Euler equations:

$$\boldsymbol{H} = \begin{pmatrix} \bar{\rho} & 0 & 0 & 0 \\ 0 & \bar{\rho} & 0 & 0 \\ 0 & 0 & \frac{1+\alpha^2}{\gamma \bar{p}} & \bar{\rho}\alpha^2 \\ 0 & 0 & \bar{\rho}\alpha^2 & \alpha^2 \gamma \bar{\rho}^2 \bar{p} \end{pmatrix}, \tag{3.15}$$

and $\alpha = \sqrt{2}$ is a real nonzero parameter. Tabandeh et al.[26] showed that when the symmetry inner product is used for projection of the linearized Euler equations, the dynamics matrix of the linear ROM in Equation (3.12) is composed of two matrices:

$$L_{ij} = -L_{ji} + b_{ij}, \tag{3.16}$$

where, L_{ji} is a skew-symmetric matrix with purely imaginary eigenvalues, and matrix b_{ij} is

identified by the boundary conditions. Thus, as a result of the anti-symmetry of matrix L_{ji}, when the boundary conditions generate a matrix b_{ij} with eigenvalues that are close to the imaginary axis in the complex plane, eigenvalues of the linear dynamics matrix L_{ij} will also be close to the imaginary axis. This property, that has been observed in several applications of the symmetry ROMs in the literature[15;24;26;27], carries significant computational benefits through stabilization and calibration of the ROMs.

The nonlinear ROMs created based on the symmetry inner product of the linearized Euler equations do not necessarily follow the error bounds obtained by Barone et al.[24], though they have shown notable improvements over the L^2 definition in terms of stability and robustness[27].

Chapter 4

Stabilization of ROMs as Linear Time-Invariant Systems

4.1 Motivation and Overview

ROMs developed by POD-Galerkin projection suffer from different instabilities in many cases[30;54;55]. Barone et al.[24] pointed out that ROM instability may come from the lack of an energy conserving definition for the inner product used in both the POD computation and the Galerkin projection, and they suggested to use a symmetry inner product which leads to a ROM in the form of a symmetric operator being applied to primary variables. Similarly, using a least-squares Petrov-Galerkin projection method instead of Galerkin projection with the L^2 inner product, theoretically provides a more stable backbone for model reduction of nonlinear equations, by minimizing the residual in projection of the governing equations[28;56]. Galerkin projection with the commonly used L^2 inner product is optimal (in minimizing the residual) when the Jacobians of the system are symmetric positive definite, which is not generally satisfied in nonlinear problems. Unfortunately, when the flow is highly inviscid and further complicated by discontinuity and unsteady perturbations, merely changing the inner product is not sufficient to stabilize a ROM. Numerical errors are inevitably generated and often amplified quickly when an aggressive truncation of high-order modes happens

without an appropriate closure model and the system itself lacks intrinsic dissipation.

The computational and theoretical simplifications offered by linearization make linear ROMs attractive in model reduction of originally nonlinear dynamical systems. To develop a general approach to stabilize ROMs as a typical linear system, Amsallem and Farhat[14] proposed an Implicit Subspace Correction (ISC) method to manipulate linearly the system dynamics matrices of a larger ROM to obtain a stable but smaller ROM by solving a convex optimization problem based on the Lyapunov stability condition. The ISC method is efficient in the stabilization of ROMs especially when the number of modes is large, while the accuracy is partly maintained by preserving the right Reduced-Order Basis (ROB). However, its accuracy is lower than other approaches that involve an explicit control of ROM accuracy in cost functions. Focusing on the accuracy, Kalashnikova et al.[30] suggested an eigenvalue reassignment (ER) method to reconfigure positive system eigenvalues to negative ones while solving an optimization problem to minimize the deviation of the ROM outputs from the outputs of the original Full-Order Model (FOM). Though the accuracy is controlled by the optimization process, the cost increases quickly when more modes are included in the ER process, and the more complicated control space of a larger ROM may eventually fail the optimization process facing the difficulty to achieve convergence .

The new Hybrid method developed here aims to take the strengths of both the ISC method[14] and the ER method[30]. Since the ISC method, though being efficient and robust, tends to excessively alter low-frequency (originally more unstable) modes and reduce the overall accuracy, the Hybrid approach takes two steps: first, uses the ISC method to stabilize all modes in an efficient manner; then, applies the ER method to fine tune the eigenvalues of a small group of low-frequency modes with a cost function defined to directly control the accuracy of the overall system outputs. With the ER method being applied at the end to handle a small number of modes despite the total number of modes used in the ROM, the Hybrid method maintains low cost and robustness (of ISC) and gets an explicit control of accuracy (via ER) independent of the ROM size. Furthermore, when a symmetry inner product[24;26;27] is implemented in the computation of POD modes and in the Galerkin projection, the ROM based on this inner product shows clear improvement of stability in

its comparison to the one based on a conventional L^2 inner product. Not to our surprise, a relatively more stable original ROM using symmetry inner product leads to a more accurate ROM at the end after stabilization. Thus, it becomes natural to adopt the original ISC and ER as well as the new Hybrid approaches to apply on a symmetry ROM to reach the ROM's full potential in terms of stability and accuracy.

Without physical dissipation, a ROM of an inviscid compressible flow is fundamentally more vulnerable to instability, and therefore an inviscid ROM is a more suitable and challenging subject for the study of ROM stabilization[14;31;37]. The low-dimensional space is here constructed by Proper Orthogonal Decomposition (POD) with snapshots from the high-fidelity simulation of the supersonic flow passing a fixed cylinder, and then Galerkin projection casts the dynamics of the flow field onto a subspace of POD modes. Though the high-fidelity snapshots are computed by a numerically stable algorithm, the highly unstable physics from the interaction of shock waves and unsteady vortex shedding often triggers numerical instability in the projected ROM that is not intrinsically formulated to keep the same stability characteristics as the original high-fidelity model. For the sake of completeness, and a smooth introduction to the new Hybrid method, the approaches introduced respectively by Amsallem and Farhat[14] and Kalashnikova et al.[30] are briefly reviewed here before the Hybrid method is proposed.

4.2 Implicit Subspace Correction (ISC)

In this method, Amsallem and Farhat[14] suggested a minimal modification of the left ROB to enhance model stability. To provide an adequate search space, a larger ROM of dimension $M + r$ is initially constructed to generate a stable ROM of a slightly smaller dimension M. The dynamics of the smaller ROM is built in a convex optimization problem that ensures the stability of the modified bases by satisfying a Lyapunov equation. The method is demonstrated for a Linear Time-Invariant (LTI) system as:

$$\boldsymbol{E}\frac{d\boldsymbol{x}}{dt}(t) = \boldsymbol{A}\boldsymbol{x}(t) + \boldsymbol{B}\boldsymbol{u}(t), \tag{4.1}$$

$$\boldsymbol{y}(t) = \boldsymbol{C}\boldsymbol{x}(t),$$

where $\boldsymbol{x} \in \boldsymbol{R}^N$ is the vector of states, $\boldsymbol{u} \in \boldsymbol{R}^S$ is the control input, and $\boldsymbol{y} \in \boldsymbol{R}^G$ is the system output. $\boldsymbol{E} \in \boldsymbol{R}^{N\times N}$, $\boldsymbol{A} \in \boldsymbol{R}^{N\times N}$, $\boldsymbol{B} \in \boldsymbol{R}^{N\times S}$ and $\boldsymbol{C} \in \boldsymbol{R}^{G\times N}$ are full-order matrices that are constant in time. $\boldsymbol{E}$ is the identity matrix due to the non-descriptor form of the equations in this case, and $\boldsymbol{u}$ is zero.

Following the Lyapunov stability condition, the equilibrium point $\boldsymbol{x}_0$ of the system in (4.1) is asymptotically stable with stability margin μ if and only if there exists a Symmetric Positive Definite (SPD) matrix $\boldsymbol{P}$ that satisfies:

$$\boldsymbol{E}^T\boldsymbol{P}(\boldsymbol{A} + \mu\boldsymbol{E}) + (\boldsymbol{A} + \mu\boldsymbol{E})^T\boldsymbol{P}\boldsymbol{E} = -\boldsymbol{Q}, \tag{4.2}$$

for any SPD matrix $\boldsymbol{Q}$. Arranging ROM ODEs in the form of the reduced-order LTI system we have:

$$\boldsymbol{E}_M\frac{d\boldsymbol{x}_M}{dt}(t) = \boldsymbol{A}_M\boldsymbol{x}_M(t) + \boldsymbol{B}_M\boldsymbol{u}(t), \tag{4.3}$$

$$\boldsymbol{y}_M(t) = \boldsymbol{C}_M\boldsymbol{x}_M(t),$$

where $\boldsymbol{x}_M \in \boldsymbol{R}^M$ is the solution to the ROM, and $\boldsymbol{y}_M \in \boldsymbol{R}^G$ is the reconstructed flow output using ROM coefficients. Similarly, $\boldsymbol{E}_M = \boldsymbol{\Phi}_M^T\boldsymbol{E}\boldsymbol{\Phi}_M \in R^{M\times M}$, $\boldsymbol{A}_M = \boldsymbol{\Phi}_M^T\boldsymbol{A}\boldsymbol{\Phi}_M \in R^{M\times M}$, $\boldsymbol{B}_M = \boldsymbol{\Phi}_M^T\boldsymbol{B} \in R^{M\times S}$ and $\boldsymbol{C}_M = \boldsymbol{C}\boldsymbol{\Phi}_M \in R^{G\times M}$ are constant matrices.

Derivations are expressed in terms of the left and right ROBs, that are the same in Galerkin projection. However, the method is directly applied to the ROM ODEs rather than the base functions, and is therefore independent of the projection method. The idea is to look for the left ROB of a target stable ROM of dimension M in the range of the bases at the dimension of $M + r$, keeping the right ROB unchanged to maintain accuracy. Assuming that $\tilde{\boldsymbol{\Phi}}_M$ is the ROB of dimension M that is being searched for in the range of the ROB of a larger ROM of dimension $M + r$, namely $\boldsymbol{\Phi}_{M+r}$, thus $\tilde{\boldsymbol{\Phi}}_M$ can be expressed in terms of a matrix $\boldsymbol{X} \in \boldsymbol{R}^{(M+r)\times M}$ of rank M, which identifies the combination towards $\tilde{\boldsymbol{\Phi}}_M$:

$$\tilde{\boldsymbol{\Phi}}_M = \boldsymbol{\Phi}_{M+r}\boldsymbol{X}. \tag{4.4}$$

Since by stabilization of the ROM ODEs we are altering the projected dynamics of the governing equations, minimum deviation of the stabilized basis from the original basis (i.e. $\left\|\tilde{\boldsymbol{\Phi}}_M - \boldsymbol{\Phi}_M\right\|$) will serve as the objective function to prevent a substantial change in the system through optimization.

In order to make the optimization problem amenable to semidefinite programming, it is expressed in terms of a SPD matrix $\hat{\boldsymbol{P}} \in \boldsymbol{R}^{(M+r)\times(M+r)}$ that satisfies the Lyapunov equation:

$$min_{\hat{\boldsymbol{P}}\in R^{(M+r)\times(M+r)}} \left\| \begin{pmatrix} \hat{\boldsymbol{P}}_{12}^T & \hat{\boldsymbol{P}}_{22} \end{pmatrix} \right\|_F + \tau \left\| \hat{\boldsymbol{P}}_{11} \right\|_F \tag{4.5}$$

$$\text{s.t.} \quad \boldsymbol{M}_E^T \hat{\boldsymbol{P}} \boldsymbol{M}_A + \boldsymbol{M}_A^T \hat{\boldsymbol{P}} \boldsymbol{M}_E = -\boldsymbol{Q},$$

$$\hat{\boldsymbol{P}} > \boldsymbol{0}_{(M+r)\times(M+r)},$$

where τ is a regularization parameter and F represents Ferobenius norm. The equality constraint in this equation is the Lyapunov stability condition that is rearranged for the system in (4.3) by expanding E_M and A_M in terms of the base functions, substituting the modified left ROB as in Equation (4.4), and defining $\boldsymbol{M}_E = \boldsymbol{\Phi}_{M+r}^T \boldsymbol{E} \boldsymbol{\Phi}_M$ and $\boldsymbol{M}_A = \boldsymbol{\Phi}_{M+r}^T (\boldsymbol{A} + \mu \boldsymbol{E}) \boldsymbol{\Phi}_M$. This minimization problem thus guarantees: a) asymptotic stability of the reduced order LTI system, b) preserving the originally stable eigendirections of the system, and c) computational cost in the order of the reduced dimension. For a feasible solution to the convex problem in (4.5), matrix $\boldsymbol{X}$ is then computed knowing $\hat{\boldsymbol{P}}$ minors:

$$\boldsymbol{X} = \begin{pmatrix} \hat{\boldsymbol{P}}_{11} \\ \hat{\boldsymbol{P}}_{12}^T \end{pmatrix}. \tag{4.6}$$

At the end, the LTI system matrices are modified to stabilize the ROM:

$$\tilde{\boldsymbol{E}}_M = \boldsymbol{X}^T \boldsymbol{M}_E, \tilde{\boldsymbol{A}}_M = \boldsymbol{X}^T (\boldsymbol{M}_A - \mu \boldsymbol{M}_E), \tilde{\boldsymbol{B}}_M = \boldsymbol{X}^T \boldsymbol{B}_{M+r}, \tilde{\boldsymbol{C}}_M = \boldsymbol{C}_{M+r}. \tag{4.7}$$

The solution of the optimization problem is computed in MATLAB by the CVX package. Provided that the optimization solver cannot reach a stable solution in the range of the larger

ROM, one may change parameter r either by altering dimension M of the target ROM or expanding the size of the ROM of dimension $M+r$, and revisit the original system identities if necessary.

Since the Galerkin system in the current study exhibits strong instability in presence of unsteady shock interactions, the modification of the system matrix to reach a stable solution may be large enough to reduce ROM accuracy in a noticeable manner or even change the dynamics of the system. It is expected that the approach may benefit from another optimization process to regulate the accuracy of ROM output and prevent deviation from the original attractor.

4.3 Optimization-based Eigenvalue Reassignment (ER)

Asymptotic stability of an LTI system is identified by the location of its eigenvalues with respect to the imaginary axis. It is possible to stabilize an originally unstable LTI system by moving the eigenvalues from the right to the left half of the complex plane passing the imaginary axis. Kalashnikova et al.[30] have used this definition as a constraint on an optimization problem that reconfigures the eigenvalues of an unstable ROM for maximum accuracy, which is implemented in the body of an objective function on deviation of the ROM output from the same output computed by the FOM. The basic concept is similar to the common practice of using a feedback signal to maintain the accurate output from a control system. However, instead of an actual feedback signal out of the ROM solution, an analytical representation of the system response is used for simplicity and low computational cost. This analytical representation here is the exact solution to the LTI system in (4.3).

Diagonalizing the system dynamics matrix $\boldsymbol{A}_M$ using eigenvalue decomposition, we have:

$$\boldsymbol{A}_M = \boldsymbol{V}_M \boldsymbol{D}_M \boldsymbol{V}_M^{-1}. \tag{4.8}$$

An optimization problem is then defined for the unstable eigenvalues of the Galerkin system:

$$min_{\lambda_j^u} \sum_{k=1}^{K} \left\| \boldsymbol{y}^k - \boldsymbol{y}_M^k \right\|_2^2, \tag{4.9}$$

$$\text{s.t.} \quad Re(\lambda_j^u) < 0, j = 1, ..., L,$$

where $\boldsymbol{y}$ is the output of the FOM provided by the original data snapshots and $\boldsymbol{y}_M$ is the ROM output reconstructed analytically by the exact solution of the LTI system:

$$\boldsymbol{y}_M(t) = \boldsymbol{C}_M[\boldsymbol{V}_M exp(t\tilde{\boldsymbol{D}}_M)\boldsymbol{V}_M^{-1}\boldsymbol{x}_M(0) + \int_0^t \boldsymbol{V}_M exp[(t-\epsilon)\tilde{\boldsymbol{D}}_M]\boldsymbol{V}_M^{-1}\boldsymbol{B}_M\boldsymbol{u}(\epsilon)d\epsilon]. \tag{4.10}$$

It is worth noting that $\boldsymbol{y}$ is a low-order projection of the original dynamics and achieved by the projection of the data snapshots to the same low-order space defined by the same number of POD modes used in ROM. Since the ROM solution is in a much lower dimensional space, instead of using the original dynamics/data in full order, it is only appropriate to use the projected dynamics of the original FOM in the same low-order space as a reference.

An iterative process between the modification of the eigenvalues and the measurement of ROM outputs against the reference is required to reach the optimal solution. In Equation (4.10), the diagonal matrix of eigenvalues $\boldsymbol{D}_M$ is substituted by $\tilde{\boldsymbol{D}}_M$, which is updated at each iteration of the optimization problem (4.9). Once the optimization problem converges, the dynamics matrix is reconstructed by eigenvectors of the original system and the optimal stable eigenvalues:

$$\tilde{\boldsymbol{A}}_M = \boldsymbol{V}_M\tilde{\boldsymbol{D}}_M\boldsymbol{V}_M^{-1}. \tag{4.11}$$

The optimization problem defined in (4.9) is a constrained nonlinear problem, which is easily implemented by the *fmincon* solver in MATLAB optimization toolbox using the interior-point algorithm.

According to the discussions on stability of an LTI system at the beginning of this approach, upper-bound constraints on real parts of eigenvalues are theoretically sufficient to solve the optimization problem for a stable ROM. Whereas, due to the large parametric

space dictated by the number of unstable eigenvalues, accuracy concerns may require further regularization of the search space by introducing lower-bound constraints, which inevitably increases the computational effort. Such limitations are stressed as more unstable eigenvalues enter the optimization problem (that is equivalent to further increase of the number of modes used in the ROM). Even worse, the algorithm may not converge when the control space becomes more complicated with the increase of control parameters, in this case, the number of unstable eigenvalues.

4.4 The Hybrid Stabilization Approach

In both of the previous stabilization methods, stable eigenvalues of the LTI system are preserved in order to maintain dynamics of the original ROM as much as possible for better accuracy. When most or all modes are stable for a ROM of dimension $M + r$, ISC provides a stable ROM of lower dimension M and keeps the accuracy across all M modes[14]. When most or all modes are unstable for the original ROM of dimension $M + r$, such as the current case, ISC still provides a stable ROM of dimension M, but loses accuracy in some eigenmodes, which in our symmetry ROM are the modes with lower-frequency response that are originally more unstable. The smaller modification to higher modes, which are originally more stable, leads to improved accuracy of dynamics in those modes. In contrast, since the L^2 ROM is initially more unstable than the symmetry ROM, even the minimal change of the left ROB in the ISC method results in considerably inaccurate time response in the L^2 ROM, regardless of the frequency.

On the other hand, ROM accuracy is regulated specifically in the ER approach and is maintained despite the number of unstable eigenmodes in the original ROM. However, with an increase in the number of unstable modes, the optimization problem in ER requires considerably higher computational cost to reach convergence, and the computational overhead may reach a point where optimization becomes infeasible in some cases. The control space also gets more complicated with larger number of control parameters (i.e. unstable modes), and it often leads to problems with poor convergence (e.g. converging to a local minimum

or not converging at all).

To achieve the best of both worlds, a Hybrid method is proposed to basically let the ISC approach handle most of the high-frequency modes and leave a few highly unstable modes at lower frequencies to be handled by the ER method. The goal is to keep the cost low and the control space smooth enough for convergence. The details are shown in Algorithm 1, where $\lambda_j^u(0)$ is the initial value of λ_j^u. η_1 and η_2 are tolerance values, b and c are small real numbers to facilitate searching the parameter space for optimal points in a limited range, and a is defined with respect to the properties of the unstable ROM generated based on a specific inner product that may naturally result in local clustering of optimal eigenvalues (e.g. close to the imaginary axis). Imaginary parts of the eigenvalues are fixed at those of the original system in the Hybrid method, therefore, only the real components of the unstable eigenvalues are changed through optimization. Generally steps 14 through 18 can be avoided for a well-behaved optimization problem with a smooth search space.

Integration of the Hybrid method with the energy conserving definition of the symmetry inner product, instead of the traditional L^2 norm, is expected to further improve the performance and robustness of this approach.

Algorithm 1 Hybrid Method

Step 1

1. Construct ROMs of dimension M, and $M + r$
2. Adjust the stability margin μ and regularization parameter τ
3. **for** $i = 1 : r$ **do**
4. Obtain M_E and M_A by the first M columns in A_{M+i} and E_{M+i}
5. Solve the optimization problem (4.5) for $\hat{\boldsymbol{P}} \in \boldsymbol{R}^{(M+i)\times(M+i)}$
6. **if** a feasible solution is obtained **then** exit
7. **end for**
8. Compute $\boldsymbol{X}$, and modify ROM matrices as in (4.7)

Step 2

9. Compute the diagonal matrix of eigenvalues ($\boldsymbol{D}_{ISC}$) of the ROM stabilized in step 1
10. Diagonalize matrix $\boldsymbol{A}_M$ of the original ROM

$$\boldsymbol{A}_M = \boldsymbol{V}_M \boldsymbol{D}_M \boldsymbol{V}_M^{-1}$$

11. Substitute selected eigenvalues of $\boldsymbol{D}_{ISC}$ in $\boldsymbol{D}_M$
12. Initialize the diagonal matrix $\tilde{\boldsymbol{D}}_M$ to $\boldsymbol{D}_M$
13. Solve the optimization problem in Equation (4.9) for λ_j^u
14. **if** $(|\lambda_j^u| > a)$ **then**
15. **while** $(|\lambda_j^u(0)| > \eta_1)$, **do** $\lambda_j^u(0) = b(\lambda_j^u(0))$ and go to 13, or
16. **while** $(|lb| > \eta_2)$, **do** $lb = lb + c$ and go to 13, or
17. Change the stability margin and go to 3
18. **end if**
19. Rearrange $\tilde{\boldsymbol{D}}_M$ with the stabilized eigenvalues
20. Compute $\tilde{\boldsymbol{A}}_M$

$$\tilde{\boldsymbol{A}}_M = \boldsymbol{V}_M \tilde{\boldsymbol{D}}_M \boldsymbol{V}_M^{-1}$$

4.5 Application: Supersonic Flow over a Circular Cylinder

Computed from snapshots of the high-fidelity simulation data, the first 16 POD modes capture 95% and 92% of the flow energy with L^2 and symmetry inner products respectively. On the other hand, adding more of the higher modes gets diminished return in its captured energy while high-frequency components from extra high modes largely reduce the efficiency of the optimization process and often lead to a less accurate ROM though at higher order. Thus, the three stabilization methods are applied to the 16 mode linear ROMs.

To compare the performance of ROMs using different stabilization methods, a relative error is defined to measure the difference between $\boldsymbol{E}^k_{POD}$, the energy of POD modes directly from the projection, and $\boldsymbol{E}^k_{ROM}$, the energy represented in ROM:

$$e = \frac{\sum_{k=1}^{K} \left\| \boldsymbol{E}^k_{POD} - \boldsymbol{E}^k_{ROM} \right\|_2^2}{\sum_{k=1}^{K} \left\| \boldsymbol{E}^k_{POD} \right\|_2^2} \quad , \tag{4.12}$$

where energy is defined by $E_{(\cdot)} = \sum_{i=1}^{M} a_i^2(t)$ with coefficients a_i from respectively the POD or ROM. Notice that this is a sensitive error metric that is only defined based on the fluctuating dynamics, while many of the flow structures are captured by the mean flow that when added to the modal approximation through reconstruction of the flow field makes it more difficult to visually recognize the order of discrepancy between the ROMs stabilized by different methods.

4.5.1 Stabilization approaches on the L^2 ROM

The horizontal velocity at a downstream probe point $(x, y) = (3, 2)$ is used as the system output in ER. In the case of L^2 ROM with 16 modes, it becomes challenging for the ER method to converge to a solution with reasonable accuracy due to the large and presumably complex parametric space. Table 4.1 shows the poor accuracy of a typical ER stabilization for the 16 mode L^2 ROM, marked by ER(1), which is most likely trapped at some local optimum

Table 4.1: Performance of the stabilization methods in the 16 mode L^2 ROM.

	ER(1)	ER(2)	ISC	Hybrid
Number of variables	16	16	153	$153+3$
Upper-bound constraints	8	8	NA	3
Lower-bound constraints	0	8	NA	3
τ	NA	NA	$1.00e-05$	$1.00e-05$
μ	NA	NA	5.00e-01	5.00e-01
Number of ER function evaluations	204	1539	NA	72
Wall-clock time (sec)	1.04	7.78	1.97	2.66
Relative error e (%)	7.76e+01	1.30e+01	4.0e+09[1]	1.51e+01

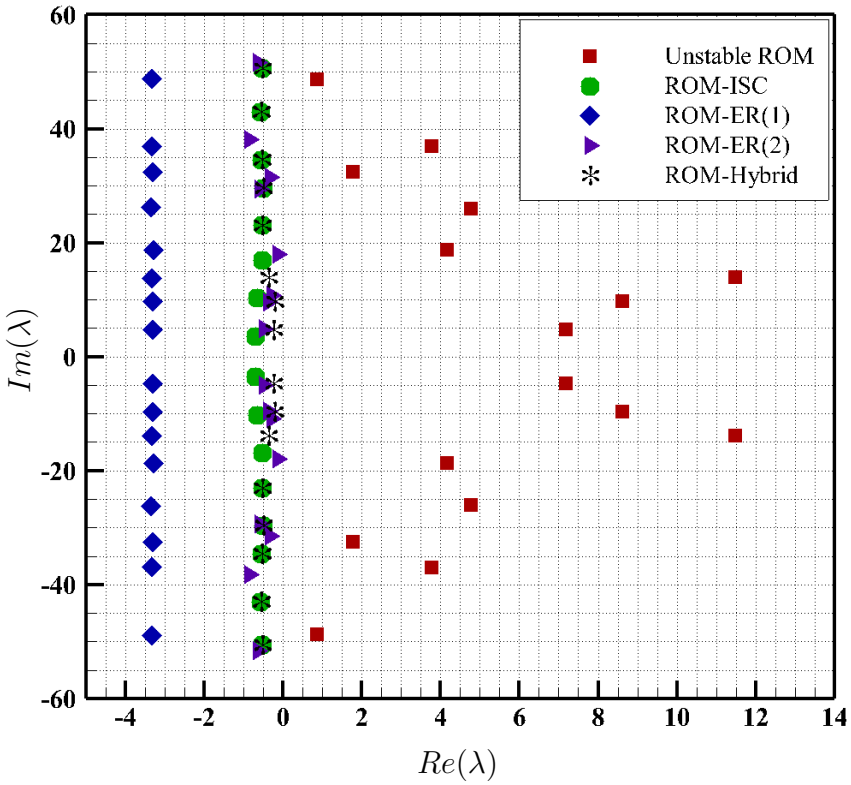

Figure 4.1: Eigenvalues of the 16 mode L^2 ROMs.

with terrible accuracy. One ad-hoc fix is to introduce empirical lower-bound constraints, which may limit the chance of being trapped by unreasonable local optima at the expense of

[1]CVX solver status shown in Matlab is "Inaccurate" for convergence, and choosing different ROM dimensions makes no improvement in this case.

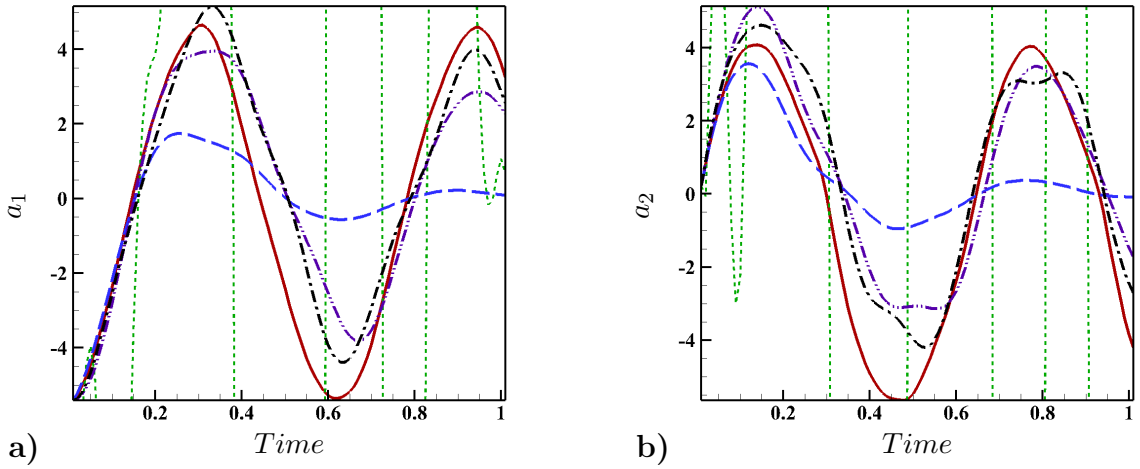

Figure 4.2: The a) first, and b) second temporal coefficients for the 16 mode L^2 ROM stabilized by ISC (----), ER(1) (——), ER(2) (- - -), and Hybrid (— -) methods compared against the POD coefficients (——).

increased computational cost. At the same time, the appropriate lower-bound constraint for each eigenvalue is not well defined and may be challenging to identify in practice. The case ER(2) in Table 4.1 shows a typical example of ER with ad-hoc lower-bound constraints for convergence to reasonable solutions. Figure 4.1 shows the new stable position of eigenvalues from ER(1) and ER(2). Apparently, ER(2) is less aggressive in modifying the eigenvalues and leads to better accuracy. In Figure 4.2, the POD coefficients are obtained by the projection of FOM state onto the POD modes, and used as a reference for evaluation of the accuracy of ROM coefficients that are computed by projection of the governing equations onto the POD subspace. Thus the time evolution of coefficients in this figure shows a more clear picture for the different levels of accuracy delivered by ER(1) and ER(2). It is worth noting that ER(2) has benefited from an empirical fix and is much more expensive than the Hybrid method though it provides similar accuracy.

ISC, as a computationally efficient method, is applied with $r = 1$ for comparison. Figure 4.1 shows that the ROM stabilized by ISC has characteristic eigenvalues in the stable half of the complex plane as expected. However, despite its computational efficiency, the performance of the ROM stabilized by ISC in Figure 4.2, where the time history of POD coefficients are shown for reference, is far worse than other approaches in the current case.

This is also confirmed by the poor convergence with the large relative error shown in Table 4.1. In fact, it has been pointed out by Amsallem and Farhat in the original work[14] that there is no guarantee for the convergence of the CVX solver in a complicated control space with increased control parameters. Choosing different ROM dimensions may help, but it does not work for the current L^2 case. Note that the number of variables shown in Table 4.1 for the convex optimization problem of the ISC method is the total number of independent components of the SPD matrix $\hat{\boldsymbol{P}} \in \boldsymbol{R}^{17\times 17}$ for stabilization of our 16-mode ROM with $r = 1$.

In order to improve the computational efficiency of ER and its reliability in stabilization of the dominant modes, the new Hybrid method stabilizes most of the high-frequency responses using the ISC method, and solves the optimization problem of the ER method for a few remaining eigenvalues controlling mostly energetic low-frequency responses, while preserving the eigenvectors of the original ROM in all directions. It is indicated by the locations of eigenvalues in Figure 4.1 that the Hybrid approach has only modified three pairs of eigenvalues (i.e. the six eigenvalues with the lowest frequencies) in its ER step on top of the initial ISC stabilization. The accuracy achieved by the Hybrid approach is about the same as ER(2) method, but with only a fractional cost as shown in Table 4.1 as well as in Figure 4.2. In fact, with a larger number of modes entering ROM stabilization, the control space gets more complicated and leads to situations where the ER(2) method fails to reach any optimal solutions at all. On the other hand, the Hybrid method limits the non-convex optimization process to only a small number of low-frequency modes, thus ensures the convergence of its ER step.

4.5.2 Stabilization approaches on the symmetrical ROM

Using a symmetry inner product, rather than a regular L^2 inner product, in the model order reduction of compressible flows has shown clear advantages, both theoretically and practically, in improving ROM stability[24;26;27].

The original ISC method is adopted and applied to a 16 mode symmetry ROM with

$r = 1$. As shown in Figure 4.3, all the eigenvalues are moved to the stable region when ISC is applied to the originally unstable symmetry ROM. It is actually more obvious in this case that the low-frequency modes, that are originally more unstable, may be "over-killed" by moving too deep into the stable region. Such over-stabilization leads to inaccuracy in the same way as it is described before for the L^2 ROM and shown again now for the symmetry ROM in Figure 4.4. Essentially, ISC shows improved performance on a symmetry ROM, but the problem of lower accuracy in low-frequency modes persists.

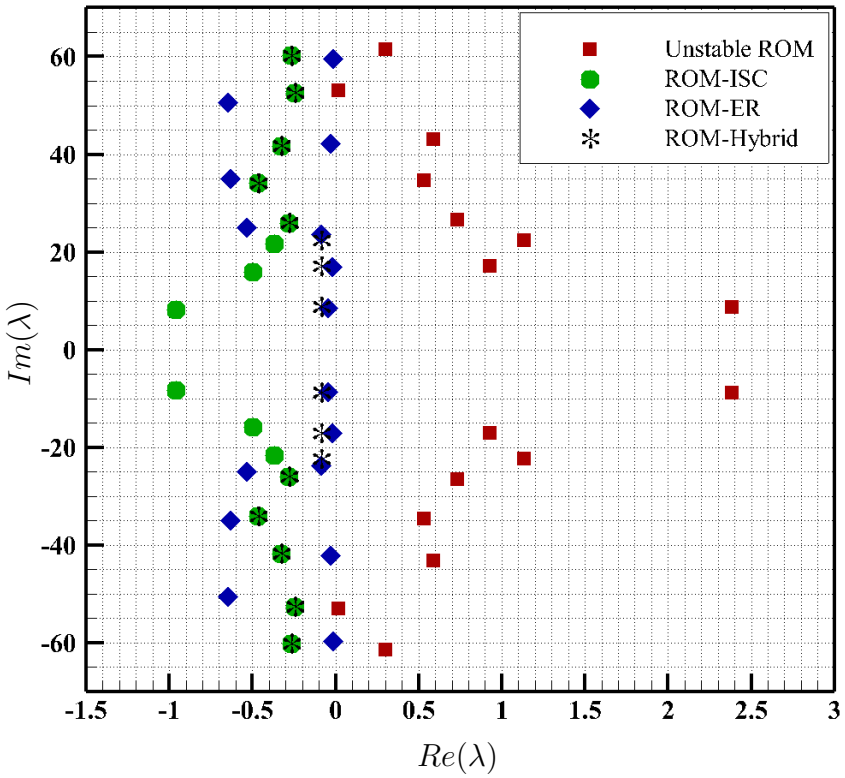

Figure 4.3: Eigenvalues of the 16 mode symmetry ROMs.

When ER is applied to the symmetry ROM, the eigenvalues are moved to the stable region, but less aggressively as shown in Figure 4.3, and according to Figure 4.4 accuracy of the ROM coefficients is also improved in comparison to the regular L^2 ROM. With the improvement in both the ISC and ER methods when being adopted for a symmetry ROM, it is not surprising to see a larger improvement in the performance of the Hybrid method. The

new eigenvalues of the ROM stabilized by the Hybrid method appear to take the features, and be a good combination of the eigenvalues of ISC and ER as shown in Figure 4.3.

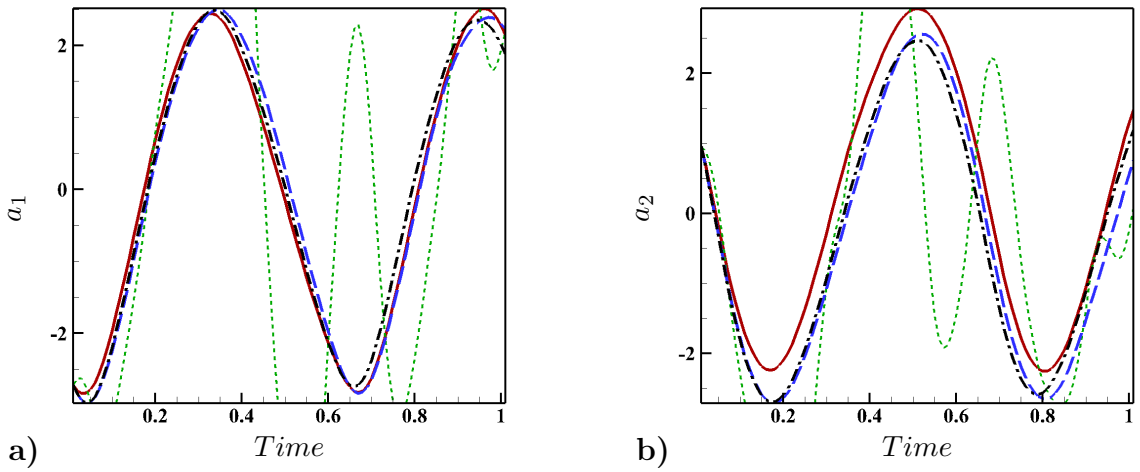

Figure 4.4: The a) first, and b) second temporal coefficients for the 16 mode symmetry ROM stabilized by ISC (), ER ( ), and Hybrid ( ) methods compared against the POD coefficients ().

Table 4.2: Performance of the stabilization methods in the 16 mode symmetry ROM.

	ER	ISC	Hybrid
Number of Variables	16	153	$153 + 3$
Upper-bound constraints	8	NA	3
Lower-bound constraints	0	NA	3
τ	NA	1.00e-05.	1.00e-05
μ	NA	2.00e-01	2.00e-01
Number of ER function evaluations	1837	NA	12
Wall-clock time (sec)	8.87	1.37	1.53
Relative error e (%)	2.76e+00	3.05e+02	3.23e+00

It is worth noting that despite the accuracy shown in the symmetry ROM, ER stabilization faces the same challenges computationally. The computational cost of the ER method is much higher than the Hybrid method, though they offer similar accuracy. Table 4.2 shows details of the computational performance of the stabilization methods for a 16 mode ROM. The advantage of the Hybrid approach in terms of computational savings is shown by the significantly smaller wall-clock time for almost the same level of accuracy obtained by the

ER method. The difference in the computational cost gets only larger when the number of modes increases. At some point with larger number of modes, the ER method may fail to converge.

Although both L^2 and symmetry ROMs are originally unstable, the maximum growth rate, measured by the real component of eigenvalues $Re(\lambda)$, is 11.48 for the L^2 ROM, which is much larger than the maximum value of 2.38 for the symmetry ROM before stabilization. The stabilization methods also perform better for the symmetry ROM. The L^2 ROM stabilized by the ER method without lower-bound constraints (i.e. ER(1)) has a poor accuracy with a relative error of 77.61%, while the symmetry ROM stabilized by the ER method with the same configuration reduces the error to only 2.76%. It is shown in chapter 7 that these observations are directly connected to the properties of the controllable space of the ROMs constructed based on the two inner products.

For a direct comparison of the flows, Figure 4.5 shows the stream-wise velocity of the reconstructed flow fields computed by different ROMs, compared against the original FOM (i.e. DNS) data. The flow computed by the ROMs stabilized by the Hybrid and ER methods reveals more details of the vortex shedding structures, while all stabilized ROMs capture the shock locations well. When a particular space-time location, at $x = 5$ (for all y locations) and $t = 0.65$, is chosen, a more quantitative comparison of ROMs is shown in Figure 4.6 for the stream-wise velocity and pressure profiles. The ROMs stabilized by the Hybrid and ER methods clearly out-perform the one stabilized by the ISC method in the comparison for both velocity and pressure profiles, though the Hybrid method is more efficient and robust than ER.

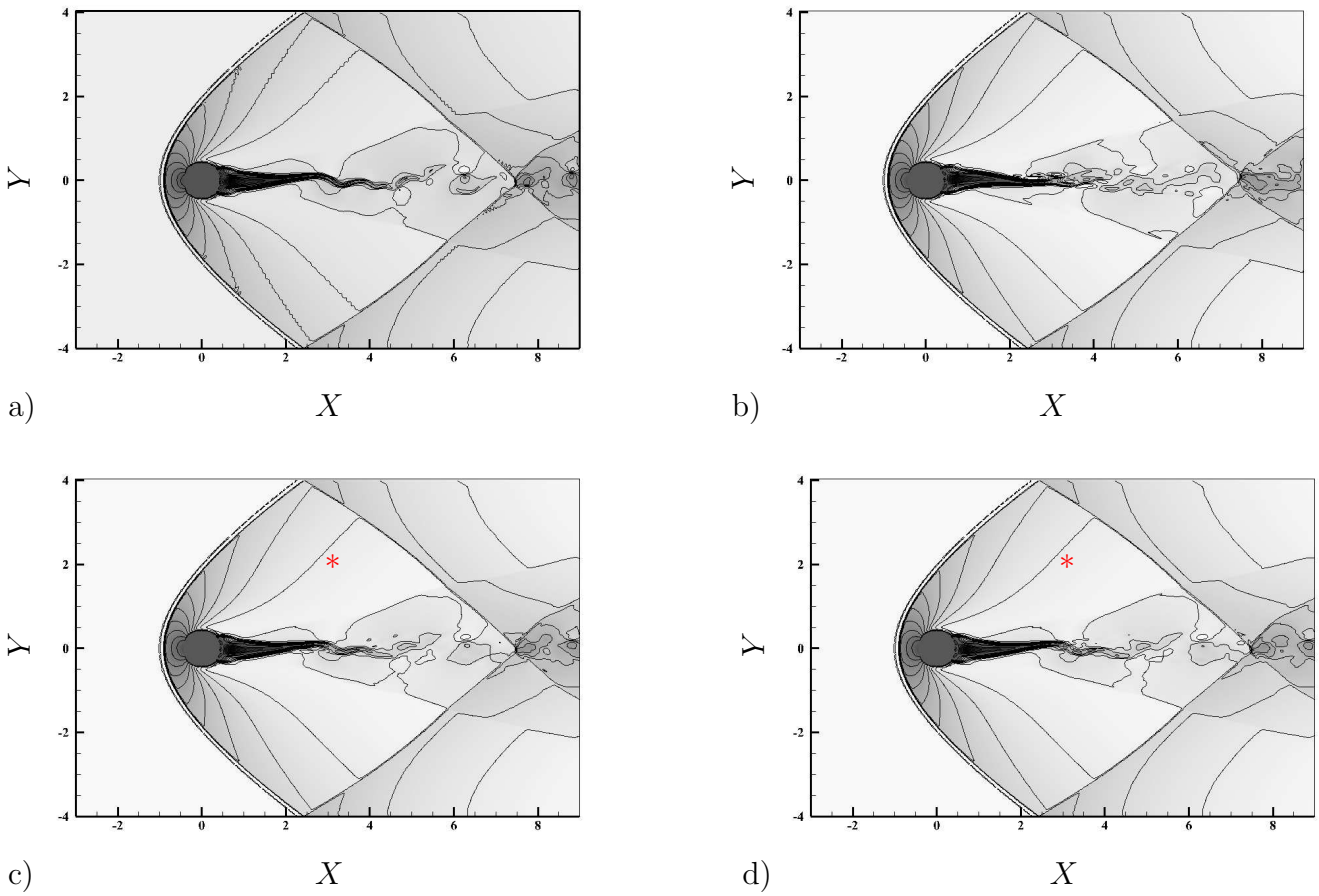

Figure 4.5: Stream-wise velocity contours of the snapshot at $t = 0.65$ computed by a) FOM, and the 16 mode symmetry ROM stabilized by b) ISC, c) ER, and d) Hybrid approaches. Velocity at the locations marked by red asterisks is used in the ER objective function for both the ER and Hybrid methods.

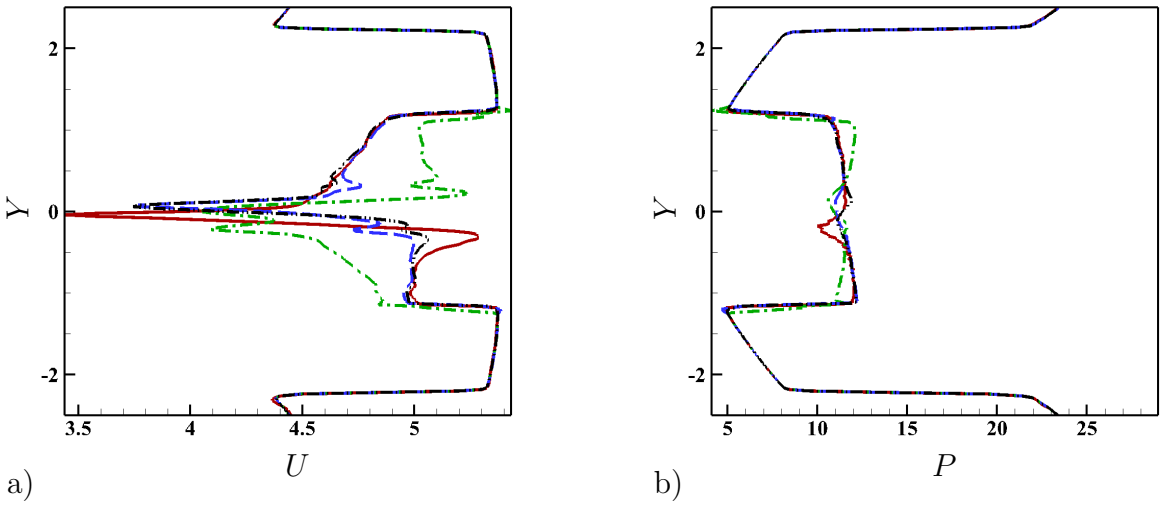

Figure 4.6: Profiles of a) horizontal component of velocity and b) pressure at $x = 5$, computed by FOM (——), and the 16 mode symmetry ROM stabilized by ISC (- -), ER (— —) and the Hybrid method (- - -).

Chapter 5

Stabilization of Nonlinear ROMs

The systematic and physics-infused construction of a projection-based Reduced-Order Model (ROM) shows the capability to replicate the dynamical evolution of the original high-dimensional system but with fractional computational cost. However, certain nonlinear features and high-frequency contributions may be lost throughout the aggressive order reduction. Thus, ROMs in a large category of fluid dynamics applications require stabilization and model closure methods to compensate key contributions missed from the model order reduction[14–17;19–21;30].

Despite the predominance of the applications that do not lend themselves to linearization, there are only a few stabilization methods that have been rigorously designed to control the nonlinear ROMs. Following the approach by Amsallem and Farhat[14], Balajewicz et al.[33;38] applied a minimal rotation of the subspace and modified the reduced-order representation at the kinematic level to obtain stabilized nonlinear ROMs for both compressible and incompressible flows. However, similar to the ISC approach, when dealing with highly unstable ROMs such as those in the current study involving strong shock-vortex interactions, the large rotation of a subspace often leads to substantial deviation of the stabilized ROM from the original dynamics and reduces the accuracy.

Inspired by the approach of Kalashnikova et al.[30], a global eigenvalue reassignment method for the stabilization of nonlinear ROMs (ERN algorithm) is developed in this chap-

ter. Using the growth rates (i.e. eigenvalues) of the linear dynamics as the control parameters, this method learns a linear control law to drive the nonlinear ROM towards maximum agreement with the Full-Order Model (FOM), where the stability of the nonlinear ROM is guaranteed by a total power constraint. Global optimization is used to improve the robustness of the method, and a multi-stage stabilization layout is developed in the next chapter to facilitate computationally efficient implementation of the ERN algorithm in strongly nonlinear applications that need a higher-dimensional linear subspace to resolve the true dynamics. Thus, the global aspect of the eigenvalue reassignment is achieved by both defining a stability condition suitable for a generic nonlinear system, and using a global optimization solver to locate the eigenvalues in the control space.

The stabilization method proposed in this work can be applied to the reduced-order models that are either constructed by projection of the governing equations onto a low-dimensional space[8;10], or discovered by system identification[2;57], and operator inference techniques[58]. The mathematically rigorous and physically informative structure of the projection-based model reduction have prompted us to use POD-Galerkin ROMs as the test-bed for implementation of the ERN algorithm. Using a symmetry inner product has improved overall stability, controllability, and robustness of compressible flow ROMs in different applications, which has turned it into a standard component of the model reduction process in this study[24;26;27].

This new stabilization approach achieves both the stability and the accuracy for the nonlinear Proper Orthogonal Decomposition (POD)-Galerkin ROM of the application with strong shock-vortex interactions and unsteady oscillations that trigger large instabilities in the original ROM before the stabilization.

The ERN algorithm is introduced in this chapter along with the details for its implementation. Then the results of applying this method for stabilization of the POD-Galerkin ROM constructed by the symmetry inner product are discussed. The nonlinear ROM is created based on the snapshots of the supersonic flow over the circular cylinder.

5.1 Power Balance and the Notion of Time-Stability

Net conservation of the Turbulent Kinetic Energy (TKE) has inspired the use of power balance as a constraint for closure and stabilization of incompressible flow ROMs based on the Navier-Stokes equations[17;38]. Noack and Niven[17] suggested several closure strategies based on the constraints that arise from the Galerkin system. Balajewicz et al.[38] used the total power balance as a constraint for the stabilization of incompressible flow ROMs that possess energy-preserving quadratic terms.

For an orthogonal subspace as POD, the total TKE is represented by:

$$E = \frac{\|\boldsymbol{q}'\|^2}{2} = \sum_{i=1}^{M} \frac{a_i^2}{2}. \tag{5.1}$$

Power is defined as the variation of TKE over time, where for a ROM with constant, linear, and quadratic terms yields:

$$\frac{dE}{dt} = \sum_{i=1}^{M} C_i \boldsymbol{a}_i + \sum_{i,j=1}^{M} L_{ij} \boldsymbol{a}_i \boldsymbol{a}_j + \sum_{i,j,k=1}^{M} Q_{ijk} \boldsymbol{a}_i \boldsymbol{a}_j \boldsymbol{a}_k. \tag{5.2}$$

Net conservation of the fluctuation energy requires the total power to be balanced on the attractor in an average sense[17]:

$$(\frac{dE}{dt}) = 0, \tag{5.3}$$

where,

$$(\frac{dE}{dt}) = \sum_{i,j=1}^{M} L_{ij} (\boldsymbol{a}_i \boldsymbol{a}_j) + \sum_{i,j,k=1}^{M} Q_{ijk} (\boldsymbol{a}_i \boldsymbol{a}_j \boldsymbol{a}_k), \tag{5.4}$$

knowing that for the POD subspace $(\boldsymbol{a}_i) = 0$. The invariance in Equation (5.3) is itself a consequence of a modal power balance at every mode. However, this condition is only satisfied by the HFM that involves the full modal interactions of the energy cascade. It is known that ignoring the multi-frequency effects due to the modal cut-off in POD-based ROMs results in accumulation of power in the system that makes ROMs unstable in turbulent flows[38;59]. Rempfer and Fasel[59] showed that the interrupted modal interactions in POD may

lead to positive, or negative modal powers at different mode numbers.

The above notion of the total power balance in turbulent flows is closely tied to the definition of exponential stability in a generic dynamical system. Exponential stability in nonlinear systems is equivalent to the time-stability, which requires a non-increasing amplitude in the dynamic response of the system. In other words, for a system to be time-stable, it has to maintain a non-positive numerical power at an arbitrary time step[60;61]:

$$\frac{dE}{dt} \leq 0. \tag{5.5}$$

In order to prevent dramatic system modifications through control, the weak form of this constraint is favored, which requires the total power to be non-positive in the average sense. At the ROM level however, the POD subspace is not complete, and partial resolution of the nonlinearities necessarily leaves a total power residual in the low-dimensional system. A positive residual corresponds to spurious accumulation of power in the system that eventually blows up the ROM response. Enforcing the reduced-order system to satisfy the average total power balance is too strong a condition, that may lead to bad or insufficient convergence in the stabilization algorithm. Thus, a less restrictive approach to guarantee the stability of the nonlinear ROM is to make the system satisfy time-stability by maintaining a negative total power residual on the average:

$$\sum_{i,j=1}^{M} L_{ij}(\boldsymbol{a}_i \boldsymbol{a}_j) + \sum_{i,j,k=1}^{M} Q_{ijk}(\boldsymbol{a}_i \boldsymbol{a}_j \boldsymbol{a}_k) = -\epsilon, \tag{5.6}$$

where ϵ is a small positive number. The exact value of the total power that leads to the most accurate ROM response is not known a priori, and has to be identified numerically in the course of optimization. While enforcing negativity to guarantee the stability of ROM through control, the influence of the magnitude of the total power residual on the optimization needs to be regulated to prioritize accuracy. This is facilitated by the specific choice of the objective function in the stabilization algorithm that is proposed in the rest of this section. Note that the total power is derived for a ROM in constant-linear-quadratic form here. Extension of

this formulation to higher-order systems is straightforward.

5.2 The ERN Stabilization Algorithm

Linearization of the nonlinear dynamical systems has long been employed as a bridge to access the mathematically rich and computationally efficient tools of the classic control theory to stabilize nonlinear systems that operate in close proximity to the fixed points. Fluid dynamics applications though more often than not involve strong nonlinearities (e.g. shock interactions, chemical reactions, turbulence, etc.) that void the reliability of the linearized counterpart of the system as a probe to model the evolution of the original nonlinear system. The stabilization method that is proposed in this study uses the eigenvalues of the linear term of the nonlinear ROM as control parameters to drive the nonlinear system towards the desired dynamics that is stable, and accurately represents the dynamics of the HFM. The eigenvalues are relocated in the complex plain via a global optimization solver until the nonlinear ROM output closely matches that of the FOM, while stability of the solution is guaranteed by enforcing the nonlinear ROM to maintain a negative total power on the average. Consider the following nonlinear system that represents a nonlinear ROM in its general form:

$$\boldsymbol{E}_M \dot{\boldsymbol{x}}_M = \boldsymbol{A}_M \boldsymbol{x}_M + \boldsymbol{f}(\boldsymbol{x}_M) + \boldsymbol{B}_M \boldsymbol{u}(t), \tag{5.7}$$

$$\boldsymbol{y}_M(t) = \boldsymbol{C}_M \boldsymbol{x}_M(t),$$

where $\boldsymbol{x}_M \in \boldsymbol{R}^M$ is the state variable, $\dot{\boldsymbol{x}}_M = \frac{d\boldsymbol{x}_M}{dt}$ is the state derivative, $\boldsymbol{u} \in \boldsymbol{R}^L$ is the control input, and $\boldsymbol{y}_M \in \boldsymbol{R}^S$ is the reconstructed output using ROM coefficients. Similarly, $\boldsymbol{E}_M = \boldsymbol{\Phi}_M^T \boldsymbol{E} \boldsymbol{\Phi}_M \in R^{M \times M}$, $\boldsymbol{A}_M = \boldsymbol{\Phi}_M^T \boldsymbol{A} \boldsymbol{\Phi}_M \in R^{M \times M}$, $\boldsymbol{B}_M = \boldsymbol{\Phi}_M^T \boldsymbol{B} \in R^{M \times L}$, and $\boldsymbol{C}_M = \boldsymbol{C} \boldsymbol{\Phi}_M \in R^{S \times M}$ are constant matrices, and $\boldsymbol{E}$, $\boldsymbol{A}$, $\boldsymbol{B}$, and $\boldsymbol{C}$ are the matrices of the N-dimensional FOM. We have $\boldsymbol{E}_M = \boldsymbol{I}$ for the system in non-descriptor form, $\boldsymbol{C}_M = \boldsymbol{1}$ for full-state output, and $\boldsymbol{u} = 0$ (no physical control inputs) in the applications discussed in this paper, where $\boldsymbol{I} \in R^{M \times M}$ is the identity matrix. Finally, $\boldsymbol{f}(\boldsymbol{x}_M)$ is a general nonlinear function that represents the nonlinear terms in the ROM equation, which in the case of

non-polynomial ROMs is obtained after lifting transformations[49], or by hyper-reduction[62] in order to keep the stabilization algorithm tractable.

The linear dynamics matrix $\boldsymbol{A}_M$ is diagonalized:

$$\boldsymbol{A}_M = \boldsymbol{V}_M \boldsymbol{D}_M \boldsymbol{V}_M^{-1}. \tag{5.8}$$

Eigenvectors of $\boldsymbol{A}_M$ are the columns of matrix $\boldsymbol{V}_M$, and are preserved through the stabilization. The diagonal matrix $\boldsymbol{D}_M$ contains the eigenvalues of $\boldsymbol{A}_M$. Unstable eigenvalues $\boldsymbol{\lambda}^u$ of this matrix are the control parameters that are reassigned in the following optimization problem to stabilize the nonlinear system:

$$min_{\boldsymbol{\lambda}^u} \sum_{k=1}^{K} \left\| \boldsymbol{y}^k - \boldsymbol{y}_M^k \right\|_2^2, \tag{5.9}$$

$$\text{s.t.} \quad (\frac{d\tilde{E}}{dt}) < 0,$$

where (.) represents time average, K is the total number of snapshots, $\boldsymbol{y}$ is the Quantity of Interest (QoI) in the FOM output that is provided by the high-fidelity snapshots, and $\boldsymbol{y}_M$ is the same QoI in the ROM output that is computed by numerical integration of the ROM ODEs. However, in the case of full-state output when the simulations are not focused on a specific QoI (e.g. drag force or Mach number at a specific location), computing the objective function in (5.9) becomes prohibitively expensive. Therefore, the objective function is modified in the following optimization problem for the stabilization of ROMs in systems with full-state output:

$$min_{\boldsymbol{\lambda}^u} \sum_{k=1}^{K} \left\| \boldsymbol{a}_{(POD)}^k - \boldsymbol{a}_{(ROM)}^k \right\|_2^2, \tag{5.10}$$

$$\text{s.t.} \quad (\frac{d\tilde{E}}{dt}) < 0,$$

where $\boldsymbol{a}_{(.)} = \sum_{i=1}^{M} a_i(t)$, $\boldsymbol{a}_{(POD)}$ is computed by the POD coefficients that are obtained by projection of the FOM state onto the POD modes, and $\boldsymbol{a}_{(ROM)}$ is determined by the ROM

coefficients that are computed by integration of the nonlinear ROM ODEs at each iteration of the optimization. For ROMs with the constant-linear-quadratic form shown in Equation (3.10), the average total power ($\frac{d\tilde{E}}{dt}$) is given by Equation (5.4), where the tilde sign shows that its value is updated at each iteration of the optimization according to the newly assigned eigenvalues.

The linear dynamics matrix $\tilde{\boldsymbol{A}}_M$ is also reconstructed at each iteration by the original eigenvectors and the modified eigenvalues contained in the diagonal matrix $\tilde{\boldsymbol{D}}_M$:

$$\tilde{\boldsymbol{A}}_M = \boldsymbol{V}_M \tilde{\boldsymbol{D}}_M \boldsymbol{V}_M^{-1}. \tag{5.11}$$

At the onset of the optimization, the diagonal entries of matrix $\tilde{\boldsymbol{D}}_M$ are initialized either randomly, with the eigenvalues in matrix $\boldsymbol{D}_M$, or with a combination of different strategies that is discussed in the multi-stage configuration in chapter 6. Regardless of the existence of an actual control input in the FOM, the ERN algorithm modifies the linear dynamics matrix by numerically applying a linear actuation of the form $\boldsymbol{u}_M = -\boldsymbol{K}_M \boldsymbol{x}_M$ in the algorithmic level, so that $\tilde{\boldsymbol{A}}_M = \boldsymbol{A}_M - \boldsymbol{B}_M \boldsymbol{K}_M$, where $\boldsymbol{K}_M$ is the gain matrix.

The average total power constraint is implemented as a penalty term:

$$min_{\boldsymbol{\lambda}^u} \{ \sum_{k=1}^{K} \left\| \boldsymbol{a}^k_{(POD)} - \boldsymbol{a}^k_{(ROM)} \right\|_2^2 + \tau [(\frac{d\tilde{E}}{dt}) + \epsilon] \}, \tag{5.12}$$

where, ϵ is a small positive number, and τ is a regularization parameter. ϵ, and τ are hyperparameters that are easily identified by trial and error here, though they can be adjusted by grid or random search in systems with more complicated control landscapes. In the case of ROMs with complex eigenvalues, the imaginary parts of the eigenvalues can be preserved through the stabilization to improve computational efficiency and accuracy. The optimization problems (5.9) and (5.10) are not necessarily convex, thus using a global optimization solver is recommended to enhance the robustness of the algorithm. Particle Swarm Optimization (PSO) is used in this work for its computational efficiency. The optimization problem can also be easily solved by the global optimization toolbox in MATLAB. Implementation

of the stabilization method is explained in Algorithm 2 for a system with full-state output.

Algorithm 2 ERN stabilization algorithm

Input: POD temporal coefficients $\boldsymbol{a}_{(POD)}$, matrix $\boldsymbol{A}_M$, nonlinear ROM tensor(s) (tensor $\boldsymbol{Q}$ in the case of quadratic nonlinearity), regularization parameter τ, and penalty parameter ϵ.

Output: Modified matrix $\tilde{\boldsymbol{A}}_M$ that stabilizes the nonlinear ROM.

1. Diagonalize matrix $\boldsymbol{A}_M$:
$$\boldsymbol{A}_M = \boldsymbol{V}_M \boldsymbol{D}_M \boldsymbol{V}_M^{-1}.$$
2. Initialize a diagonal matrix $\tilde{\boldsymbol{D}}_M$.
3. Solve the optimization problem:
$$min_{\boldsymbol{\lambda}^u}\{\sum_{k=1}^{K} \left\| \boldsymbol{a}_{(POD)}^k - \boldsymbol{a}_{(ROM)}^k \right\|_2^2 + \tau[(\tfrac{d\tilde{E}}{dt}) + \epsilon]\}.$$
4. Construct the modified matrix $\tilde{\boldsymbol{A}}_M$:
$$\tilde{\boldsymbol{A}}_M = \boldsymbol{V}_M \tilde{\boldsymbol{D}}_M \boldsymbol{V}_M^{-1}.$$

5.3 Particle Swarm Intelligence

The nonlinear optimization problem (5.9) that is not necessarily convex, along with the non-analytical nature of the objective function motivated us to use an optimization algorithm that can deal with a broader range of problem types than this particular application. Meanwhile, with the big picture of ultimate application of ROMs in many-queries applications, the computational efficiency of the global optimization method becomes more important.

Developed by Kennedy and Eberhart[63], Particle Swarm Intelligence, also known as Particle Swarm Optimization (PSO), attains a stochastic approach to model the adaptation of social behavior in morphing for the optimal swarm dynamics, and uses this model for solving optimization problems. PSO initially scatters a given number of particles in random positions in the search space. Assuming that r particles are initialized in an L-dimensional space, then it uses an inertia-based formulation to populate the group of agents about the optimal points from one iteration to the next. Each particle is characterized by a position vector (i.e. the L unstable eigenvalues) and a velocity vector, which represents the step size in modification of the eigenvalues towards the next iteration. Typically, larger population and step size values are required in a larger domain in order to accurately capture the global minimum point. The basic form of this algorithm updates the step size and the position of each particle as follows:

$$\Delta\boldsymbol{\lambda}_{i+1} = \Delta\boldsymbol{\lambda}_i + \boldsymbol{U}(0,\psi_1)(\boldsymbol{\lambda}_p - \boldsymbol{\lambda}_i) + \boldsymbol{U}(0,\psi_2)(\boldsymbol{\lambda}_g - \boldsymbol{\lambda}_i), \tag{5.13}$$

$$\boldsymbol{\lambda}_{i+1} = \boldsymbol{\lambda}_i + \Delta\boldsymbol{\lambda}_{i+1}, \tag{5.14}$$

where i is the iteration index, and $\boldsymbol{\lambda}_p$ is the vector that contains the best position of a particle in its own history. In other words, each particle keeps track of its best function value through iterations, by marking the position at which the smallest cost function is obtained. Whereas, $\boldsymbol{\lambda}_g$ is the position of the particle with the least cost function value among the population. In this formulation, $\boldsymbol{U}$ is a vector of random numbers in the range of $(0,\psi_1)$ for the second term, and $(0,\psi_2)$ for the third term, where ψ_1 and ψ_2 are acceleration coefficients. These

coefficients act like weighting factors that respectively attract the population towards the local, and global best solutions. Therefore, the global optimization algorithm maintains a stable behavior if there is a balance between the values of these two parameters[64;65].

Many studies are conducted on further improvement of PSO in various perspectives. In order to control smoothness of the search, a relaxation factor ($\omega < 1$) is introduced in Equation (5.13). Larger values of this factor encourage a global swarm attribute, and smaller values motivate a local attribute:

$$\Delta\boldsymbol{\lambda}_{i+1} = \omega\Delta\boldsymbol{\lambda}_i + \boldsymbol{U}(0,\psi_1)(\boldsymbol{\lambda}_p - \boldsymbol{\lambda}_i) + \boldsymbol{U}(0,\psi_2)(\boldsymbol{\lambda}_g - \boldsymbol{\lambda}_i). \tag{5.15}$$

Clerk and Kennedy[64] proposed a formulation with constriction coefficients, that contributes in reducing the sensitivity of the algorithm to the step size, and therefore improving its stability and robustness:

$$\Delta\boldsymbol{\lambda}_{i+1} = \chi(\Delta\boldsymbol{\lambda}_i + \boldsymbol{U}(0,\psi_1)(\boldsymbol{\lambda}_p - \boldsymbol{\lambda}_i) + \boldsymbol{U}(0,\psi_2)(\boldsymbol{\lambda}_g - \boldsymbol{\lambda}_i)), \tag{5.16}$$

where the constriction coefficient χ is obtained by:

$$\chi = \frac{2}{\psi - 2 + \sqrt{\psi^2 - 4\psi}}, \tag{5.17}$$

and $\psi = \psi_1 + \psi_2$, where $\psi > 4$.

Parameters χ, ψ_1 and ψ_2 are optimally adjusted in their study[64]. Based on the promising behavior of this formulation, it is adopted here for implementation of PSO, with the values of $\chi = 0.7298$, and $\psi_1 = \psi_2 = 2.05$[64].

Defining topology as the architecture adopted for communication among the particles in the population, the topology in the above algorithm is known as"gbest", which stems from the fact that besides its own best position, each particle is also communicating with the global best member of the population. Various architectures are designed for implementation of PSO, that also affect local and global search attributes according to the number of the

neighborhoods each particle in the population interacts with[66–68]. The results obtained by the current topology are quite convincing in the applications of this study. However, flexibility of PSO in working with various topologies encourages parallelization in more expensive optimization problems.

5.4 Application: Supersonic Flow over a Circular Cylinder

The nonlinear ROM is constructed by projection of the nonlinear Euler equations onto the POD subspace computed by 101 snapshots in this case. The first 16 POD modes capture 92 percent of the flow energy, and are used to construct the subspace for projection.

Similar to the linear ROM, the nonlinear ROM of this case is highly unstable, with the temporal coefficients shown in Figure 5.1. The POD coefficients are computed by projection of the FOM state onto the low-dimensional space, and the ROM coefficients are computed by numerical integration of the ROM ODEs. The ERN algorithm is then used to stabilize the nonlinear ROM, with $\epsilon = 10^{-5}$, and $\tau = 0.001$. The optimization parameters and results are reported in Table 5.1, where $\Delta\boldsymbol{\lambda}_{max}$ is the maximum step size (velocity), and population represents the number of particles in PSO. The difference between two consecutive best objective function values (among all particles) is chosen as the stopping criterion. The stabilized ROM results shown in this application are obtained by optimization in Domain 1. The problem is also implemented with larger bounds (Domain 2) to exhibit the robustness of the ERN algorithm with respect to the bound constraints. The relative error of 0.31% percent, and the agreement between the POD and ROM coefficients in Figure 5.1 show that this method has successfully stabilized the system and recovered accuracy to match the dynamics of the FOM. Despite the original system is highly unstable, the stabilization algorithm only appends a small computational overhead to the model reduction process. The wall-clock time of the offline stage of model reduction in Table 5.1 includes the time required for constructing the POD modes and construction of the ROM matrices.

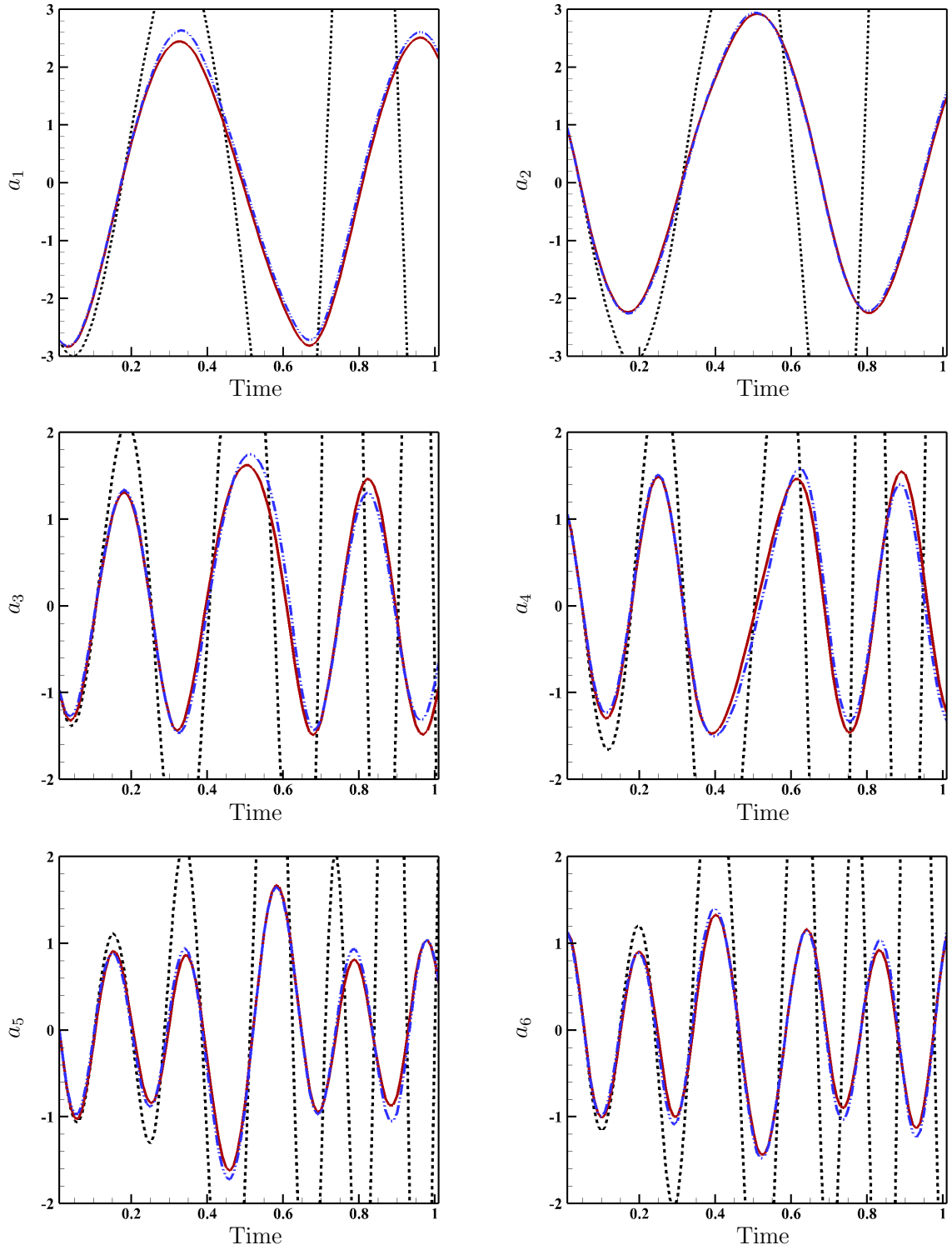

Figure 5.1: Modal coefficients of the 16 mode stabilized nonlinear ROM (- -) compared against the POD coefficients (—), and the unstable nonlinear ROM (------).

Table 5.1: Performance of the ERN algorithm in stabilization of the 16 mode ROM.

	Domain 1	Domain 2
Bound constraints	[-2, 2]	[-100, 50]
$\Delta\boldsymbol{\lambda}_{max}$	1.0	1.0
Population	15	15
Iterations	78	394
Minimum function value	1.71e-02	1.69e-02
Wall-clock time (Sec): ROM (offline): 8.95e+01 ROM (online): 3.30e-03	Stabilization: 1.18e+00	Stabilization: 7.1e+00
Relative error $e\%$	0.31	0.29

Indeed, solving the optimization problem in a larger domain takes more computational effort as reflected by the larger wall-clock time in Domain 2, and may need further adjustment of the population and $\Delta\boldsymbol{\lambda}_{max}$. It is the advantage of the symmetrization that has enabled us to implement the stabilization algorithm within the smaller bounds of Domain 1. ROMs constructed based on the symmetry inner product with certain boundary conditions are known to maintain eigenvalues in the vicinity of the imaginary axis, thus prevent exhausting computational resources for optimization in an excessively large domain[27].

Eigenvalues of the linear term of the nonlinear ROM are shown in Figure 5.2 for the unstable and stabilized POD-Galerkin ROMs. These eigenvalues are the control parameters that are adjusted through the stabilization to reach maximum agreement between the ROM and FOM outputs, or the temporal coefficients in the case of full-state output. Note that there is an eigenvalue pair with a positive real component in the stabilized nonlinear system. Transferring this eigenvalue pair to the left half of the complex plane attenuates the corresponding low-frequency modes, therefore the linear matrix needs to be unstable for the nonlinear ROM to accurately follow the FOM attractor in this case. This could not be captured by linearization, or using a linear stability condition in the optimization problem of the ERN algorithm.

In order to obtain a visual perception of the accuracy in the stabilized ROM, Figure 5.3 shows the stream-wise velocity contours of the FOM and ROM reconstruction at a specific

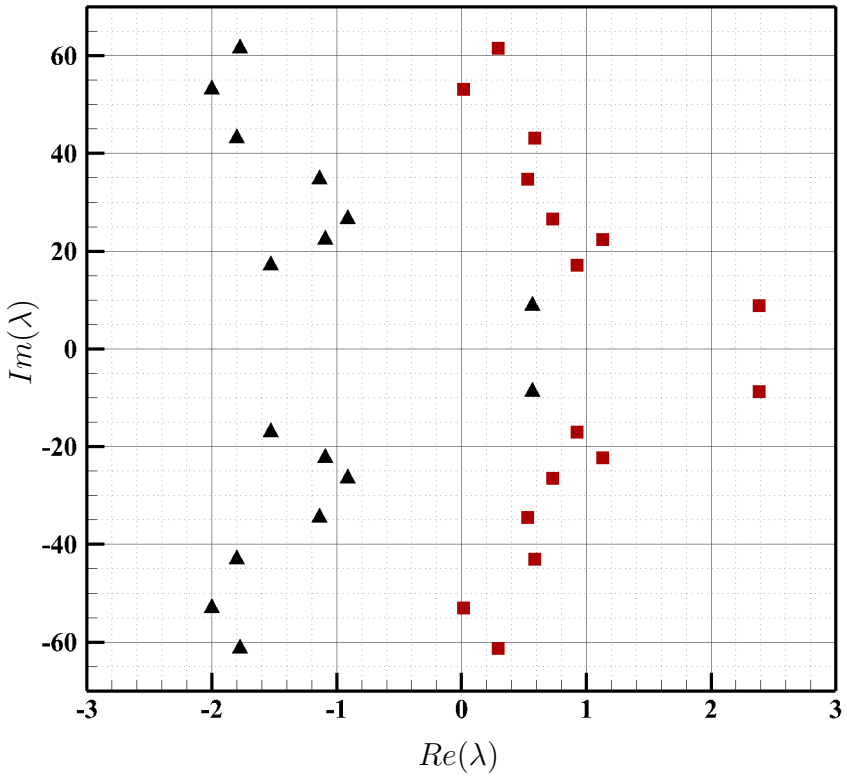

Figure 5.2: Eigenvalues of the linear term in the 16 mode unstable (■), and stabilized (▲) ROMs.

time instant. The agreement between the stabilized ROM and the high-fidelity simulations is a result of the direct monitoring of accuracy in the stabilization method.

The ultimate goal in constructing ROMs is to facilitate accurate replication of the dynamics of the FOM almost independently of the high-fidelity snapshots. One way to discover the ability of ROMs to stand alone in a flow control or optimization setup is to observe the predictive performance of the model, that is, to track the dynamics predicted by the ROM beyond the interval of the snapshots that have been originally used to construct the low-dimensional space. Figure 5.4 compares the temporal coefficients predicted by the stabilized ROM beyond the interval of the 101 snapshots that are used to construct the subspace. The POD coefficients in this figure serve as the reference, and are computed by projection of the FOM state in the reconstruction and prediction interval (i.e. 601 snapshots) onto the

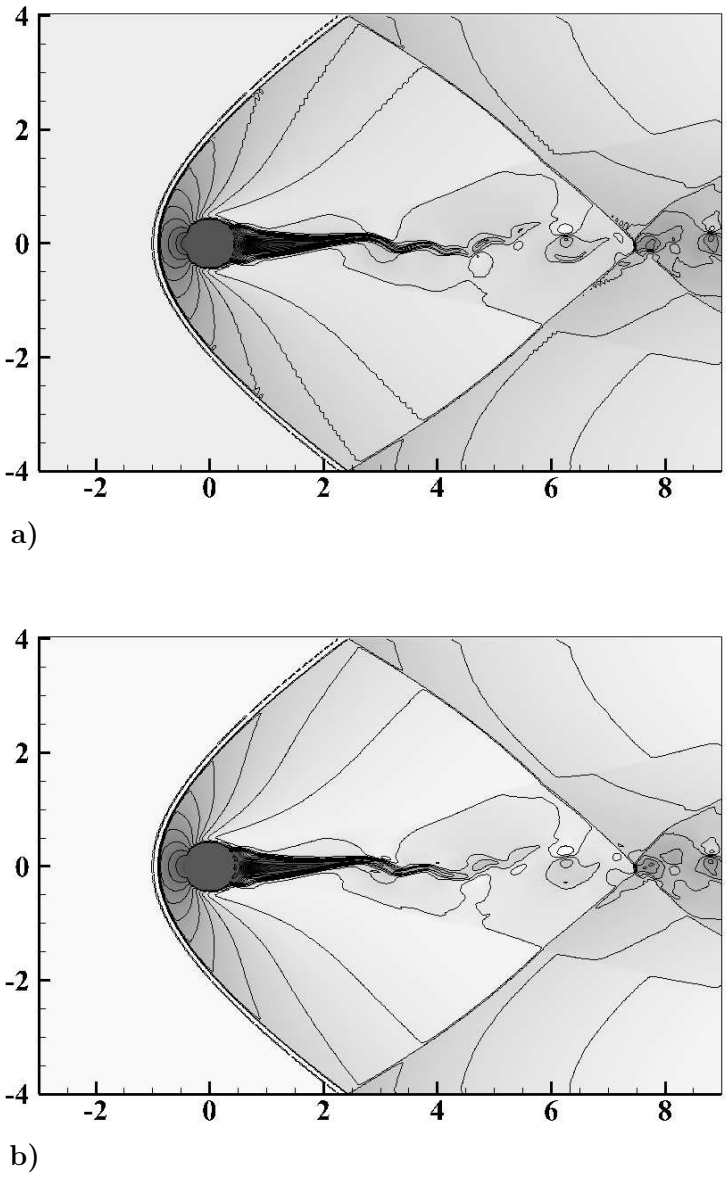

Figure 5.3: Stream-wise velocity contours of the snapshot at $t = 0.65$, computed by a) FOM, and b) the 16 mode nonlinear ROM stabilized with the ERN algorithm. Non-dimensional time is computed from the beginning of the snapshot collection for model reduction. Contour lines are plotted within the range of -2.5 to 5.5.

POD modes obtained by the 101 snapshots of the reconstruction interval alone. The stabilized ROM coefficients remain in good agreement with the true dynamics in the prediction window.

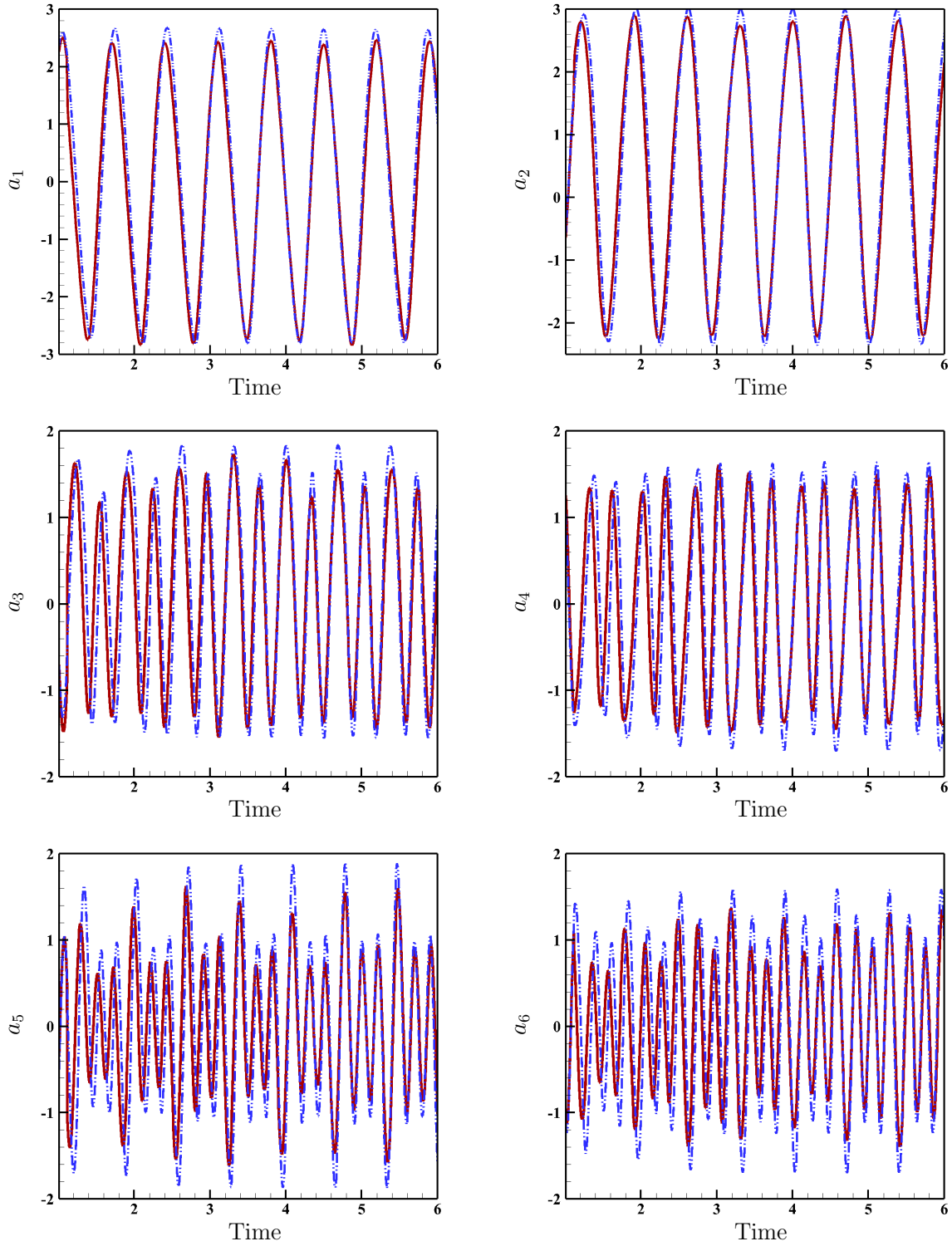

Figure 5.4: Prediction of the temporal coefficients by the 16 mode stabilized ROM ( ), compared against the POD coefficients ( ) obtained by projection of 601 snapshots onto the POD modes of the first 101 snapshots.

Chapter 6

Stabilization of ROMs in Strongly Nonlinear Systems

The standard model order reduction procedure by POD-Galerkin projection does not guarantee the closure of reduced-order dynamical systems, thus the stability and accuracy of the models may be compromised when the dynamically observable signatures are not populated in low-frequency responses. The situation is further complicated in advection-dominated flows, and in general strongly nonlinear systems, where capturing the nonlinearity with a linear subspace requires a lot of base functions[22;29;51]. Thus the typically larger dimension of ROMs in these systems makes stabilization expensive, and even intractable in higher dimensions. Efficient stabilization algorithms are therefore essential to the projection-based model reduction procedure.

Supersonic flows governed by the Euler equations, that ignore any physical dissipation mechanism by the viscous effects, are the extreme example for advection-dominated flows. When strong unsteady shock-wake interactions, a highly nonlinear phenomenon, are present in the flow, a linearized ROM is not accurate even after stabilization. A nonlinear ROM on the other hand may keep the accuracy after stabilization, but requires a fairly large number of bases for convergence. Despite its computational efficiency in smaller ROMs, the ERN algorithm becomes computationally more expensive and may fail as the number of unstable

modes increases in ROMs with larger number of bases. The importance of this aspect culminates as the large number of control parameters (i.e. unstable modes) also complicates the optimization landscape and impairs accuracy.

To solve this problem in the stabilization of relatively large-size nonlinear ROMs, a multi-stage approach is proposed to divide the optimization process of the ERN algorithm into a few stages, where each stage contains only a small number of unstable modes for an overall more efficient and robust algorithm. It is shown that the computational cost and accuracy of the ERN algorithm significantly benefits from the new stabilization layout. This chapter explains the framework of the multi-stage layout, and the results of its application to the nonlinear ROM created from the snapshots of supersonic flows over the triangular prism, and the circular cylinder.

6.1 The Multi-Stage Stabilization Layout

Global optimization of the objective function that is computed by integration of the nonlinear ROM ODEs in the ERN algorithm can become expensive as the number of modes increases. It is shown in previous studies that robustness of the symmetry ROMs makes them amenable to local optimization[27]. Nevertheless, the computation cost of the stabilization methods typically rises nonlinearly with the number of unstable modes[15;34]. POD-based model reduction of highly nonlinear systems on the other hand is challenged by demanding a large number of POD modes to sufficiently describe the flow field. This is a direct consequence of the linearity of the POD subspace, and is recently addressed by using nonlinear manifolds instead, which introduce other sources of computational and theoretical complications (e.g. in computing the manifold itself, projection, and hyper-reduction over the generally non-orthogonal manifold)[22;23].

A multi-stage layout is proposed in this work that facilitates robust stabilization with the ERN algorithm, in strongly nonlinear systems that require a larger linear subspace for the ROM to accurately replicate the dynamics of the high-dimensional system. This is achieved by constructing and stabilizing a few smaller ROMs, and using their eigenvalues to accelerate

stabilization of the larger ROM.

Assuming that a stable ROM of dimension M is the final target of the multi-stage stabilization method, P ROMs of dimensions $r_1, r_2, \ldots, r_P$ are constructed, where $r_{(\cdot)} < M$. The ERN method shown in Algorithm 1 is used to stabilize the smallest ROM (of dimension r_1). In the next stage, the ROM of dimension r_2 is stabilized with the same method. However, this time the first r_1 eigenvalues of the ROM are frozen at the values obtained by stabilization of the smaller (r_1-dimensional) ROM, and the remaining $(r_2 - r_1)$ eigenvalues are reassigned by Algorithm 1 using global optimization. This process is repeated up to the last stage (i.e. stabilization of the target M-dimensional ROM). Unlike the previous stages, the first r_P eigenvalues of the M-dimensional ROM are not frozen at the values obtained by stabilization of the r_P-dimensional ROM, which are instead used to initialize local optimization of the first r_P eigenvalues in the M-dimensional ROM for further calibration, while the remaining $(M - r_P)$ eigenvalues are obtained by global optimization. At each stage, the eigenvalues entering global optimization are initialized randomly. Implementation of this stabilization layout is described in Algorithm 3.

Local optimization is here approximated by enhancing exploitation, and damping exploration in the optimization solver. This can be easily achieved by controlling the optimization parameters in any global optimization solver. In the case of PSO, this adjustment is applied by reducing the upper-limit on the step size ($\Delta\lambda_{max}$).

The procedure can therefore be parameterized based on the step size as shown in Figure 6.1. Stages with global optimization are characterized by a larger step size that allows for

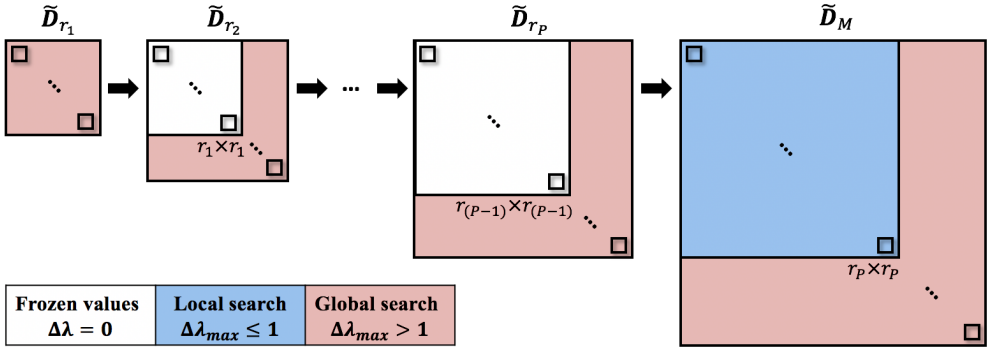

Figure 6.1: Schematic of the multi-stage stabilization layout.

exploration, the local optimization of the first r_P eigenvalues in the last stage is achieved by a relatively smaller step size that facilitates exploitation, and the frozen eigenvalues in the intermediate stages are referenced with zero step size.

Algorithm 3 Multi-stage stabilization algorithm

Input: POD temporal coefficients $\boldsymbol{a}_{(POD)}$, matrix $\boldsymbol{A}_{(\cdot)}$, and tensor(s) of the unstable ROMs of dimensions $r_1, \ldots, r_P, M$.

Output: Modified matrix $\tilde{\boldsymbol{A}}_M$ that stabilizes the nonlinear M-dimensional ROM.

1. **for** $m = 1, \ldots, P$ **do**
2. Diagonalize matrix $\boldsymbol{A}_{r_m}$:
$$\boldsymbol{A}_{r_m} = \boldsymbol{V}_{r_m} \boldsymbol{D}_{r_m} \boldsymbol{V}_{r_m}^{-1}.$$
3. **if** $m = 1$ **then**
4. Use Algorithm 1 (steps 2 to 4) to stabilize the ROM with global optimization.
5. **else**
6. **for** $i = 1, \ldots, r_{m-1}$ **do**
7. $\tilde{\lambda}_i^{r_m} = \tilde{\lambda}_i^{r_{m-1}}$, where i is the eigenvalue index, and the superscript shows the dimension of the ROM the eigenvalue belongs to.
8. **end for**
9. Use Algorithm 1 (steps 2 to 4) to reassign the remaining $(r_m - r_{m-1})$ eigenvalues with global optimization.
10. **end if**
11. **end for**
12. Diagonalize matrix $\boldsymbol{A}_M$.
13. **for** $i = 1, \ldots, r_P$ **do**
14. Initialize $\tilde{\lambda}_i^M = \tilde{\lambda}_i^{r_P}$.
15. **end for**
16. Use Algorithm 1 (steps 2 to 4) to calibrate the first r_P eigenvalues of the M-dimensional ROM with local optimization, and reassign the remaining $(M - r_P)$ eigenvalues with global optimization.

6.2 Application I: Supersonic Flow over a Triangular Prism

The unsteady shock-wake interactions in this case are not properly resolved by the leading POD modes. Under inviscid flow assumptions, this aspect creates highly unstable ROMs[15;34;37]. Unlike the diffusion-dominated flows, energy accumulation by the POD modes is rather slow here in converging to the energy of the FOM, thus demanding a larger number of modes (in this case 60). In the mean time, a linear ROM is not capable of accurately representing the flow field as a result of the strongly nonlinear nature of the shock-wake interactions. Therefore, an efficient stabilization method is required that can recover the rather large nonlinear ROM of this problem.

According to the normalized cumulative energy shown in Figure 6.2, at least 28 modes are required to capture above 90 percent of the flow energy. The POD-Galerkin ROM of this case is constructed based on the first 60 POD modes that capture nearly 96 percent of the energy.

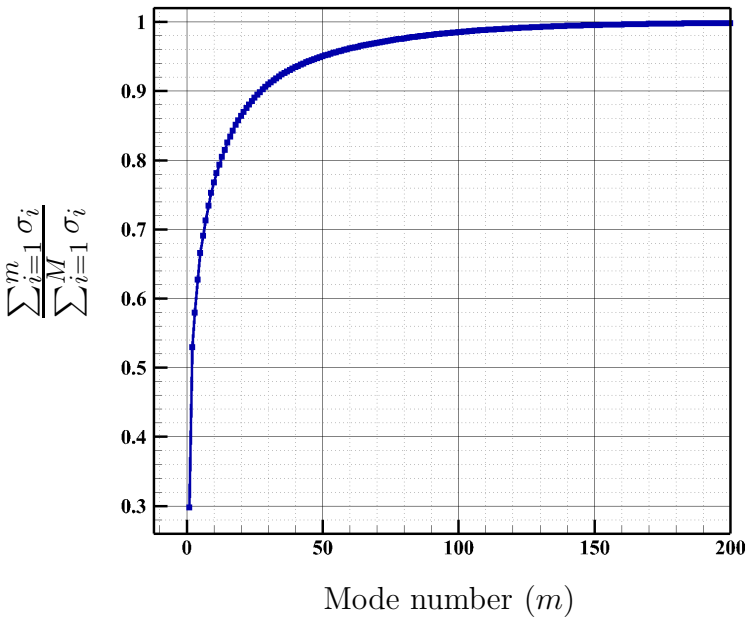

Figure 6.2: Normalized cumulative energy of the POD modes computed with the symmetry inner product.

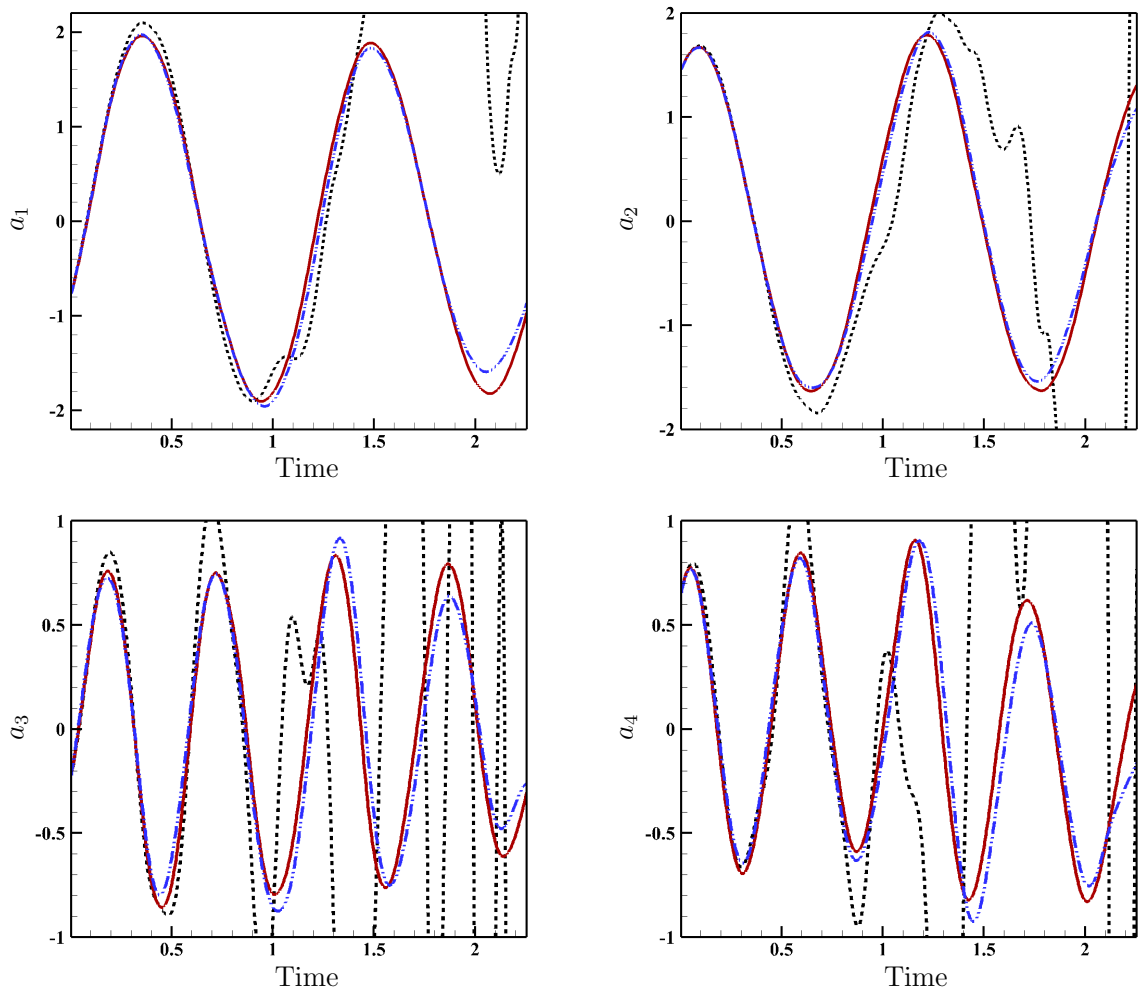

Figure 6.3: Modal coefficients of the 60 mode nonlinear ROM stabilized by the multi-stage layout (- - -), compared against the POD coefficients (——), and the unstable ROM (·····).

The temporal coefficients of the originally unstable ROM is shown in Figure 6.3, that also compares the ROM coefficients against the POD coefficients obtained by projection of the state onto the POD subspace. Applying the bare bone ERN algorithm for the stabilization of the 60 mode ROM of this case becomes expensive. Thus, the multi-stage configuration is implemented to reduce the computational cost of the stabilization.

Table 6.1 lists the optimization parameters and the results obtained by the vanilla ERN algorithm, and those by the multi-stage configuration, both applied with $\epsilon = 10^{-8}$, and $\tau = 0.02$. In the multi-stage configuration, $P = 3$, and ROMs of dimensions $r_1 = 16$, $r_2 = 30$, and $r_3 = 50$ are constructed for the stabilization of the 60 mode ROM. Local optimization

of the first 50 eigenvalues is in this method achieved with a smaller upper-bound on the step size (i.e. $\Delta\boldsymbol{\lambda}_{max} = 1.0$), and the larger upper-bound of $\Delta\boldsymbol{\lambda}_{max} = 10.0$ encourages a global search attribute in reassigning the remaining eigenvalues. Using global optimization for the reassignment of all 60 eigenvalues in the vanilla ERN algorithm requires a larger population, which eventually adds up to a high computational cost that is in the same order as the offline phase of the model reduction. Thus, the vanilla ERN algorithm can become intractable in larger ROMs, that commonly arise in fluid flows with strong nonlinearities. Implementation of this algorithm with the multi-stage layout has reduced the wall-clock time by one order of magnitude. The small relative error and the temporal coefficients in Figure 6.3 show that the stabilized system is evolving on the same attractor as the FOM, and closely follows the original dynamics. The ROM results shown in this application are obtained by the multi-stage layout, and the details of the vanilla ERN algorithm are merely discussed in Table 6.1 for the matter of comparison.

Table 6.1: Performance of the ERN and multi-stage ERN algorithms in stabilization of the 60 mode ROM. In the multi-stage layout, only the values of the last stage of optimization are reported, unless otherwise noted.

	Vanilla ERN	Multi-stage ERN
Bound constraints	[-120, 2]	[-120, 2]
Population	50	15
$\Delta\boldsymbol{\lambda}_{max}$	5.0	1.0 (local), 10.0 (global)
Iterations	583	106
Minimum function value	5.42e-02	4.16e-02
Wall-clock time (Sec)		
Stabilization:	1.76e+04	1.32e+03 (4 stages)
ROM (offline):	2.08e+04	3.19e+04 (4 stages)
ROM (online):	6.55e-01	6.55e-01
Relative error $e\%$	3.12	0.47

Figure 6.4 shows the distribution of the eigenvalues of the linear term in the unstable and stabilized nonlinear ROMs. Similar to the previous application, some of the eigenvalue pairs in the stabilized system have taken a positive real component. Likewise, a negative real component in the eigenvalues of the original system do not necessarily mean that those

eigenmodes are originally stable. The location of the eigenvalues of the linear term in a strongly nonlinear system cannot be used to identify the stability or instability of the nonlinear system, but they are merely treated as the control parameters in the ERN algorithm to facilitate the modification of the nonlinear ROM in order to guide the system towards maintaining a negative total power (that guarantees the stability of the nonlinear ROM), and maximum agreement with the FOM dynamics.

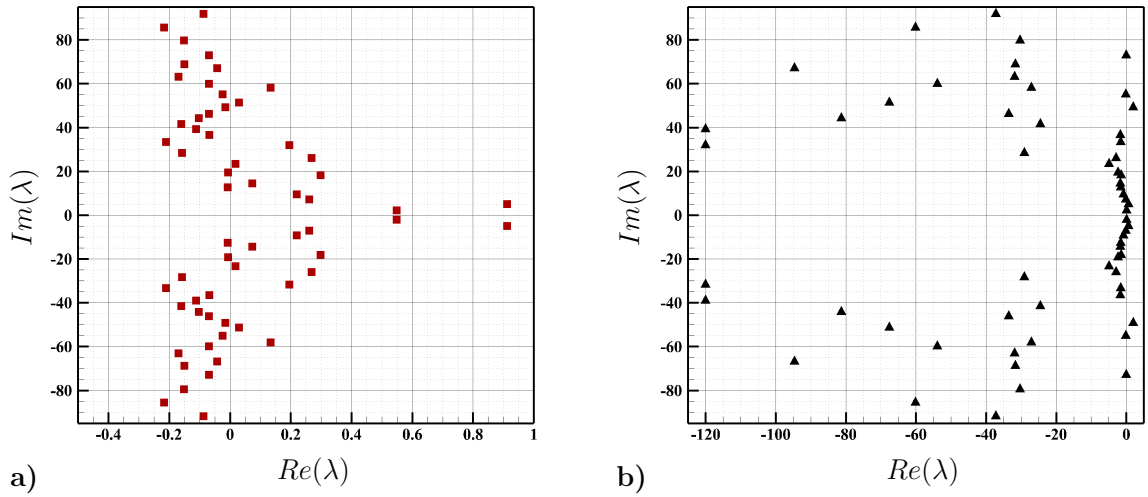

Figure 6.4: Eigenvalues of the 60 mode a) unstable, and b) stabilized ROMs.

Stream-wise velocity contours of the snapshot at $t = 1.02$ in Figure 6.5 visualize the similarity between the flow structures captured by the FOM, and those reconstructed by the stabilized nonlinear ROM.

Performance of the stabilized ROM in the prediction window is shown in Figure 6.6, where the ROM coefficients are compared against the POD coefficients obtained by projection of 1650 snapshots of the FOM onto the POD subspace constructed based on the first 550 snapshots. Despite the large number of control parameters, the stabilized ROM predicts the dynamics of the flow with reasonable accuracy.

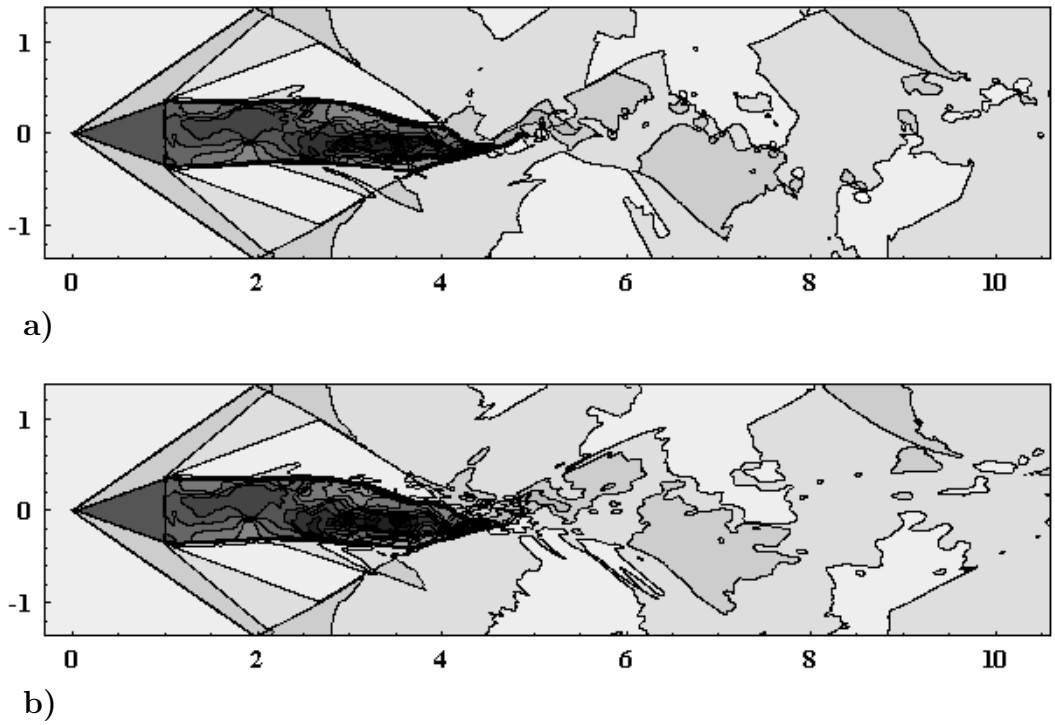

Figure 6.5: Stream-wise velocity contours of the snapshot at $t = 1.02$, computed by a) FOM, and b) 60 mode nonlinear ROM. Non-dimensional time is computed from the beginning of the snapshot collection for model reduction. Contour lines are plotted within the range of -2.5 to 4.5.

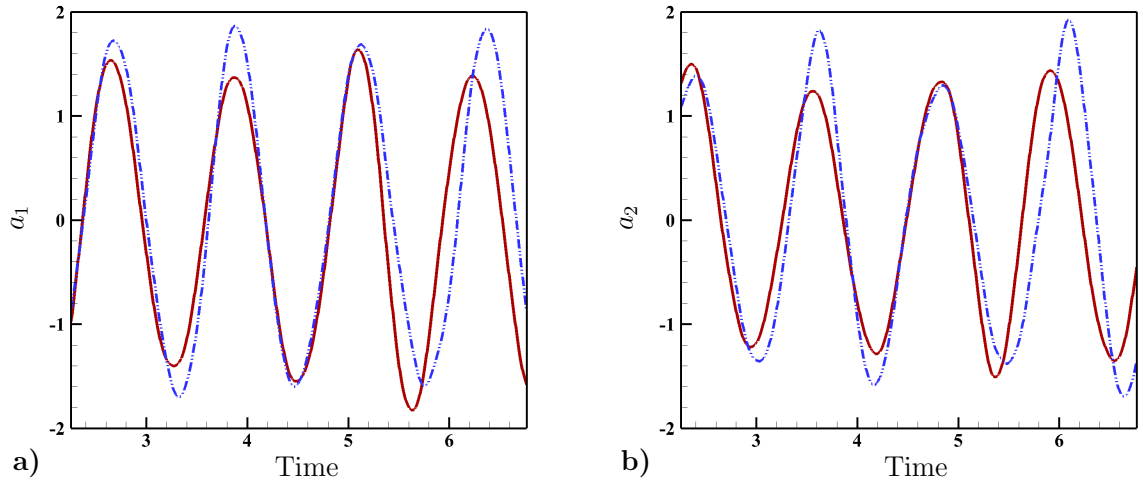

Figure 6.6: Prediction of the a) first, and b) second temporal coefficients by the 60 mode stabilized ROM ( ) and compared against the POD coefficients ( ) obtained by projection of 1650 snapshots onto the POD modes of the first 550 snapshots.

6.3 Application II: Supersonic Flow over a Circular Cylinder

According to the results shown in the previous chapters, the first 16 POD modes are sufficient in this application to capture most of the flow energy, and stabilization of the 16 mode ROM with the ERN algorithm has recovered the stability and accuracy within a small computation cost, when compared to the offline phase of model reduction. In the meantime, the linear ROM of this case that is constructed based on the linearized Euler equations, has more or less recovered the accuracy of the FOM. This is not surprising, as the unsteady shock oscillations caused by the shock-vortex interactions in this case maintain smaller amplitudes compared to the case of supersonic flow over the triangular prism. Large-amplitude oscillations of the reflected shock waves in the latter, intensify the nonlinearity, that on one hand requires a much larger number of POD modes to capture the true physics of the flow, and on the other hand degrades accuracy in a linear ROM.

Knowing that the existence of strong nonlinearities is the norm rather than exception in practical applications, it is important to probe the performance of the stabilization algorithm as the number of unstable modes increases, and the optimization landscape becomes more complicated. Theoretically, as the dimension of ROM increases, the additional information that is absorbed in the low-dimensional space is expected to improve the stability and accuracy of the model. In practice however, it is often the case that the numerical errors encountered with the high-frequency modes contaminate the subspace and trigger larger instabilities in the ROM. A similar situation occurs in this application. Thus, the more complicated, and more unstable control landscape of an 80 mode ROM is used to challenge the ERN algorithm, and investigate the potential of the multi-stage layout to deliver robust stabilization.

The multi-stage layout is implemented with $P = 3$, and ROMs of dimensions $r_1 = 16$, $r_2 = 30$, and $r_3 = 50$, are constructed and stabilized to guide the optimization solver through the stabilization of the 80 mode ROM using algorithm 3. Table 6.2 shows the performance

of the vanilla, and multi-stage ERN algorithms. The penalty term is applied with $\epsilon = 10^{-5}$, and $\tau = 0.001$. Population, and $\Delta\boldsymbol{\lambda}_{max}$ are the hyper-parameters that facilitate adjusting the search attribute in PSO. In the multi-stage layout, the smaller value of $\Delta\boldsymbol{\lambda}_{max}$ enhances exploitation towards modeling a local behavior for fine-tuning the eigenvalues corresponding to the low-frequency response, and the larger $\Delta\boldsymbol{\lambda}_{max}$ belongs to the remaining 30 eigenvalues that are reassigned with global optimization. Similarly, a larger population is adopted in the vanilla ERN algorithm to improve the global search in the absence of the guidance from the smaller ROMs.

Table 6.2: Performance of the ERN and multi-stage ERN algorithms in stabilization of the 80 mode ROM. In the multi-stage layout, only the values of the last stage of optimization are reported, unless otherwise noted.

	Vanilla ERN	Multi-stage ERN
Bound constraints	[-120, 5]	[-120, 5]
Population	30	15
$\Delta\boldsymbol{\lambda}_{max}$	10.0	1.0 (local), 10.0 (global)
Iterations	949	326
Minimum function value	3.51e-02	3.42e-02
Wall-clock time (Sec)		
Stabilization:	1.30e+04	2.32e+03 (4 stages)
ROM (offline):	6.32e+03	8.29e+03 (4 stages)
ROM (online):	4.55e-01	4.55e-01
Relative error $e\%$	0.26	0.28

According to the values of the relative error, accuracy has been recovered by both algorithms, though the wall-clock time shows that the multi-stage approach has reduced the cost of stabilization by one order of magnitude, and the computational saving delivered by this layout dominates the additional offline cost of constructing the smaller ROMs. Thus, the multi-stage approach has provided a robust framework for the stabilization of the 80-dimensional nonlinear ROM with the ERN algorithm. Figure 6.7 shows that stabilization has recovered the accuracy in the originally unstable 80 mode ROM coefficients. Performance of the linear and nonlinear ROMs of this case are visualized in the previous chapters, hence repeating the illustration of the reconstructed flow field is avoided here for the 80 mode

ROM that is merely constructed for the purpose of comparing the computational efficiency of the vanilla and multi-stage ERN algorithms.

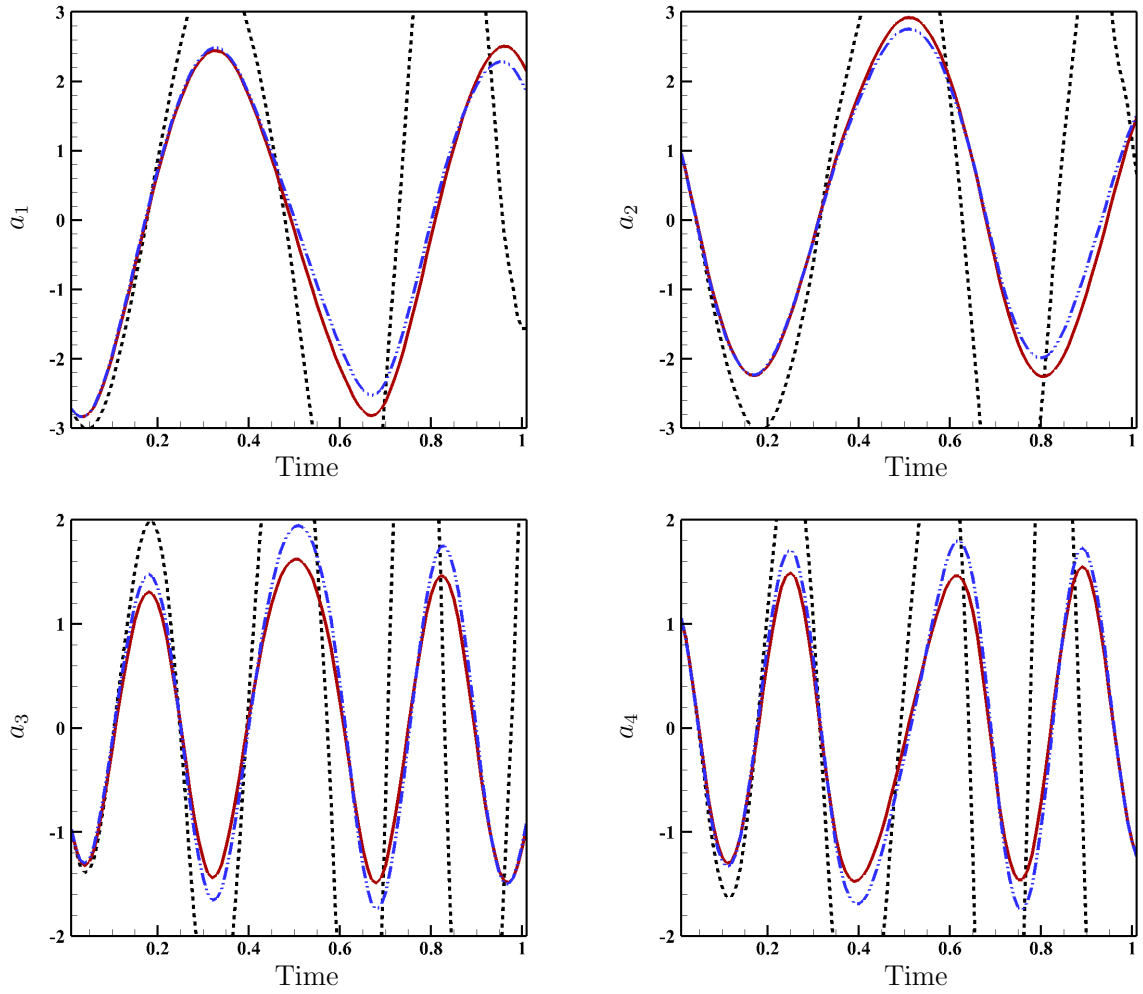

Figure 6.7: Modal coefficients of the 80 mode nonlinear ROM stabilized by the multi-stage layout (- - -), compared against the POD coefficients (——), and the unstable ROM (·····).

Chapter 7

Impact of Symmetrization on the Robustness of ROMs

Proper Orthogonal Decomposition (POD) retains the most energetic modes for construction of the low-dimensional space. POD is popular for its computational efficiency as it captures the most energy by the fewest number of modes among linear dimensionality reduction methods. However, the most energetic structures are not always the only principal components that drive the flow dynamics. Turbulent flows and compressible flows with unsteady shock waves are examples in which an energy-based metric is not merely sufficient for identification of the most informative low-dimensional space[14;15;31;34;37;69;70]. This issue has been addressed to some degree in the dimensionality reduction methods with balancing transformations, such as Balanced Truncation[44] and Balanced Proper Orthogonal Decomposition (BPOD)[9;71], by transforming the system to the coordinates in which the leading modes correspond to the most observable directions that are also the most controllable.

The influence of the inner product definition is taken for granted in BPOD, where the observability Gramian of the snapshot data naturally arises as the inner product in the model reduction routine. On the other hand, better stability properties of the symmetrized equations has inspired the use of a symmetrizing matrix to derive inner products in POD-Galerkin ROMs. Previous studies have shown that when the governing equations are symmetrizable,

using the symmetry inner product in construction of ROMs preserves the stability of the high-fidelity numerical simulations through model reduction[24;26]. Similar stability bounds are also guaranteed in the least-squares Petrov-Galerkin projection by optimal projection in a least-squares problem that minimizes the residual in the low-dimensional representation of the original nonlinear system[10;28]. This research pushes the horizons of the impact of symmetrization farther by showing that using the symmetry inner product in the POD-Galerkin ROMs of compressible flows not only improves their stability properties, but makes them more controllable, and enhances their robustness[27].

In this chapter, the eigenvalue reassignment method of Kalashnikova et al.[30] (ER), and the ERN algorithm[27;72] are used for the stabilization of the linear and nonlinear ROMs that are separately constructed by L^2 or symmetry inner products. The ER method also is implemented here with a global optimization algorithm (PSO) in order to ensure that the solver is not trapped in local minima that compromise the comparison of the influence of the inner product definition on the performance of ROMs. The results show that although both models are originally unstable, the symmetry ROM is more stable than the L^2 ROM. After stabilization, an analysis of the controllability Gramians of the stabilized linear ROMs shows that the symmetry ROM has a larger controllable space, which facilitates feasible and efficient placement of the system poles for maximum resemblance with the original full-order system. On the other hand, the small controllable space and complicated control landscape of the L^2 ROM prevents optimal modification of the eigenvalues, and increases the optimization cost. Decomposition of the controllability Gramians shows that the symmetry ROM is more controllable than the L^2 ROM in most directions. Similarly, the smooth control landscape of the nonlinear symmetry ROM has substantially enhanced its robustness with respect to sub-optimal control laws, which results in the accuracy of the dynamics predicted by the symmetry ROM, regardless of the type of the optimization solver implemented for stabilization.

The controllability and sensitivity approaches adopted to examine the control space of the L^2 and symmetry ROMs are explained in this chapter. Then the L^2 and symmetry ROMs based on the snapshots of the two supersonic flow applications are compared before

and after stabilization.

7.1 Controllability Analysis in the Linear ROMs

The main objective in control and stabilization of ROMs is to drive the system towards maximum agreement with the FOM, which is implemented in the ER and Hybrid methods through an optimization process that minimizes the deviation of the ROM output from the FOM output. A full-ranked controllability matrix in an LTI system indicates that the system is controllable in all directions. However, the extent to which one succeeds in keeping the controlled (stabilized) ROM close to the FOM, and how challenging it is to do so through solving the optimization problem is the matter of the degree of controllability. This is a criterion that cannot be determined merely by the rank of the controllability matrix, and is rather defined by the controllability Gramian of the stabilized system. The controllability Gramian is a hermitian matrix with real eigenvalues, that provides a relative measure of the required actuation energy at each direction to drive the system towards any state. The determinant of this Gramian represents the volume of the controllable space, which if consistent in all directions, it can explain the smooth or otherwise difficult behavior of the system in being controlled towards the desired state; in this case maximum agreement with the FOM.

Kalashnikova et al.[30] have shown that for the LTI system in (4.3), ER is equivalent to full-state feedback control with control input $\boldsymbol{u} = -\boldsymbol{K}\boldsymbol{x}_M$ and the specific choice of $\boldsymbol{B}_M$ and $\boldsymbol{K}$ matrices:

$$\boldsymbol{B}_M = \begin{bmatrix} \boldsymbol{V}_1 & \boldsymbol{V}_2 & \dots & \boldsymbol{V}_M \end{bmatrix}, \tag{7.1}$$

$$\boldsymbol{K} = \begin{bmatrix} \lambda_1^u - \tilde{\lambda}_1 & 0 & 0 & \dots & 0 \\ 0 & \lambda_2^u - \tilde{\lambda}_2 & 0 & \dots & 0 \\ \vdots & \vdots & \ddots & \vdots & \vdots \\ 0 & 0 & 0 & \lambda_M^u - \tilde{\lambda}_M & 0 \end{bmatrix} \boldsymbol{V}^{-1}, \tag{7.2}$$

where λ^u is the unstable eigenvalue and $\tilde{\lambda}$ is the new eigenvalue assigned by ER. This definition, that is not immediately available for the ISC and therefore Hybrid methods, has made it possible to compute the controllability matrix and Gramian for the L^2 and symmetry ROMs that are stabilized by ER in this study. The analysis is then used to explain certain similar behavior observed in stabilization of ROMs by ISC and Hybrid methods as well. To that end, the controllability matrix $\mathscr{C}$ is computed for the LTI system (4.3) with the control matrix $\boldsymbol{B}_M$ shown in Equation (7.1):

$$\mathscr{C} = \begin{bmatrix} \boldsymbol{B} & \boldsymbol{A}\boldsymbol{B} & \boldsymbol{A}^2\boldsymbol{B} & \dots & \boldsymbol{A}^{M-1}\boldsymbol{B} \end{bmatrix}. \tag{7.3}$$

The subscripts M of the reduced-order matrices are dropped for simplicity. Matrix $\mathscr{C}$ is full-rank for all of our ROMs and the systems are controllable regardless of the definition of the inner product. Therefore, the controllability Gramian $\boldsymbol{W}_{\mathscr{C}}$ of the stabilized ROMs is:

$$\boldsymbol{W}_{\mathscr{C}} = \int_0^\infty e^{(\boldsymbol{A}\epsilon)}\boldsymbol{B}\boldsymbol{B}^T e^{(\boldsymbol{A}^T\epsilon)} d\epsilon. \tag{7.4}$$

The determinant of this Gramian is then used to reveal the connection between the volume of the controllable space in the L^2 or symmetry ROMs and the performance of the stabilization algorithms in driving the ROMs towards the desired state. It should be noted that since the optimization problem in the ER method is not necessarily convex, global optimization (PSO) is used in this chapter for the stabilization of the linear ROM also, to improve the robustness of the stabilization, and enable a more accurate comparison of the controllable space in the L^2 and symmetry ROMs.

7.2 Sensitivity Analysis in the Nonlinear ROMs

One way of quantifying the robustness of the nonlinear ROMs is to observe the sensitivity of these models to sub-optimal control laws through the stabilization. The choice of a population-based global optimization solver allows us to easily achieve this by variation of the

number of optimization agents. Thus, by decreasing the number of particles in PSO, search attribute gradually changes from global to local, where the local search results deliver the desired sub-optimality for the sensitivity study. In order to clear the analysis from the effects of random initialization of the particles, and the random coefficients in the PSO formulation, each population is tested through five trials with constant and consistent hyperparameters (i.e. bound constraints and $\Delta\boldsymbol{\lambda}_{max}$). This factor prevents contamination of the results with the influence of multiple hyperparameters, and enhances sub-optimality of the local search results without the help of hyperparameter adjustments. The upper limit on the step size ($\Delta\boldsymbol{\lambda}_{max}$) in PSO is adjusted for the largest population through the sensitivity analysis in each application. In order to accurately capture the global minimum point (i.e. the optimal control law) as the population decreases, this hyperparameter has to be re-adjusted (increased) to allow for adequate exploration of the search space by the smaller population. Therefore, keeping $\Delta\boldsymbol{\lambda}_{max}$ constant while decreasing the population, introduces the desired sub-optimality for the sensitivity study.

7.3 Application I: Supersonic Flow over a Circular Cylinder

In order to study the influence of the inner product definition on the performance of the linear and nonlinear ROMs of this case, L^2 and symmetry inner products are separately used to construct the POD modes that serve as the low-dimensional space for both linear and nonlinear ROMs. Figure 7.1 shows the cumulative energy captured at each mode number using each of the inner product definitions. The energy captured by both sets of POD modes converges to more than 99 percent of the total energy at 38 modes for the L^2 inner product, and 49 modes for the symmetry inner product. The first 16 POD modes that are used to build the linear and nonlinear ROMs capture about 90 percent of the flow energy with the L^2, and 84 percent with the symmetry inner product. Figures 7.2, and 7.3 demonstrate the first eight POD modes of the vertical component of velocity, computed by the L^2 and

symmetry inner products.

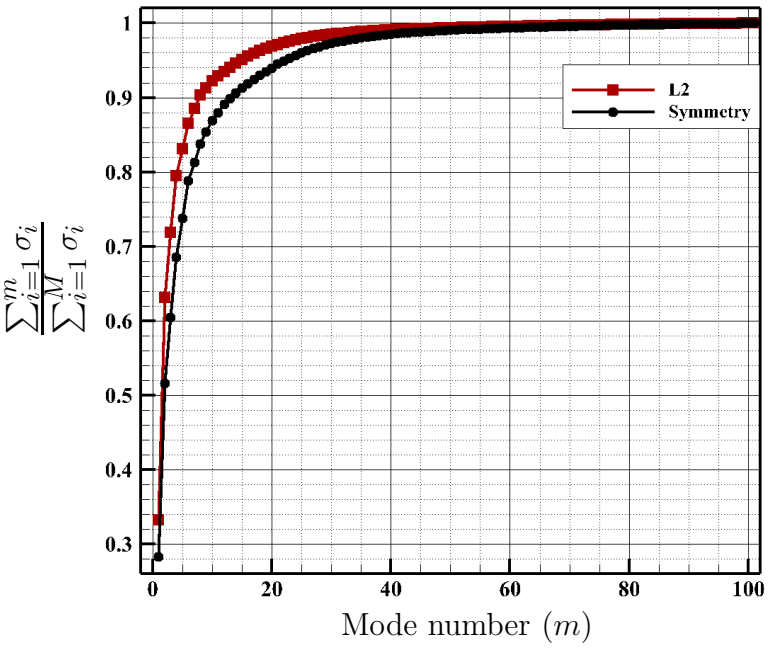

Figure 7.1: Normalized cumulative energy of the POD modes computed by L^2 and symmetry inner products.

The linear ROM is constructed first using L^2 and symmetry inner products separately to project the linearized Euler equations onto the subspace generated by the same inner product definition. Note that each reduced-order modeling procedure involves only one inner product definition through both dimensionality reduction, and projection steps, resulting in two ROMs: an L^2 ROM, and a symmetry ROM. Both of these ROMs are initially unstable, with eigenvalues shown in Figure 7.4. The eigenvalue configurations in this figure agree with the analysis of Tabandeh et al.[26] in Equation (3.16), showing that for the symmetry ROM, the eigenvalues of the linear matrix L_{ij} are close to the imaginary axis. According to Figure 7.4, the maximum real part (Re_{max}) among the eigenvalues of the unstable symmetry ROM is 2.4, while in the L^2 ROM, $Re_{max}(\lambda^u) = 11.5$. Thus, the original symmetry ROM is more stable than the L^2 ROM.

In the next step, the ER method is implemented with PSO to stabilize the two linear ROMs. Table 7.1 shows the global optimization parameters and results. According to this

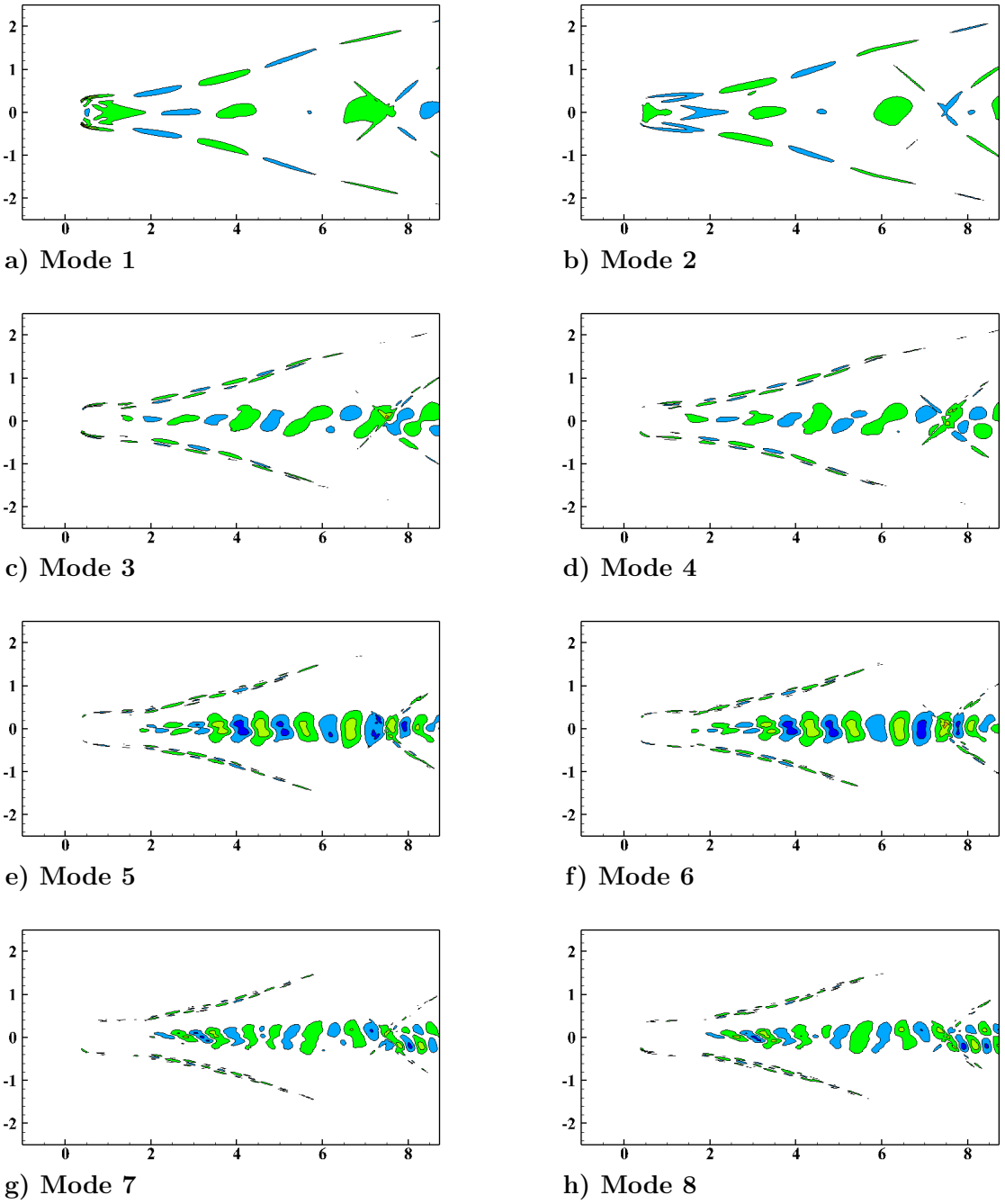

Figure 7.2: POD modes of the vertical component of velocity constructed by the L^2 inner product.

table, compared to the L^2 ROM, the symmetry ROM is more accurate, with almost the same computation cost. Eigenvalues of the stabilized ROMs in Figure 7.4 however show that in the symmetry ROM, with the eigenvalues that are fairly close to the imaginary axis, the

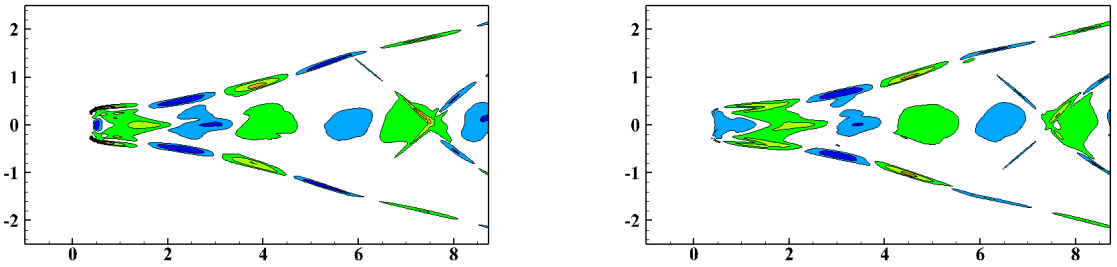

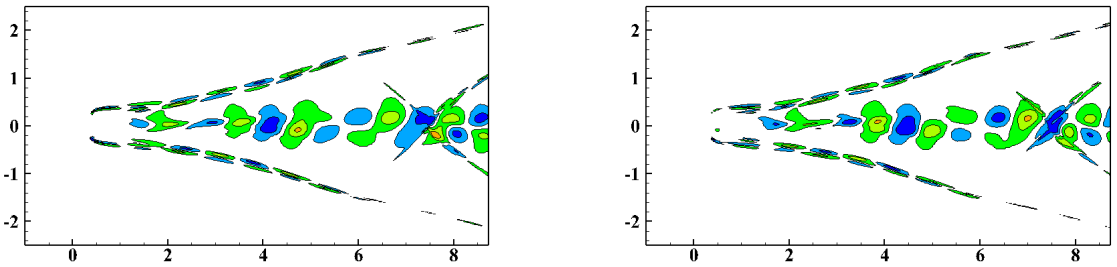

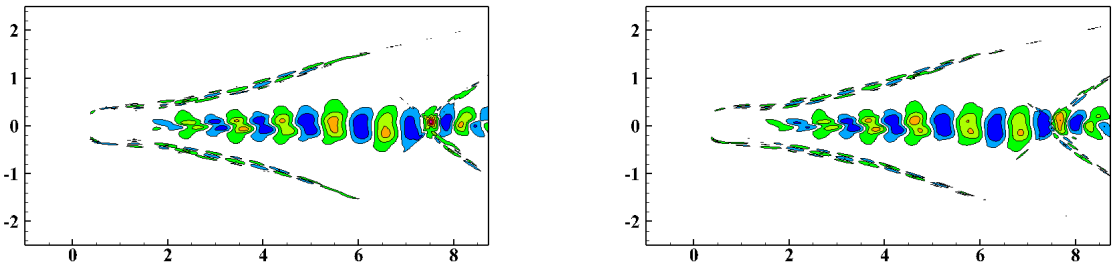

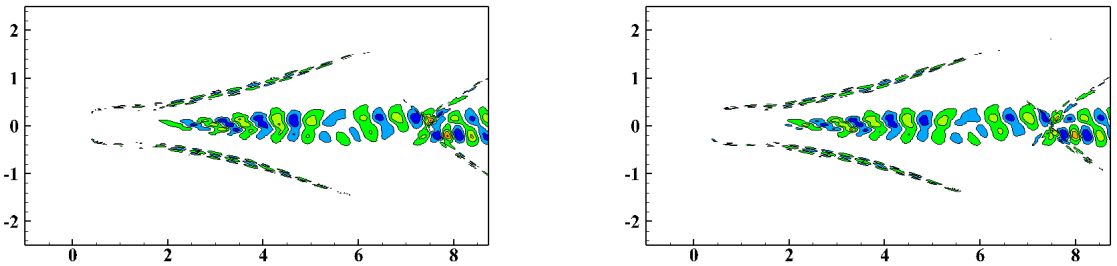

Figure 7.3: POD modes of the vertical component of velocity constructed by the symmetry inner product.

global optimization solver can be operated as well in a smaller area (e.g. bounded within [-10, 0]) to reduce the computation cost. The same cannot be achieved in the L^2 ROM with the stabilized eigenvalues that are scattered in a large area in the left half of the complex

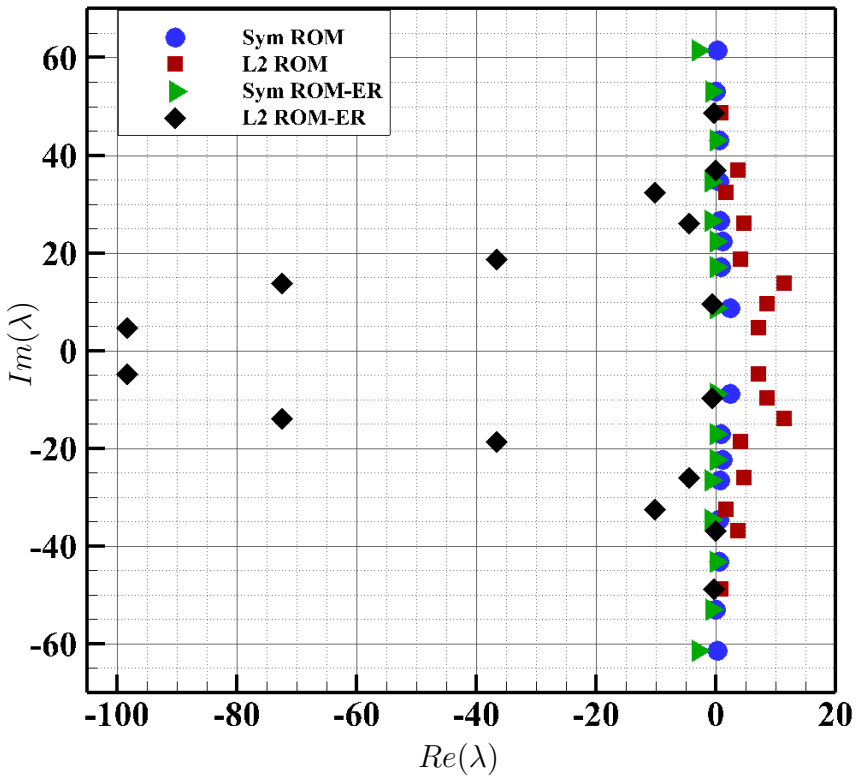

Figure 7.4: Eigenvalues of the 16 mode linear L^2 and symmetry ROMs.

plane (as far as $Re_{min}(\lambda) = -98.29$), thus making it impossible to predict the approximate location of the optimal eigenvalues, and shrink the search space.

Table 7.1: Stabilization of the 16 mode linear L^2 and symmetry ROMs

	L^2 ROM	Symmetry ROM
Bound Constraints	[-100, 0]	[-100, 0]
Population	60	55
$\Delta\boldsymbol{\lambda}_{max}$	2.0	2.0
Iterations	123	160
Minimum function value	0.400	0.182
Wall-clock time (Sec)	2.233	2.657

Figure 7.5 that compares the ROM coefficients with the POD temporal coefficients, agrees with the smaller objective function value of the symmetry ROM that is captured by the global optimization in Table 7.1. Both ROMs are originally unstable, but after stabilization, the

symmetry ROM shows a better resemblance with the POD coefficients. The small phase shift in the first, and second coefficients is further amplified in higher modes. This phase shift and the amplitude deviations in the stabilized ROM coefficients are a result of the approximation of the nonlinear FOM with a linear ROM, and have been removed in the nonlinear symmetry ROM.

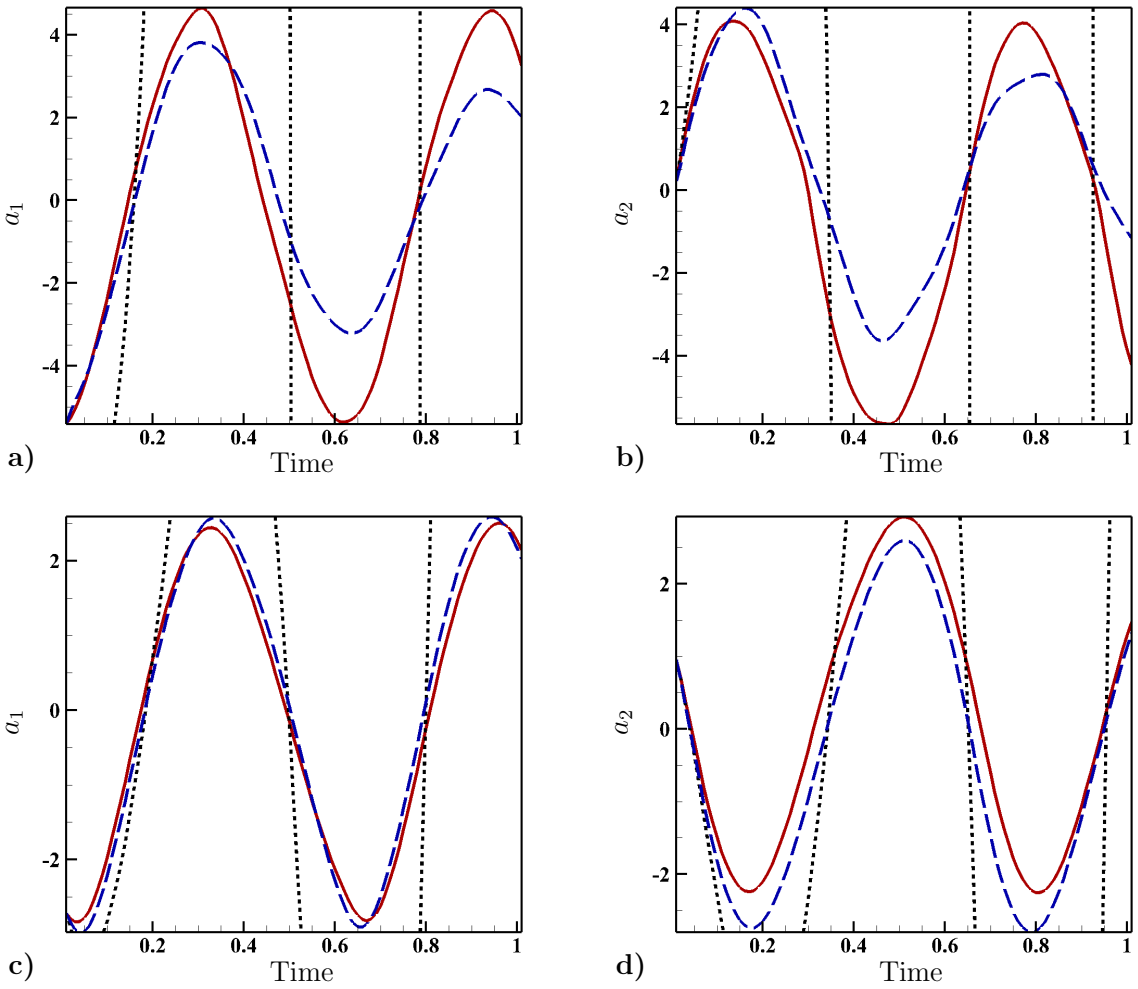

Figure 7.5: Modal coefficients of the 16 mode stabilized linear ROMs (– –), compared against the POD coefficients (——), and the unstable ROM coefficients (···), based on the L^2 (a, b), and symmetry (c, d) inner products.

An analysis of the controllability Gramians of the two ROMs shows that the complicated eigenvalue configuration and lower accuracy in the stabilized L^2 ROM is in fact connected to the properties of its controllable space. Degrees of controllability corresponding to each eigen-mode, and the volume of the controllable space are shown in Table 7.2. The symmetry

ROM is more controllable than the L^2 ROM in most directions, with a controllable space that is orders of magnitude larger. The immediate consequence of a large controllable space is that the system can be easily controlled towards the desired state, where in the current application is interpreted as the computation cost the global optimization solver spends on finding the optimal solution, and how close to the desired state that optimal solution can get. Apparently the small controllable space in the L^2 ROM means that it is very difficult to drive the system towards maximum resemblance with the FOM, thus, stabilization in a complicated control landscape has led to an eigenvalue configuration that is not necessarily optimal in terms of accuracy. This was also observed through the stabilization of the linear L^2 ROM with the ISC and Hybrid methods in chapter 4.

In the mean time, proximity of the stabilized eigenvalues to the imaginary axis in the symmetry ROM shows that the problem of stabilization of a linear symmetry ROM can be handled with a local optimizer within an acceptable tolerance. In other words, the symmetry ROM is robust with respect to the search attribute, which is also shown for the nonlinear ROMs in the remainder of this chapter.

Table 7.2: Degree of controllability ($\|\boldsymbol{V}^*\boldsymbol{W}_{\mathscr{C}}\boldsymbol{V}\|$) corresponding to each pair of eigen-modes, and volume of the controllable space ($det(\boldsymbol{W}_{\mathscr{C}})$) in the 16 mode L^2 and symmetry ROMs.

	L^2 ROM	Symmetry ROM
Mode 1, 2	$1.170e+01$	$4.896e+03$
Mode 3, 4	$5.038e+01$	$4.915e+03$
Mode 5, 6	$3.201e+01$	$4.924e+03$
Mode 7, 8	$1.662e+01$	$1.565e+02$
Mode 9, 10	$6.017e+02$	$2.263e+01$
Mode 11, 12	$1.844e+03$	$5.194e+03$
Mode 13, 14	$4.975e+03$	$1.656e+01$
Mode 15, 16	$3.816e+02$	$4.190e+00$
$det(\boldsymbol{W}_{\mathscr{C}})$	$1.666e-11$	$6.929e+26$

Although the controllability analysis is merely applied to the linear system here, it remotely explains some of the challenges in the stabilization of the nonlinear L^2 ROM. Eigenvalues of the linear matrix L_{ij} of the nonlinear ROM in Equation (3.10) are the control parameters in the ERN algorithm. Figure 7.6 shows these eigenvalues for the nonlinear

ROMs before and after stabilization. Note that since it is the nonlinear system that is being controlled here, the optimal eigenvalues do not necessarily need to be on the left half of the complex plane for the system to be stable. The eigenvalue configurations in the L^2 and symmetry ROMs follow a pattern similar to that in the linear ROMs. In the stabilized L^2 ROM, the reassigned eigenvalues are distributed between $Re_{min}(\lambda) = -25.92$ and $Re_{max}(\lambda) = 1.10$, while this range is reduced to -2.0 to 0.59 in the stabilized symmetry ROM. Thus, the optimization problem in the symmetry ROM can be efficiently solved in a smaller area. This is shown in Table 7.3, where the wall-clock time of 8.32 seconds for the stabilization of the L^2 ROM has decreased to 0.45 seconds in the symmetry ROM.

By reducing the number of modes from 16 to 8, eigenvalues of the stabilized L^2 ROM in Figure 7.6 exhibit an abnormal distribution with $Re_{min}(\lambda) = -216.92$. This is an indication of an ill-behaved optimization problem, potentially due to a very small controllable space, and a complicated control landscape when the ROM is built with this specific mode number. The situation goes back to normal by further reducing the number of modes from 8 to 4. The eigenvalues of the 4 mode stabilized L^2 ROM are not shown in Figure 7.6, but their real parts are distributed in the smaller range of -7.88 to 0.75.

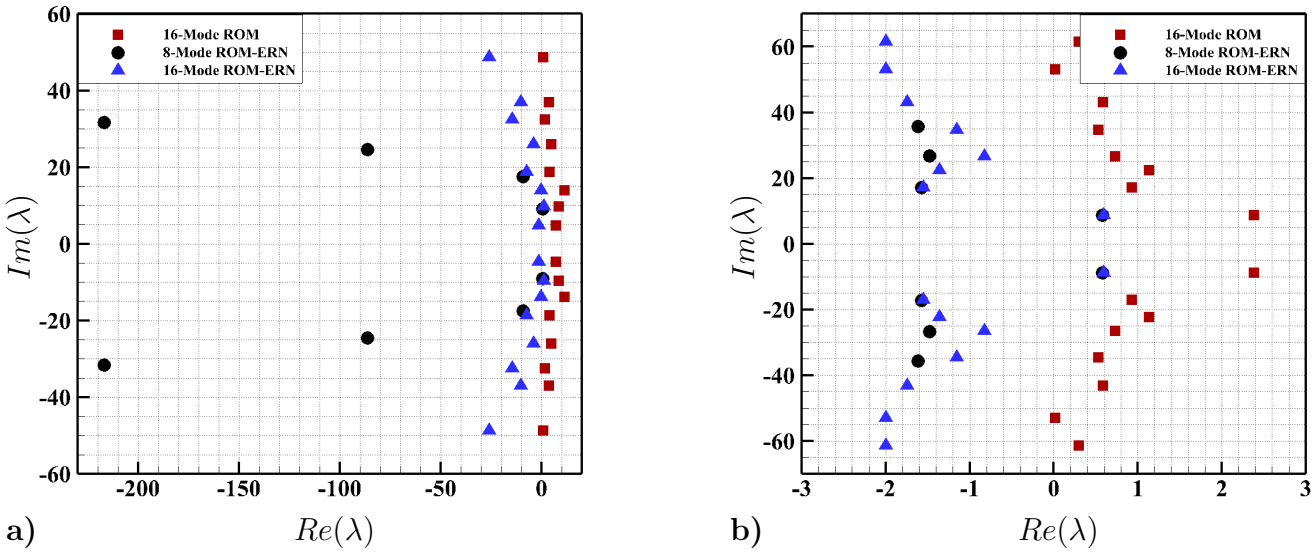

Figure 7.6: Eigenvalues of the nonlinear a) L^2 and b) symmetry ROMs.

Table 7.3 shows that the symmetry ROM allows for consistent optimization hyperparam-

eters through the stabilization of nonlinear ROMs of different dimensions. This consistency is a direct consequence of the robustness of the symmetry ROM, that facilitates easy and reliable implementation of the stabilization algorithm. The L^2 ROM on the other hand, is not gifted with this property as the optimization hyperparameters have to be readjusted for every mode number according to the complicated optimization landscape that affects the behavior of the optimization problem as the dimension of the subspace changes.

Table 7.3: Stabilization of the nonlinear L^2 and symmetry ROMs

	L^2 ROM			Symmetry ROM		
ROM dimension	16 mode	8 mode	4 mode	16 mode	8 mode	4 mode
Bound constraints	[-50, 50]	[-250, 250]	[-50, 50]	[-2, 2]	[-2, 2]	[-2, 2]
Population	75	300	25	5	5	5
$\Delta\boldsymbol{\lambda}_{max}$	1	8	1	1	1	1
Iterations	144	58	87	115	66	60
Minimum function value	9.60e-2	0.24	0.25	1.76e-2	1.54e-2	3.17e-2
Wall-clock time (Sec)	8.32	1.7	4.0e-2	0.45	4.6e-2	9.3e-3

Reconstruction of the stream-wise velocity contours by the stabilized nonlinear ROMs at $t = 0.65$ in Figure 7.7 shows a noticeable improvement in the accuracy of ROM when the symmetry inner product is used through the model reduction process.

The robustness of the nonlinear ROMs with respect to sub-optimal control is studied by observing the variations of the captured minimum objective function value with the population, where each of the tested populations includes five trials with different random initialization of the particle locations. All optimization hyperparameters are constant, except for the number of particles that is changed from 5 to 55 in 10 intervals. Figure 7.8 shows the best, and the mean of the minimum objective function values captured by the five trials at each target population. Starting with the local searches in the left side of the plot and moving in the direction of increasing the number of particles, the symmetry ROM shows almost no sensitivity to the search attribute, thus the local search results are almost as good as the global results. Agreement of the best and mean values shows that all trials have converged within the same level of accuracy. This property is a consequence of the smooth control landscape and better controllability of the symmetry ROM that is directly studied

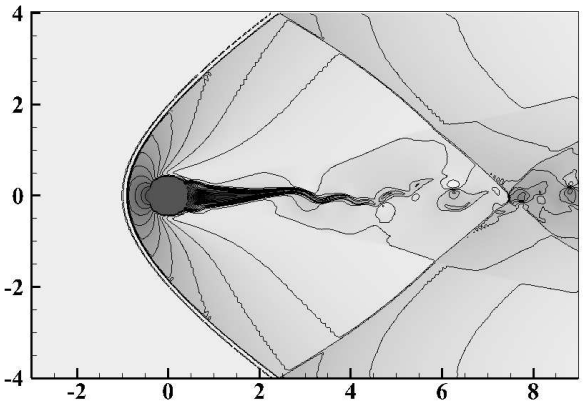

a)

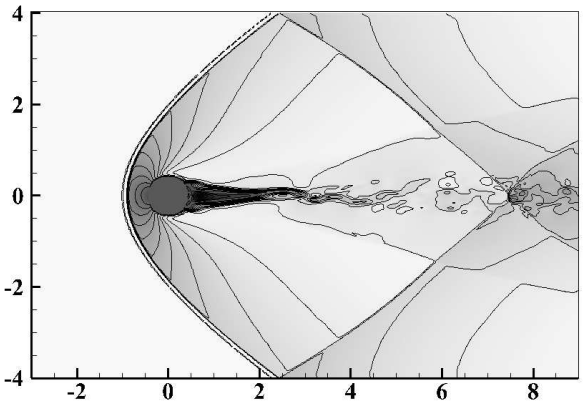

b)

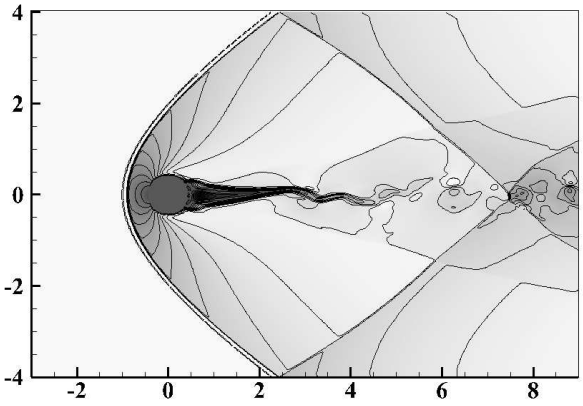

c)

Figure 7.7: Stream-wise velocity contours of the snapshot at $t = 0.65$, computed by a) FOM, and 16 mode nonlinear b) L^2 and c) symmetry ROMs. Non-dimensional time is computed from the beginning of snapshot collection for model reduction. Contour lines are plotted within the range of -2.5 to 5.5.

in the linear system.

The L^2 ROM shows a very different behavior with most of its trials deviating from the best value captured, which is itself an order of magnitude larger than the optimal solutions in the symmetry ROM. Similar to the properties observed in the linear L^2 ROM, variations of the mean value, and failure of most trials in finding the minimum point in the nonlinear ROM are the indications of a complicated control space.

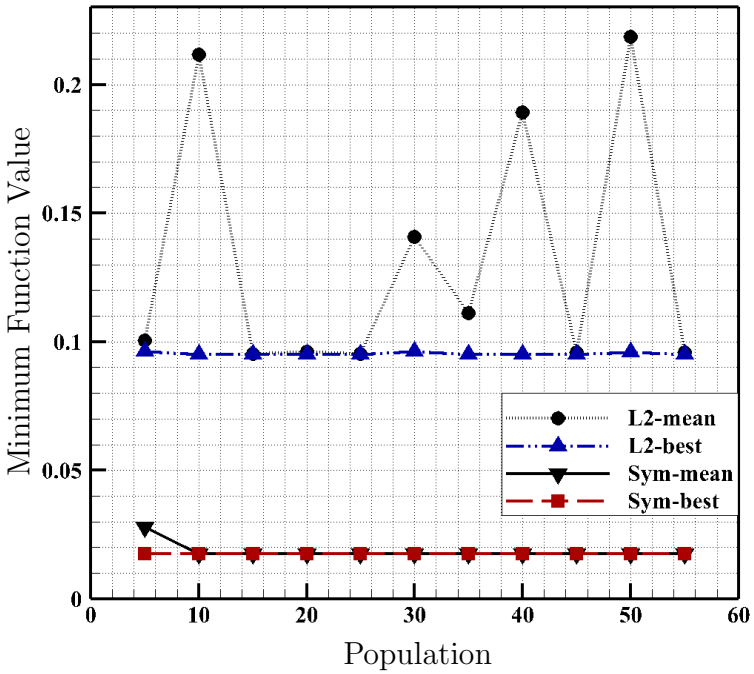

Figure 7.8: Sensitivity of the 16 mode nonlinear L^2 and symmetry ROMs with respect to the search attribute. From left to right, search attribute changes from local to global by increasing the number of global optimization agents. Each point corresponds to the best, or mean of the objective function values of five trials with different random initializations. L^2 and Sym stand for ROMs built by L^2 and symmetry inner products.

7.4 Application II: Supersonic Flow over a Triangular Prism

The influence of the inner product definition on the stability, controllability, and robustness of ROMs is also studied for the linear and nonlinear ROMs created based on the snapshots of the Mach 3.5 flow over the triangular prism. Figure 7.9 shows convergence of the POD modes computed based on the L^2 and symmetry inner products, where 262 modes are required to capture precisely 100 percent of the total energy with the L^2 inner product, and 314 modes with the symmetry inner product. The first 16 modes that capture 89 percent of the energy with the L^2 and 83 percent with the symmetry inner product are used as the bases for construction of the linear and nonlinear ROMs. Figures 7.10, and 7.11 show the first eight POD modes of pressure computed based on the L^2, and symmetry inner products.

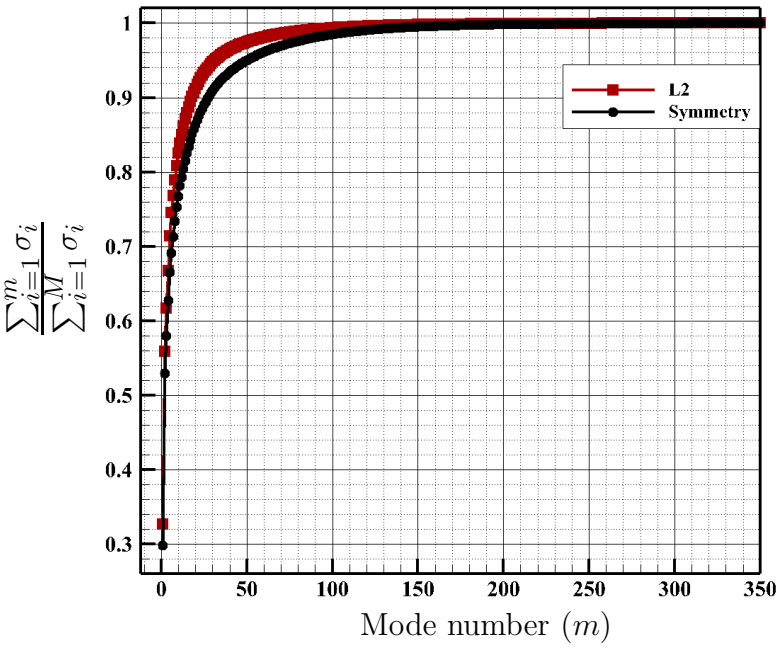

Figure 7.9: Normalized cumulative energy of the POD modes computed by L^2 and symmetry inner products.

The linearized Euler equations are projected onto the POD modes to build the linear ROMs with eigenvalues shown in Figure 7.12. The L^2 ROM has 12 unstable eigenvalues with

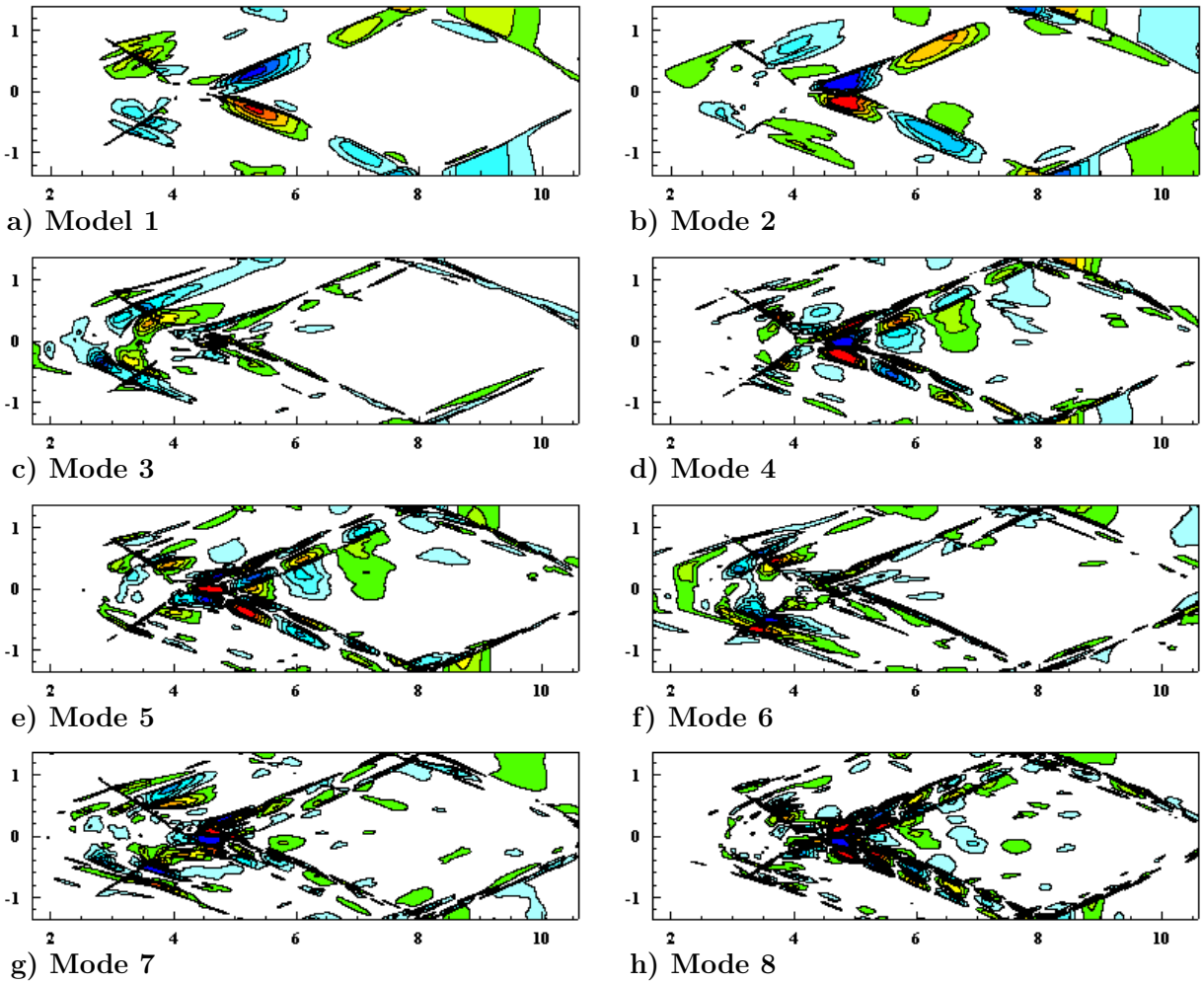

Figure 7.10: POD modes of pressure computed by the L^2 inner product.

$Re_{max}(\lambda^u) = 1.08$, and the symmetry ROM has 14 unstable eigenvalues with $Re_{max}(\lambda^u) = 0.88$. Eigenvalues in both ROMs are originally close to the imaginary axis in this case with a slightly more compact distribution in the symmetry ROM, which is not surprising according to the properties of the symmetry ROM.

After stabilizing the two ROMs with the ER method, the eigenvalues of the symmetry ROM remain in the vicinity of the imaginary axis with $Re_{min}(\lambda) = -6.6$, while the eigenvalues of the stabilized L^2 ROM spread out with an eigenvalue pair that is located as far as $Re_{min}(\lambda) = -44.49$. Consequently, the optimization problem in the L^2 ROM has to be solved in a large area that necessarily imposes additional computation cost. This is shown in Table 7.4 that includes the global optimization parameters and results. The stabilized

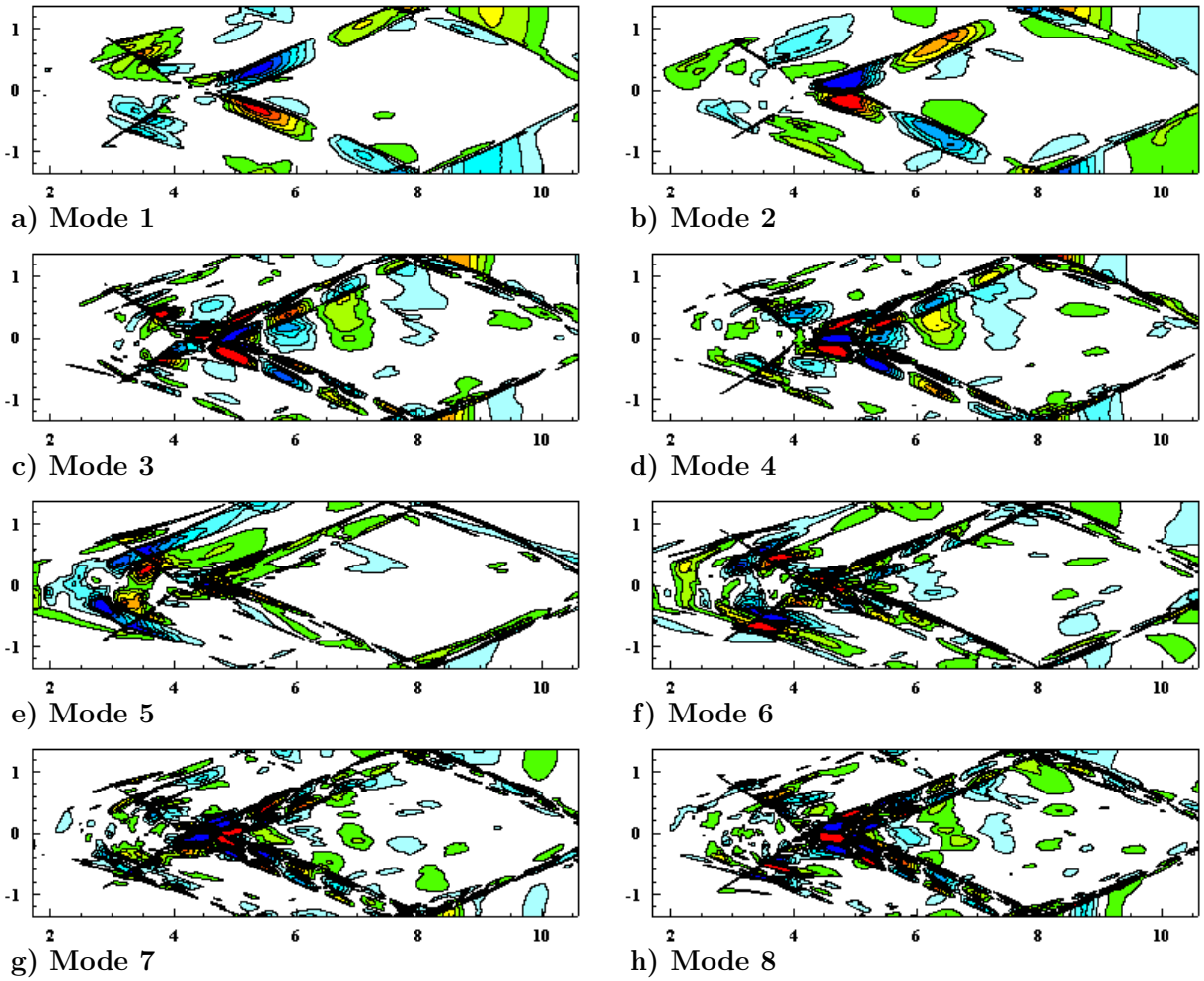

Figure 7.11: POD modes of pressure computed by the symmetry inner product.

Table 7.4: Stabilization of the 16 mode linear L^2 and symmetry ROMs

	L^2 ROM	Symmetry ROM
Bound Constraints	[-100, 0]	[-20, 0]
Population	100	30
$\Delta\boldsymbol{\lambda}_{max}$	5.0	3.0
Iterations	871	100
Minimum function value	0.364	0.308
Wall-clock time (Sec)	794.92	4.78

eigenvalues in Figure 7.12 are obtained by global optimization within a range of $[-100, 0]$ for the L^2 ROM, which converges in about 13.25 minutes of wall-clock time. The optimization problem for the symmetry ROM on the other hand is solved within the smaller bounds of

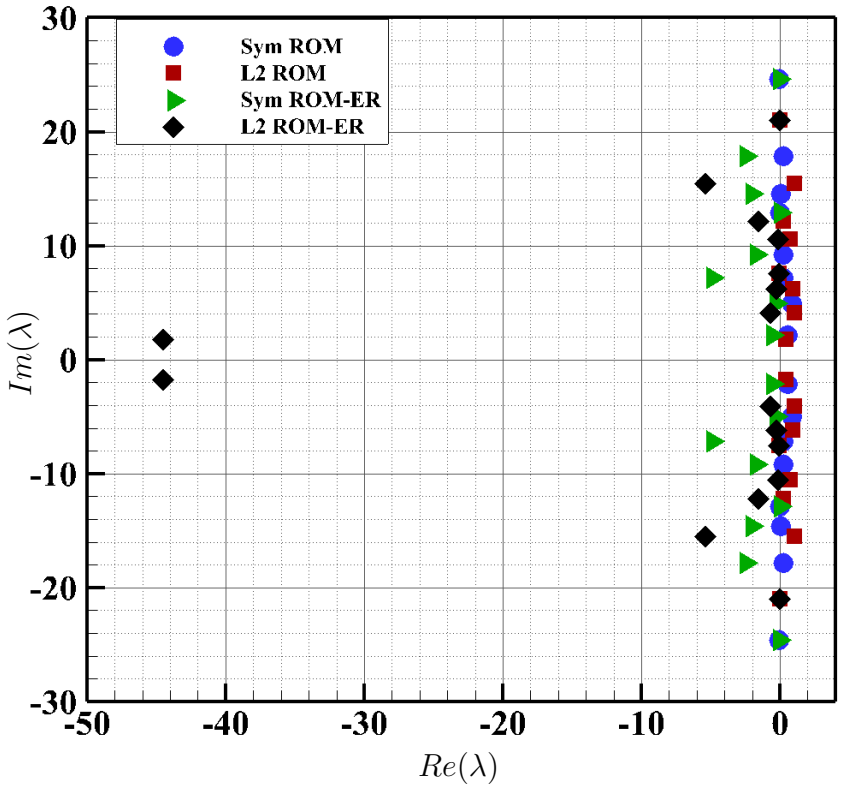

Figure 7.12: Eigenvalues of the 16 mode linear L^2 and symmetry ROMs.

$[-20, 0]$, that apparently result in a lower computation cost. This operational advantage is provided by the compact distribution of the eigenvalues in the symmetry ROM.

Temporal coefficients of the two linear ROMs are also compared against the original unstable ROMs, and the POD coefficients in Figure 7.13. The stabilized L^2 and symmetry ROMs of this case are very similar in terms of accuracy, as also suggested by the minimum objective function values reported in Table 7.4.

Analysis of the controllability Gramian shows the connection between the smooth, low-cost optimization problem of the symmetry ROM, and the properties of the controllable space of this model as a linear system. Table 7.5 lists the degrees of controllability in all eigen-directions, and the volume of the controllable space for the L^2 and symmetry ROMs. The symmetry ROM is more controllable than the L^2 ROM in most directions, and the volume of the controllable space of the symmetry ROM, that is 4 orders of magnitude larger

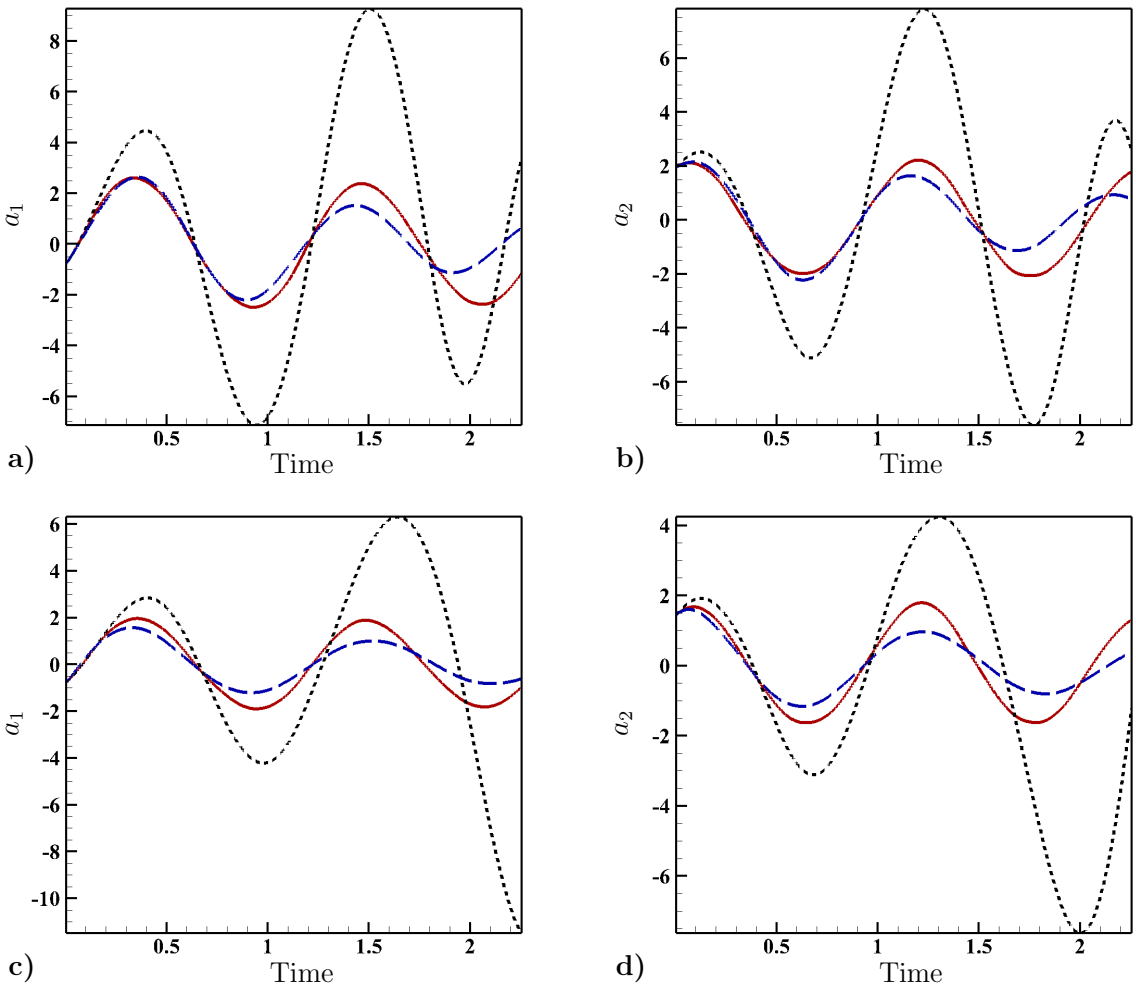

Figure 7.13: Modal coefficients of the 16 mode stabilized linear ROMs (– –), compared against POD coefficients (—), and the unstable ROMs (·····), based on the L^2 (a, b), and symmetry (c, d) inner products.

than the L^2 ROM, explains the better properties of the optimization problem in both linear and nonlinear symmetry ROMs.

The unstable nonlinear ROMs are next stabilized by the ERN algorithm. The original, and reassigned eigenvalues of the linear matrix in the nonlinear L^2 and symmetry ROMs are shown in Figure 7.14. Similar observations are also made in the nonlinear ROMs. The eigenvalues of the stabilized L^2 ROM are distributed in a large region with $Re_{min}(\lambda) = -24.40$ and $Re_{max}(\lambda) = 0.52$, which in the stabilized symmetry ROM is reduced to $Re_{min}(\lambda) = -8.07$ to $Re_{max}(\lambda) = 0.61$.

The compact distribution of the eigenvalues in the symmetry ROM allows for global

Table 7.5: Degree of controllability ($\|\boldsymbol{V}^*\boldsymbol{W}_{\mathscr{C}}\boldsymbol{V}\|$) corresponding to each pair of eigen-modes, and volume of the controllable space ($det(\boldsymbol{W}_{\mathscr{C}})$) in the 16 mode L^2 and symmetry ROMs.

	L^2 ROM	Symmetry ROM
Mode 1, 2	$1.079e-01$	$2.891e+00$
Mode 3, 4	$9.732e-01$	$2.338e+00$
Mode 5, 6	$2.496e+00$	$7.243e+00$
Mode 7, 8	$7.327e+00$	$6.887e+00$
Mode 9, 10	$4.143e+00$	$8.408e+01$
Mode 11, 12	$4.699e-01$	$5.079e+03$
Mode 13, 14	$3.907e-01$	$7.531e+01$
Mode 15, 16	$1.695e+01$	$1.047e+01$
$det(\boldsymbol{W}_{\mathscr{C}})$	$3.660e-02$	$1.188e+03$

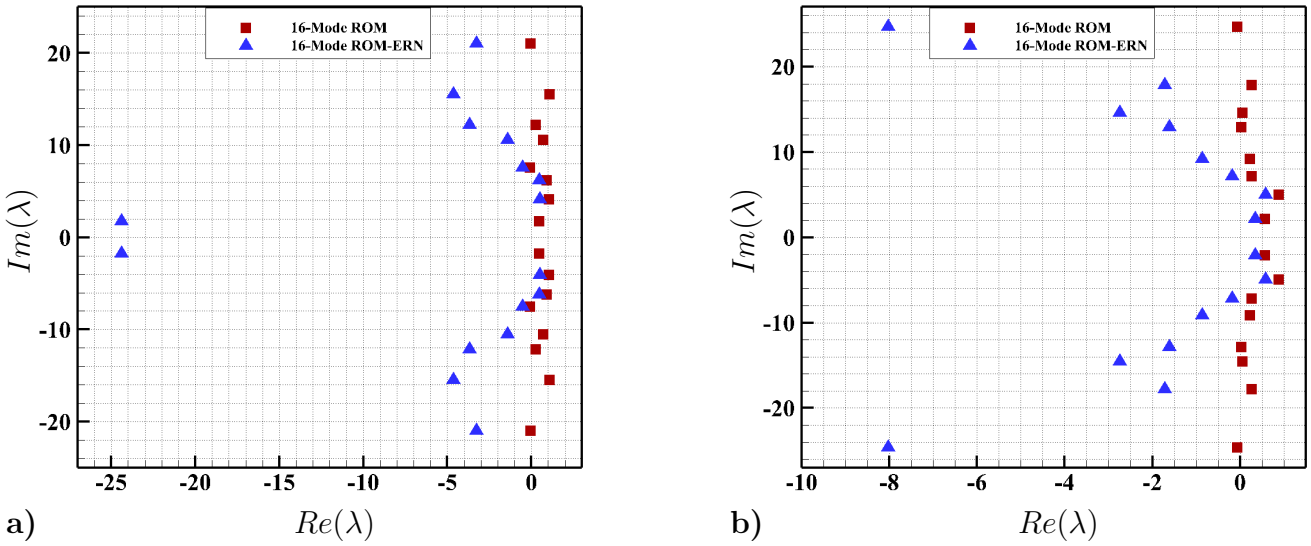

Figure 7.14: Eigenvalues of the 16 mode nonlinear a) L^2 and b) symmetry ROMs.

search within smaller bounds, that according to Table 7.6 leads to slightly better computational performance. Note that based on the information in Table 7.5, the contrast between the volume of the controllable spaces in the linear L^2 and symmetry ROMs is not as large as in the case of the supersonic flow over the cylinder. Consistently, controllability of the two systems, thus the accuracy of the optimal solutions captured through the stabilization of the L^2 and symmetry ROMs (linear and nonlinear) do not deviate as much as in the cylinder case. Nevertheless, better accuracy of the symmetry ROM is evident in Figure 7.15, that

shows the stream-wise velocity contours reconstructed by the 16 mode L^2 and symmetry ROMs at $t = 1.02$, compared against the same snapshot computed by the FOM.

Table 7.6: Stabilization of the 16 mode nonlinear L^2 and symmetry ROMs

	L^2 ROM	Symmetry ROM
Bound Constraints	[-50, 5]	[-20, 5]
Population	60	25
$\Delta\boldsymbol{\lambda}_{max}$	3.0	2.0
Iterations	101	203
Minimum function value	6.959e-2	2.572e-2
Wall-clock time (Sec)	25.547	21.28

Sensitivity of ROMs with respect to sub-optimal control laws is studied by changing the population in PSO, where the influence of random initialization and parameters is eliminated by averaging between five different trials at each population. The best and mean values of the minimum objective function captured by each group of the trials are plotted in Figure 7.16 for the 16 mode L^2 and symmetry ROMs, as the population of particles is changed between 5 to 60 in 11 intervals. Besides the test with five particles, the symmetry ROM shows a very small sensitivity to sub-optimal eigenvalue locations. Large variations of the mean values in the L^2 ROM, that considerably deviate from the captured best objective function value in all of the tested populations, show that most of the trials have failed to find the global minimum point, and the system is very sensitive to sub-optimal eigenvalue configurations. These observations are also consistent with the results delivered by controllability analysis of the linear ROMs.

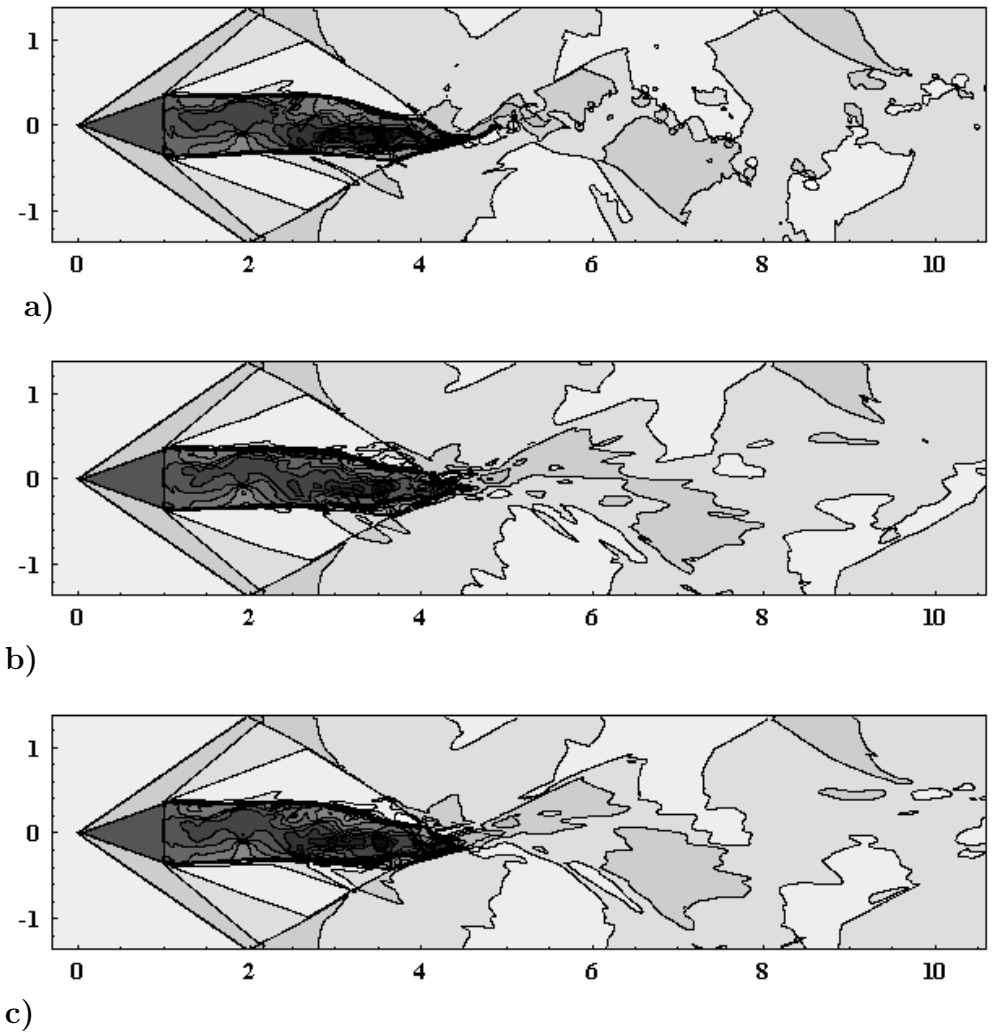

Figure 7.15: Stream-wise velocity contours of the snapshot at $t = 1.02$, computed by a) FOM, and 16 mode nonlinear b) L^2 and c) symmetry ROMs. Contour lines are plotted within the range of -2.5 to 5.18.

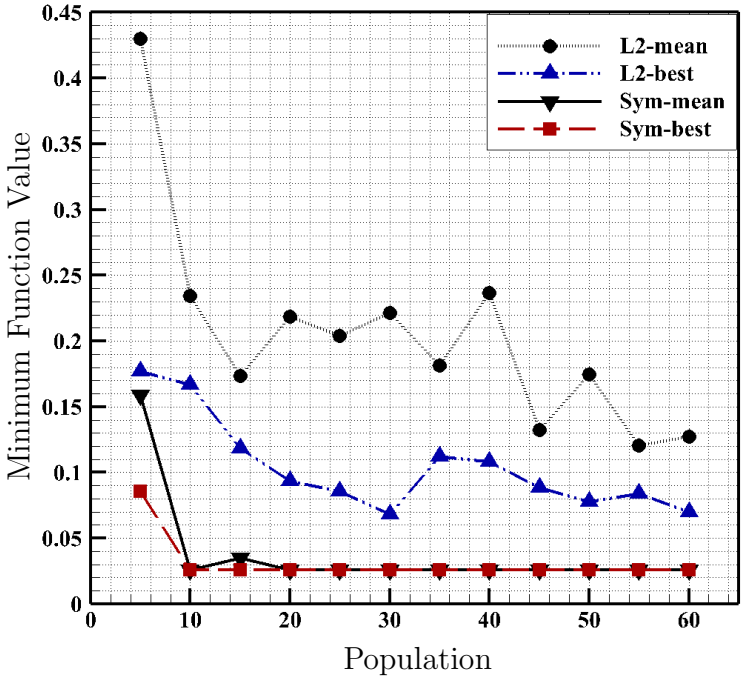

Figure 7.16: Sensitivity of the 16 mode nonlinear L^2 and symmetry ROMs with respect to the search attribute. From left to right, search attribute changes from local to global by increasing the number of global optimization agents. Each point corresponds to the best, or mean of the objective function values of five trials with different random initializations. L^2 and Sym stand for ROMs built by L^2 and symmetry inner products.

Chapter 8

Summary and Conclusion

Since the advent of ROMs, model reduction procedure has been modified and enhanced to stand alone in prediction of the dynamics beyond the jurisdiction of the high-fidelity simulations. The computational speed-up delivered by ROMs that makes them an indispensable component of fast or real-time control and optimization, comes with additional challenges that have paced down their implementation in practical applications. POD-based ROMs regularly suffer from instabilities when the flow field involves dynamically critical high-frequency signatures that are naturally truncated through the construction of the POD subspace. This difficulty is commonly observed in flows with unsteady moving shock waves, and in turbulent flows that are characterized with multi-frequency interactions. In the latter case, inadequate resolution of the multi-scale interactions leads to the so-called POD closure problem that compromises the accuracy and stability of ROM. Thus, the simplicity, mathematical power, and computational savings that accompany the orthogonal linear POD subspace may be compromised by the incomplete representation of the strongly nonlinear structures as to produce ROMs that are unstable, or barely replicate the behavior of the original high-dimensional attractor. Recent studies have shown that the transition to a nonlinear subspace is not a process free of theoretical and computational complexities. This study attempts to generate viable ROMs, while still benefiting from the mathematical and computational advantages of POD in the model reduction routine.

In the two applications discussed in this work, the two-dimensional Euler equations are solved to simulate the supersonic flow over a circular cylinder, and a triangular prism. Both flow fields involve unsteady shock-wake interactions. Galerkin projection over the POD subspace that is computed based on the high-fidelity snapshots of these flows, invoke severe instabilities in the constructed ROMs. The influence of symmetrization on the improvement of stability in hyperbolic equations has fostered the evolution of the symmetry inner product for POD-Galerkin ROMs of compressible flows. However, large instabilities as a result of the unresolved dynamics, similar to those in the supersonic flow applications of this study, cannot be contained within the error bounds provided by the symmetrization. Thus, even the symmetric ROMs need further stabilization and calibration, which opens a new path to study the controllability and robustness of ROMs created based on different inner product definitions. With the aid of the controllability analysis conducted in this work via the controllability Gramian, and a sensitivity analysis, it is shown that the advantage of using a symmetry inner product, instead of the common L^2 inner product, is not merely limited to the improvement of stability. Symmetrization leads to ROMs with better controllability: models that easily lend themselves to post-process stabilization and calibration. Thus, not only the symmetry ROMs allow accurate control towards maximum agreement with the FOM, but they are also robust against potentially imperfect hyperparameters of the stabilization method that may lead to sub-optimal control laws.

For the linear ROMs, two different stabilization algorithms, the ISC method proposed by Amsallem and Farhat[14] and the ER method proposed by Kalashnikova et al.[30] are compared. ISC appears to be computationally efficient but it fails to generate accurate results when the original ROM is highly unstable. ER on the other hand directly monitors accuracy through the objective function that constructs a feedback signal of the ROM output, but its computational efficiency and robustness are challenged when the number of unstable modes grows. In this work, a new Hybrid approach is proposed to integrate the computational efficiency of ISC with the accuracy of ER. The three stabilization methods are tested on numerical simulation data, where a Mach 2.8 flow passes a fixed cylinder and the flow is featured by shock waves and their interaction with shedding vortices. The eigenvalues

of the linear matrices are compared for ROMs before and after stabilization. Though all stabilization approaches work to some degree, the Hybrid method shows clear advantages by keeping both efficiency and accuracy for ROMs with a large number of unstable eigenvalues.

Presence of strongly nonlinear phenomena, like turbulence, unsteady shock waves, and chemical reactions, can render linear models inaccurate, or even invalid. This aspect highlights the importance of the development of stabilization methods for nonlinear ROMs, that can also respond to a broader class of applications. A second stabilization method (the ERN algorithm) is proposed in this study, that uses global optimization to modify the eigenvalues of the linear term of the nonlinear ROM to control the nonlinear system dynamics, while stability is guaranteed by enforcing the ROM to maintain a negative total power residual. The proposed method has effectively recovered stability and accuracy in the applications. In the mean time, a multi-stage stabilization layout is proposed to facilitate computationally efficient implementation of this method in strongly nonlinear systems. Such applications usually require a large number of POD modes to resolve the nonlinearities, thus leaving the bare bone stabilization techniques often intractable. The designed multi-stage configuration has reduced the computation cost of the ERN algorithm by an order of magnitude, and improved its robustness through the stabilization of the large nonlinear ROMs of the supersonic flow applications.

This study seeks a complete framework for POD-based model reduction in compressible flows. However, the proposed stabilization methods are founded over global principles, and can be readily adopted for the stabilization of ROMs in other applications that do not necessarily relate to fluid dynamics. The proposed algorithms are non-intrusive, thus they do not depend on the dimensionality reduction method, neither do they rely on a specific projection type, and in general, model reduction technique. Therefore, the suggested approaches can be easily applied to the ROMs constructed by system identification and operator inference techniques. In this light, the future line of research is directed towards evaluation of the performance of the proposed methods for the stabilization and enhancement of ROMs created through other channels, and for different, more complicated dynamical systems (e.g. turbulent flows).

Bibliography

[1] A. Chaudhuri, A. Hadjadj, and A. Chinnayya. On the use of immersed boundary methods for shock/obstacle interactions. *J Comput Phys*, 230(5):1731–1748, 2011.

[2] S.L. Brunton and B.R. Noack. Closed-loop turbulence control: progress and challenges. *Appl Mech Rev*, 67(5):050801, 2015.

[3] M. Wei and J.B. Freund. A noise-controlled free shear flow. *J Fluid Mech*, 546:123–152, 2006.

[4] M. Wei and C.W. Rowley. Low-dimensional models of a temporally evolving free shear layer. *J Fluid Mech*, 228:113–134, 2009.

[5] M. Wei, B.R. Qawasmeh, M. Barone, B.G. van Bloemen Waanders, and L. Zhou. Low-dimensional model of spatial shear layers. *Phys Fluids*, 24(1):014108, 2012.

[6] J. Xu and K. Duraisamy. Multi-level convolutional autoencoder networks for parametric prediction of spatio-temporal dynamics. *arXiv preprint arXiv:1912.11114*, 2019.

[7] F.J. Gonzalez and M. Balajewicz. Deep convolutional recurrent autoencoders for learning low-dimensional feature dynamics of fluid systems. *arXiv preprint arXiv:1808.01346*, 2018.

[8] C.W. Rowley, T. Colonius, and R.M. Murray. Model reduction for compressible flows using POD and Galerkin projection. *Physica D*, 189(1):115–129, 2004.

[9] C.W. Rowley. Model reduction for fluids, using balanced Proper Orthogonal Decomposition. *Int J Bifurcat Chaos*, 15(3):997–1013, 2005.

[10] T. Bui-Thanh, K. Willcox, and O. Ghattas. Model reduction for large-scale systems with high-dimensional parametric input space. *SIAM J Sci Comput*, 30(6):3270–3288, 2008.

[11] G. Berkooz, P. Holmes, and L. Lumley. The proper orthogonal decomposition in the analysis of turbulent flows. *Ann Rev Fluid Mech*, 25:539–575, 1993.

[12] P. Holmes, J.L. Lumley, and G. Berkooz. *Turbulence, Coherent Structures, Dynamical Systems and Symmetry*. Cambridge University Press, New York, 1996.

[13] L. Sirovich. Turbulence and the dynamics of coherent structures. *Q Appl Math*, 45(3): 561–590, 1987.

[14] D. Amsallem and C. Farhat. Stabilization of projection-based reduced-order models. *Int J Numer Methods Eng*, 91(4):358–377, 2012.

[15] E. Rezaian and M. Wei. A hybrid stabilization approach for reduced-order models of compressible flows with shock-vortex interaction. *Int J Numer Methods Eng*, 121(8): 1629–1646, 2020.

[16] M. Bergmann, C. Bruneau, and A. Lollo. Enablers for robust POD models. *J. Comp. Phys.*, 228:516–538, 2009.

[17] B. Noack and R. Niven. A hierarchy of maximum entropy closures for Galerkin systems of incompressible flows. *Comput Math Appl*, 65:1558–1574, 2013.

[18] B. Noack and R. Niven. Maximum-entropy closure for a galerkin model of an incompressible periodic wake. *J Fluid Mech*, 700:187–213, 2012.

[19] Z. Wang, I. Akhtar, J. Borggaard, and T. Iliescu. Proper Orthogonal Decomposition closure models for turbulent flows: a numerical comparison. *Comput Methods Appl Mech Eng.*, 237:10–26, 2012.

[20] V. Resseguier, E. Memin, D. Heitz, and B. Chapron. Stochastic modelling and diffusion modes for POD models of small-scale flow analysis. *J Fluid Mech*, 826:888–917, 2017.

[21] S. Pan and K. Duraisamy. Data-driven discovery of closure models. *SIAM J Appl Dyn Syst*, 17(4):2381–2413, 2018.

[22] K. Lee and K.T. Carlberg. Model reduction of dynamical systems on nonlinear manifolds using deep convolutional autoencoders. *J Comp Phys.*, 404:108973, 2020.

[23] H. Jain, P. Tiso, J.B. Rutzmoser, and D.J. Rixen. A quadratic manifold for model order reduction of nonlinear structural dynamics. *Comput Struct*, 188:80–94, 2017.

[24] M.F. Barone, I. Kalashnikova, D.J. Segalman, and H.K. Thornquist. Stable Galerkin reduced order models for linearized compressible flow. *J Comput Phys*, 228(6):1932–1946, 2009.

[25] I. Kalashnikova and M.F. Barone. On the stability and convergence of a Galerkin reduced order model ROM of compressible flow with solid wall and far-field boundary treatment. *Int J Numer Methods Eng*, 83(10):1345–1375, 2010.

[26] M. Tabandeh, M. Wei, and J. Collins. On the symmetrization in POD-Galerkin model for linearized compressible flows. AIAA 2016-1106. 54th AIAA Aerospace Sciences Meeting, San Diego, California, 2016.

[27] E. Rezaian and M. Wei. Impact of symmetrization on the robustness of POD-Galerkin ROMs for compressible flows. AIAA 2020-1318. AIAA Scitech 2020 Forum, Orlando, Florida, 2020.

[28] K. Carlberg, C. Bou-Mosleh, and C. Farhat. Efficient non-linear model reduction via a least-squares Petrov-Galerkin projection and compressive tensor approximations. *Int J Numer Meth Eng*, 86(2):155–181, 2011.

[29] S. Grimberg, C. Farhat, and N. Youkilis. On the stability of projection-based model order reduction for convection-dominated laminar and turbulent flows. *J Comp Phys.*, 419:109681, 2020.

[30] I. Kalashnikova, B. van Bloemen Waanders, S. Arunajatesan, and M.F. Barone. Stabilization of projection-based reduced order models for linear time-invariant systems via optimization-based eigenvalue reassignment. *Comput Methods Appl Mech Eng*, 272: 251–270, 2014.

[31] D.J. Lucia and P.S. Beran. Projection methods for reduced order models of compressible flows. *J Comp Phys.*, 188(1):252–280, 2003.

[32] B.N. Bond and L. Daniel. Guaranteed stable projection-based model reduction for indefinite and unstable linear systems. Proceedings of the 2008 IEEE/ACM International Conference on Computer-Aided Design, pages 728–735, 2008.

[33] M. Balajewicz, I. Tezaur, and E. Dowell. Minimal subspace rotation on the Stiefel manifold for stabilization and enhancement of projection-based reduced order models for the compressible Navier-Stokes equations. *J Comp Phys*, 321:224–241, 2016.

[34] E. Rezaian and M. Wei. Eigenvalue reassignment by particle swarm optimization toward stability and accuracy in nonlinear reduced-order models. AIAA 2018-3095. Fluid Dynamics Conference, Atlanta, Georgia, 2018.

[35] L. Cordier, B. Noack, G. Tissot, G. Lehnasch, J. Delville, M. Balajewicz, G. Daviller, and R. Niven. Identification strategies for model-based control. *Exp Fluids*, 54(8):1580, 2013.

[36] B.R. Noack, M. Schlegel, B. Ahlborn, G. Mutschke, M. Morzyński, and P. Comte. A finite-time thermodynamics of unsteady fluid flows. *J Non-Equil Thermody*, 33(2): 103–148, 2008.

[37] E. Rezaian and M. Wei. Obtaining a stable Galerkin ROM in presence of shock-vortex interaction. AIAA 2017-1008. 55th AIAA Aerospace Sciences Meeting, Grapevine, Texas, 2017.

[38] M.J. Balajewicz, E.H. Dowell, and B.R. Noack. Low-dimensional modelling of high-Reynolds-number shear flows incorporating constraints from the Navier-Stokes equation. *J Fluid Mech*, 729:285–308, 2013.

[39] M. Xu. Understanding flapping-wing aerodynamics through adjoint-based approach; ph.d. Thesis; dept. of mechanical and aerospace engineering, new mexico state univ. 2014.

[40] M. Xu and M. Wei. Implementation of immersed boundary method in WENO scheme to simulate shock structure interaction. Proceedings of the ASME 2017 Fluids Engineering Division Summer Meeting, page 69217, 2017.

[41] C. Shu. *Essentially Non-Oscillatory and Weighted Essentially Non-Oscillatory Schemes for Hyperbolic Conservation Laws*. Springer, 1998.

[42] P. Woodward and P. Colella. The numerical simulation of two-dimensional fluid flow with strong shocks. *J Comput Phys*, 54(1):115–173, 1984.

[43] G. Rozza. Reduced basis approximation and error bounds for potential flows in parametrized geometries. *Commun Comput Phys*, 9(1):1–48, 2011.

[44] B. Moore. Principal component analysis in linear systems: Controllability, observability, and model reduction. *IEEE transactions on automatic control*, 26(1):17–32, 1981.

[45] P.J. Schmid. Dynamic mode decomposition of numerical and experimental data. *J Fluid Mech*, 656:5–28, 2010.

[46] B.R. Qawasmeh and M. Wei. Low-dimensional models for compressible temporally developing shear layers. *J Fluid Mech*, 731:364–393, 2013.

[47] H. Gao and M. Wei. Global model reduction for flows with moving boundary. AIAA 2014-0222. 52nd AIAA Aerospace Sciences Meeting, National Harbor, Maryland, 2014.

[48] H. Gao, M. Wei, and K. Jia. Model adaptation of an improved global pod-galerkin model. AIAA 2019-1898. 57th AIAA Aerospace Sciences Meeting, San Diego, California, 2019.

[49] B. Kramer and K.E. Willcox. Nonlinear model order reduction via lifting transformations and proper orthogonal decomposition. *AIAA Journal*, 57(6):2297–2307, 2019.

[50] E. Qian, B. Kramer, B. Peherstorfer, and K. Willcox. Lift & learn: Physics-informed machine learning for large-scale nonlinear dynamical systems. *arXiv preprint arXiv:1912.08177*, 2019.

[51] M. Ohlberger and S. Rave. Reduced basis methods: Success, limitations and future challenges. *arXiv preprint arXiv:1511.02021*, 2015.

[52] I. Akhtar, A.H. Nayfeh, and C.J. Ribbens. On the stability and extension of reduced-order Galerkin models in incompressible flows. *Theoret Comput Fluid Dyn*, 23(3):213–237, 2009.

[53] H. Gao and M. Wei. Domain decomposition in POD-Galerkin projection for flows with moving boundary. AIAA 2016-1102. 54th AIAA Aerospace Sciences Meeting, San Diego, California, 2016.

[54] I. Kalashnikova and M.F. Barone. Stable and efficient Galerkin reduced order models for non-linear fluid flow. AIAA 2011-3110. 6th AIAA Theoretical Fluid Mechanics Conference, Honolulu, Hawaii, 2011.

[55] I. Kalashnikova and M.F. Barone. Efficient non-linear Proper Orthogonal Decomposition/Galerkin reduced order models with stable penalty enforcement of boundary conditions. *Int J Numer Methods Eng*, 90(11):1337–1362, 2012.

[56] T. Bui-Thanh, K. Willcox, and O. Ghattas. Model reduction for large-scale systems with high-dimensional parametric input space. *SIAM J Sci Comput*, 30(6):3270–3288, 2008. doi: 10.1137/070694855.

[57] Z. Ma, S. Ahuja, and C.W. Rowley. Reduced-order models for control of fluids using the eigensystem realization algorithm. *Theoret Comput Fluid Dyn*, 25(1-4):233–247, 2011.

[58] S. Pan and K. Duraisamy. Data-driven operator inference for nonintrusive projection-based model reduction. *Comput Methods Appl Mech Eng*, 306:196–215, 2016.

[59] D. Rempfer and H.F. Fasel. Dynamics of three-dimensional coherent structures in a flat-plate boundary layer. *J Fluid Mech*, 275:257–283, 1994.

[60] I. Kalashnikova, S. Arunajatesan, M.F. Barone, B.G. van Bloemen Waanders, and J.A. Fike. Reduced order modeling for prediction and control of large-scale systems. *Sandia National Laboratories Report*, SAND 2014-4693, 2014.

[61] B. Gustafsson, H.O. Kreiss, and J. Oliger. *Time dependent problems and difference methods*. John Wiley & Sons, 1995.

[62] S. Chaturantabut and D.C. Sorensen. Nonlinear model reduction via discrete empirical interpolation. *SIAM J Sci Comput*, 32(5):2737–2764, 2010.

[63] J. Kennedy and R. Eberhart. Particle swarm optimization. In Proceedings of the IEEE International Conference on Neural Networks IV, Perth, Australia, 1995.

[64] M. Clerk and J. Kennedy. The particle swarm explosion, stability, and convergence in a multidimensional complex space. *IEEE Transaction on Evolutionary Computation*, 6 (1):58–73, 2002.

[65] R. Perez and K. Behdinan. Particle swarm approach for structural design optimization. *Comput Struct*, 85:1579–1588, 2007.

[66] R. Eberhart and J. Kennedy. A new optimizer using particle swarm theory. In Micro Machine and Human Science, Proceedings of the Sixth International Symposium, IEEE, Nagoya, Japan, 1995.

[67] J. Kennedy. Small worlds and mega-minds: effects of neighborhood topology on particle swarm performance. In Proceedings of the IEEE Congress on Evolutionary Computation, 1999.

[68] J. Kennedy and R. Mendes. Population structure and particle swarm performance. In Proceedings of the IEEE Congress on Evolutionary Computation, Honolulu, HI, 2002.

[69] E. Memin. Fluid flow dynamics under location uncertainty. *Geophys Astro Fluid*, 108 (2):119–146, 2014.

[70] Z.Y. Wan, P. Vlachas, P. Koumoutsakos, and T. Sapsis. Data-assisted reduced-order modeling of extreme events in complex dynamical systems. *PloS One*, 13:e0197704, 2018.

[71] K. Willcox and J. Peraire. Balanced model reduction via the proper orthogonal decomposition. *AIAA journal*, 40(11):2323–2330, 2002.

[72] E. Rezaian and M. Wei. Multi-stage stabilization of ROMs in strongly nonlinear systems. AIAA 2020-3083. AIAA Aviation Forum, 2020.